Summer 2018

The separation of shear-driven liquid films from a sharp corner

Zahra Sadeghizadeh

Department: Mechanical and Aerospace Engineering

THE SEPARATION OF SHEAR-DRIVEN LIQUID FILMS FROM A SHARP CORNER

by

ZAHRA SADEGHIZADEH

A DISSERTATION

Presented to the Graduate Faculty of the

MISSOURI UNIVERSITY OF SCIENCE AND TECHNOLOGY

In Partial Fulfillment of the Requirements for the Degree

DOCTOR OF PHILOSOPHY

in

AEROSPACE ENGINEERING

2018

Approved by

James A. Drallmeier, Advisor
Kelly Homan
David Riggins
Joseph D. Smith
Cheng Wang

PUBLICATION DISSERTATION OPTION

This dissertation consists of the following three articles which are published, submitted or will be submitted for publication as follows:

Paper I: Pages 7-42 have been published in Journal of Fluids Engineering ASME.

Paper II: Pages 43-74 have been submitted to International Journal of Multiphase Flow.

Paper III: Pages 75-93 are intended for submission to the journal of Atomization and Sprays.

ABSTRACT

The separation of shear-driven liquid films occurs in many engineering applications such as port fuel injected engines, demisters, and gas transfer lines. Despite the importance of this problem, the details of the interaction between operating parameters such as liquid flow rate, gas velocities and liquid film properties on the forces at the expanding corner are still not clear. To enhance the insight on the complicated interaction between the gas and liquid phases, the shear-driven liquid flow around a corner has been studied both experimentally and analytically in this work. The effect of the complex liquid film structure on liquid mass separation is significant. For some operating conditions the liquid film can be modeled as a smooth layer, which drives the liquid mass separation due to its inertia. However, for some other gas-liquid flow conditions, the formation of large amplitude waves at the interface also contributes to liquid mass separation at the corner. The focus of this study was to enhance the understanding of the effect of both mean film inertia and large amplitude waves on the mass separation mechanism. To develop a physical understanding of the effect of liquid film properties on both mean film inertia and large amplitude wave formation and growth, experimental studies on liquids with different viscosities and surface tensions have been performed in this work. It is shown that the interaction between the gas and liquid phase transfer controls the inertial force of the liquid film as well as wave propagation. Two distinct correlations based on this physical insight have been proposed for liquid mass separation based on dividing the shear-driven flow regimes into flow regimes without large amplitude waves and flow regimes with large amplitude waves.

ACKNOWLEDGMENTS

I would like to express my sincere gratitude to my advisor, Dr. James A. Drallmeier, for his invaluable guidance, support, caring and patience during my Ph.D. He served as an excellent role model and valuable source of advice, not only on the research, but also on all other aspects of life throughout my PhD study. I consider myself lucky and privileged for having the opportunity to be a part of his excellent research group. Additionally, I would like to extend my appreciation to my committee members, Drs. Kelly Homan, David Riggins, Joseph D. Smith, and Cheng Wang, for their time and guidance and kind support on my research.

A special thanks to my lovely family. Words cannot express how grateful I am to my father, mother, and my sisters, Somayeh and Maryam, for all the scarifies that they have made on my behalf. I am blessed beyond measure to have you all in my life.

Furthermore, I would also like to present my thankfulness to the good friends whose support drove me forward everyday: Dr. Hassan Golpour, Marcia Golmohammadi, Maryam Khanjani, Zahra Manzoor and Alireza Toghraee and fellow graduate students in my lab: Allen Ernst, Krishawn Ridenhour, Mahdi Ghareh Baygloo and Rachel Stiffler. We have worked together, lived together, and in the end we all learned from one another and made good friends.

I would like to dedicate this doctoral dissertation to my father, Gholamreza Sadeghizadeh, for his constant inspiration and unconditional love.

TABLE OF CONTENTS

Page

LIST OF ILLUSTRATIONS

Figure Page

PAPER I

PAPER III

LIST OF TABLES

SECTION

1. INTRODUCTION

Shear-driven liquid films that are driven by adjacent gas phase flow have applications in various engineering problems, such as the design of air-blast atomizers, fuel systems in internal combustion engines, transfer lines, demisters, and refrigerant flows. Despite the extensive application of shear-driven flows, there are limited studies in the literature which have considered the separation of shear-driven films from expanding corners. Development and validation of engineering models for predicting liquid mass separation at expanding corners requires comprehensive insight regarding the complicate interaction between the gas and liquid phases. The mass, moment and energy transfer between the gas and liquid film occur as liquid film is driven along the wall, which leads to formation of layers with different characteristics in the liquid film: uniform film layer, and the wavy layer at the interface including waves with different amplitudes, wavelengths, and frequencies. As a liquid film reaches a sharp corner the force imbalance between the forces that are exerted at the corner determines whether the liquid film remains attached or becomes separated completely or partially from the sharp corner. Formation of large amplitude waves (LAWs) at the interface, which have significant mass content is also correlated well to mass separation at the sharp corner.

The key to develop a practical prediction model for liquid mass separation is to determine the mechanisms that impact uniform and wavy layers prior to the corner. The lack of a practical, reliable, parametric model for predicting mass separation motivates the current work.

This work is divided into three papers. Paper I discusses the two coupled mechanisms that impact liquid mass separation at expanding corners: mean film inertia and large

amplitude waves (LAW) at the interface. The liquid mass separation was correlated to the operating flow conditions. Paper II investigates the effect of liquid film properties such as viscosity and surface tension on the mean film and LAWs at the interface, which consequently affect the liquid mass separation. To study the effect of film properties, an experimental liquid matrix was developed to isolate the viscosity and surface tension effects. Paper III is the major part of this work and includes the development of two distinct maps for predicting liquid mass separation at sharp corners.

1.1. LITERATURE REVIEW

Thin liquid films driven by gas shear stress have received significant attention during the past decades because of their application in engineering problems such as refrigerant systems in the chemical industry, fuel atomizers in gas turbines, fuel film transport in internal combustion engines and gas condensate lines. Despite the extensive research on the liquid atomizers and spray systems, the complicate interaction between gas and liquid in these systems demands comprehensive research on the characteristics of liquid sheets under the gas phase influence. The recent experimental and numerical studies reveal the significance of improving the efficiency of spray systems such as elliptical jets, transonic three-stream airblast injector, and splash plate nozzles. See for example Zhao *et al.* (2017), Strasser and Battaglia (2016), and Thunivumani and Gadgil (2018)

For these applications, after the liquid film forms on wall surfaces, it is driven by the shear force of the parallel gas flow along the wall. At the gas-liquid interface, the pressure fluctuations and shear stress generate instabilities on the liquid film surface due to gas phase turbulence. Recent studies show that the dynamic pressure ratio between the gas-liquid phase, thickness of the gas boundary layer as well as the velocity difference between the liquid and gas phase are relevant parameters that control the peak frequencies and the growth rates of the instabilities at the interface as shown by Fuster *et al.* (2013) and Matas (2015). Depending on gas-liquid flow rate conditions and substrate geometry, the liquid film may

be detached from the surface at a geometric singularity (e.g., corner), resulting in droplets in the gas field. This may be detrimental in some applications of chemical engineering, such as gas-liquid separators, transfer lines, and condensers, where the liquid and gas need to be maintained in separated phases. Hence, preventing liquid films from separating and consequent entrainment in the gas phase is a critical challenge in these applications. In other applications, liquid detachment from the surface is a desirable occurrence. For example, in pre-filming air-assisted atomizers, the liquid film undergoes a geometrical singularity to be detached from the wall and generate small atomized droplets.

Shear driven liquid films can be divided into two layers with different characteristics: liquid film substrate and wavy layer at the interface. The liquid film substrate is the uniform layer beneath the wavy layer that generally has small mean thickness and velocity compared to the wavy layer. The wavy layer is a complicated structure at the interface made of various waves with different wavelengths and frequencies. This layer includes ripple waves (also called capillary waves) which have small amplitude, small wavelength and high frequency alongside large amplitude waves (LAW) with large wavelength and low frequency. Depending on the gas-liquid flow rate conditions and liquid properties, the distribution of these two types of waves may change. The film mass separation models available in the open literature may be categorized into two different groups according to the liquid film model: Liquid film is modeled as a smooth layer with mean characteristics, and liquid film is modeled as series of disturbance waves.

In the first approach, the liquid film was simplified as a smooth layer. In an attempt to define and quantify controlling parameters for the liquid film passing over a corner, Owen and Ryley (1985) presented a theoretical analysis to model the radial stress distribution on the film at the corner. They assumed that the liquid has smooth interface, negligible viscosity dissipation, and linear liquid velocity profile. This model has been verified experimentally in their studies for thin film thickness less than 0.1 *mm*. O'rourke and Amsden (1996) proposed another model to predict liquid separation from the corner by calculating the balance

between the liquid film inertia and the pressure difference between gas and liquid phase at the point of liquid separation. However, this model was not verified with experimental studies. Friedrich *et al.* (2008) developed a model based on the momentum conservation on the liquid film control volume at the point of separation. This is the most practical model available in literature, which has been used by others to predict separation including Zhang *et al.* (2017) who modeled the separation of the liquid fuel film at expanding corners under different fuel film forming conditions. The Friedrich *et al.* (2008) model considers that the liquid film has a smooth interface and predicts the liquid mass separation for thin films in the range of $0.1\ mm < h_f < 0.5\ mm$. The advantage of this model is in its simplicity to predict the liquid mass separation based on mean properties of gas and liquid phase. The correlation provided in Friedrich *et al.* (2008) for different gas-liquid flow conditions suggests that the gas impacts the liquid mass separation criteria only through its effects on liquid film momentum. However, the uncertainty of this model to predict the onset of separation can be high. For example, experimental results showed liquid mass separation between $10-15\%$ for cases that the proposed model predicted zero liquid mass separation.

In the second approach, separation is presumed to be controlled by a series of LAWs. Bacharoudis *et al.* (2014) presented a film separation model where the film substrate is neglected and the liquid film is modeled as a series of disturbance waves with specific frequency and wavelength that negotiate the sharp corner. The force balance on the wave control volume determines if the wave either remains attached to the wall or becomes separated from liquid substrate at the sharp corner. Following Friedrich's approach, the force ratio model was defined on the wave control volume by considering the ratio of destabilizing forces to stabilizing forces for each single disturbance wave turning the corner. Experimental validation in this study indicated that the characteristics of disturbance waves are the most appropriate parameters to determine liquid mass separation quantity at the sharp corner. However, this approach is more difficult to apply compared to the model by Friedrich *et al.* (2008), which uses only mean values. Also, this model fails to explain the

separation of liquid films in cases where liquid is being separated from the sharp corner in the absence of disturbance waves. In sum, the above studies have considered separately the inertial force of the substrate as the effective mechanism on liquid mass separation, and specific disturbance waves that are influential on liquid mass separation criteria by affecting the local variation of inertia. It should be noted that regardless of LAW existence, in all cases inertia is the dominant destabilizing force, which needs to overcome the restoring forces such as surface tension and gravity. The liquid film substrate and LAWs have been considered separately to enable construction of predictive models for liquid mass separation. The limitations displayed by both approaches suggest both effects are important.

There are limited studies available that consider a range of liquid properties on LAW formation and film inertia in shear-driven flows. At a fixed gas-liquid flow rate, the liquid film properties such as viscosity and surface tension influence the film characteristics in terms of mean film thickness, film width, and interface instabilities. Wegener (2009) studied the effect of surface tension and viscosity on liquid film characteristics, using the laser focused displacement(LFD) method to measure mean film thickness and an estimate of film velocity. For all flow conditions in this study an increase in viscosity resulted in formation of thicker mean film thickness and a decreases in mean film velocity. Also, the experimental results showed that surface tension influenced the mean film thickness and mean film velocity indirectly through variation in film width. Increases in surface tension resulted in smaller film width, which led to thicker mean film thickness and higher mean film velocity. Hoogendoorn (1959) used water and oil as working fluids to study the effect of viscosity and surface tension on film in a stratified flow regime. This flow regime occurs where both phases are separated from one another with a definite interface and usually takes place at low gas velocity in pipes. The observations in this study showed that the transition to stratified flow occurred at higher gas velocity for air-oil mixture compared to the air-water mixture due to surface tension reduction. Moreover, Andreussi *et al.* (1985) studies showed that the liquid viscosity affected the transition between flow regimes in

two-phase flow. Weisman *et al.* (1979) prepared a liquid matrix in order to change one liquid properties while the other properties remained approximately constant. This study showed that the transition from smooth stratified flow to wavy stratified regime occurred at higher gas velocity as surface tension decreased. It should be mentioned that the wavy flow regime in all these studies includes both ripple waves and large amplitude waves (LAWs) at the interface. Furthermore, based on observations by Thwaites *et al.* (1976), reducing the liquid surface tension by adding a surfactant led to more damping of ripple waves and reduction in LAWs frequency at the interface. The limited range of operating conditions studied in the literature along with the assumptions that consider the liquid film either as a smooth surface or a wavy structure are barriers for drawing a general conclusion on the effect of liquid film properties on mean film characteristics, instabilities at the interface and subsequent liquid mass separation. This literature clearly shows liquid film properties impact film characteristics and instabilities at the interface, which are important parameters for prediction of liquid mass separation at expanding corners. Despite the importance of liquid film properties on liquid mass separation, this problem has not studied extensively in literature.

The complexity of liquid mass separation from expanding corners demands deep insight into the important physical aspects of the problem in order to establish a comprehensive model for predicting the liquid mass separation. The available models in open literature (Friedrich *et al.* (2008), Bacharoudis *et al.* (2014), Wang *et al.* (2004), O'rourke and Amsden (1996), Owen and Ryley (1985), and Steinhaus *et al.* (2007)) do not capture the complete physics of the film separation in a shear-driven flow problems. In this work empirical liquid mass separation maps are generated based on nondimensional operating conditions, liquid film properties, and the corner geometry to help in refining existing models.

PAPER

I. EFFECT OF LARGE AMPLITUDE WAVES AND FILM INERTIA ON MASS SEPARATION AT A SHARP CORNER

Z. Sadeghizadeh, James A. Drallmeier

Department of Mechanical & Aerospace Engineering

Missouri University of Science and Technology

Rolla, Missouri 65409–0050

Tel: 573–341–6622, Fax: 573–341–4115

Email: zsp7c@mst.edu

ABSTRACT

The separation of a shear-driven thin liquid film from a sharp corner is studied in this paper. Partial or complete mass separation at a sharp corner is affected by two different mechanisms: liquid film inertia, which affects liquid mass separation through force imbalance at the sharp corner, and large amplitude waves at the interface, which contributes to liquid instability at the corner. Experimental results for *Re* number varies from 100 to 300 and mean film thickness from 130 to 290 micron show that both film inertia and large amplitude wave effects correlate to mass separation results. The results suggest that while both inertia of the film substrate and large amplitude wave effects enhance the mass separation, the correlations between large amplitude wave characteristics and mass separation results provide better insight into the onset of separation and the impact of the gas phase velocity on separation for the conditions studied.

Keywords: shear driven liquid film, film inertia, Large Amplitude Waves

1. INTRODUCTION

Thin liquid films driven by gas shear stress have received significant attention during the past decades because of their application in engineering problems such as refrigerant systems in the chemical industry, fuel atomizers in gas turbines, fuel film transport in internal combustion engines and gas condensate lines. Despite the extensive research on the liquid atomizers and spray systems, the complicate interaction between gas and liquid in these systems demands comprehensive research on the characteristics of liquid sheets under the gas phase influence. The recent experimental and numerical studies reveal the significance of improving the efficiency of spray systems such as elliptical jets, transonic three-stream airblast injector, and splash plate nozzles.Zhao *et al.* (2017)Strasser and Battaglia (2016)Thunivumani and Gadgil (2018)

For these applications, after the liquid film forms on wall surfaces, it is driven by the shear force of the parallel gas flow along the wall. At the gas-liquid interface, the pressure fluctuations and shear stress generate instabilities on the liquid film surface due to gas phase turbulence. Recent studies show that the dynamic pressure ratio between the gas-liquid phase, thickness of the gas boundary layer as well as the velocity difference between the liquid and gas phase are relevant parameters that control the peak frequencies and the growth rates of the instabilities at the interface. Fuster *et al.* (2013)Matas (2015) Depending on gas-liquid flow rate conditions and substrate geometry, the liquid film may be detached from the surface at a geometric singularity (e.g., corner), resulting in droplets in the gas field. This may be detrimental in some applications of chemical engineering, such as gas-liquid separators, transfer lines, and condensers, where the liquid and gas need to be maintained in separated phases. Hence, preventing liquid films from separating and consequent entrainment in the gas phase is a critical challenge in these applications. In other applications, liquid detachment from the surface is a desirable occurrence. For example, in pre-filming air-assisted atomizers, the liquid film undergoes a geometrical singularity to be detached from the wall and generate small atomized droplets.

Shear driven liquid films can be divided into two layers with different characteristics: liquid film substrate and wavy layer at the interface. The liquid film substrate is the uniform layer beneath the wavy layer that generally has small mean thickness and velocity compared to the wavy layer. The wavy layer is a complicated structure at the interface made of various waves with different wavelengths and frequencies. This layer includes ripple waves (also called capillary waves) which have small amplitude, small wavelength and high frequency alongside large amplitude waves (LAW) with large wavelength and low frequency. Depending on the gas-liquid flow rate conditions and liquid properties, the distribution of these two types of waves may change. The film mass separation models available in the open literature may be categorized into two different groups according to the liquid film model: Liquid film is modeled as a smooth layer with mean characteristics, and liquid film is modeled as series of disturbance waves.

In the first approach, the liquid film was simplified as a smooth layer. In an attempt to define and quantify controlling parameters for the liquid film passing over a corner, Owen and Ryley (1985) presented a theoretical analysis to model the radial stress distribution on the film at the corner. They assumed that the liquid has smooth interface, negligible viscosity dissipation, and linear liquid velocity profile. This model has been verified experimentally in their studies for thin film thickness less than 0.1 *mm*. O'rourke and Amsden (1996) proposed another model to predict liquid separation from the corner by calculating the balance between the liquid film inertia and the pressure difference between gas and liquid phase at the point of liquid separation. However, this model was not verified with experimental studies. Friedrich *et al.* (2008) developed a model based on the momentum conservation on the liquid film control volume at the point of separation. This is the most practical model available in literature, which has been used by others to predict separation including Zhang *et al.* (2017) who modeled the separation of the liquid fuel film at expanding corners under different fuel film forming conditions. The Friedrich *et al.* (2008) model considers that the liquid film has a smooth interface and predicts the liquid

mass separation for thin films in the range of 0.1 $mm < h_f <$0.5 mm. The advantage of this model is in its simplicity to predict the liquid mass separation based on mean properties of gas and liquid phase. The correlation provided in Friedrich *et al.* (2008) for different gas-liquid flow conditions suggests that the gas impacts the liquid mass separation criteria only through its effects on liquid film momentum. However, the uncertainty of this model to predict the onset of separation can be high. For example, experimental results showed liquid mass separation between $10 - 15\%$ for cases that the proposed model predicted zero liquid mass separation.

In the second approach, separation is presumed to be controlled by a series of LAWs. Bacharoudis *et al.* (2014) presented a film separation model where the film substrate is neglected and the liquid film is modeled as a series of disturbance waves with specific frequency and wavelength that negotiate the sharp corner. The force balance on the wave control volume determines if the wave either remains attached to the wall or becomes separated from liquid substrate at the sharp corner. Following Friedrich's approach Friedrich *et al.* (2008), the force ratio model was defined on the wave control volume by considering the ratio of destabilizing forces to stabilizing forces for each single disturbance wave turning the corner. Experimental validation in this study indicated that the characteristics of disturbance waves are the most appropriate parameters to determine liquid mass separation quantity at the sharp corner. However, this approach is more difficult to apply compared to the model by Friedrich *et al.* (2008), which uses only mean values. Also, this model fails to explain the separation of liquid films in cases where liquid is being separated from the sharp corner in the absence of disturbance waves. In sum, the above studies have considered separately the inertial force of the substrate as the effective mechanism on liquid mass separation, and specific disturbance waves that are influential on liquid mass separation criteria by affecting the local variation of inertia. It should be noted that regardless of LAW existence, in all cases inertia is the dominant destabilizing force, which needs to overcome the restoring forces such as surface tension and gravity. The liquid film substrate and LAWs have been

considered separately to enable construction of predictive models for liquid mass separation. The limitations displayed by both approaches suggest both effects are important.

The purpose of this paper is to study the effect of both liquid substrate inertia and LAWs on liquid mass separation. To calculate the liquid substrate inertial force, a numerical model was used to find the liquid film mean velocity and thickness. To quantify the LAWs at the liquid interface, a threshold value for interface height was defined for the liquid film's high-speed images to distinguish LAWs from ripple waves at the interface. Results are then investigated under varying flow conditions to differentiate the effect of both phenomena.

2. EXPERIMENTAL SETUP

The experimental unit was designed to study the characteristics of a shear-driven liquid film and separation phenomena that occur at the sharp corner. The apparatus shown in Fig.1 represents a rectangular flow duct consisting of four sections. Air is pulled from the ambient air through the test section by a liquid ring vacuum pump. Volume flow rate of air through the duct was determined using a laminar flow element (LFE), which correlates the pressure drop through the LFE with the volumetric gas flow rate from which the mean gas velocity was calculated for a known cross-sectional area. By adjusting the manual control valve on the suction pump, the average gas velocity varies from 10 to 40 m/s.

The first section of the test unit is the air entrance region, which has a length of 1.43 m and provides a fully developed turbulent flow at the point of liquid film introduction in the second section. The cross section before the sharp corner is a rectangle with a height of 2 cm and a width of 10 cm, giving the aspect ratio of 5. Neglecting the limited wall effects, simulations indicate that for this aspect ratio, the entrance length of 1.43 m should provide a 2D flow at the center 7.5 cm of the test section. Consequently, the film is introduced over the center 7.62 cm width of the test section. The liquid film is introduced through a porous brass medium at the bottom wall at the film introduction point in the test section. Liquid volume flow rate is regulated by using a valve and rotameter with an uncertainty of 2.5%. A

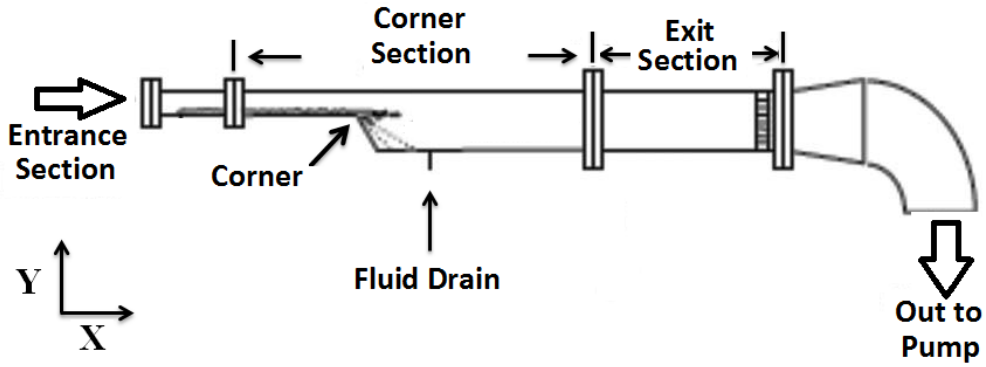

Figure 1. Schematic of experimental unit

liquid filter has been applied before the brass medium to filter any contamination in liquids larger than 8 micron. The third section is the test section with a sharp corner, which is 23 cm downstream of the liquid film introduction point and has an angle of 60° to the horizontal. In order to measure film width nearest to the corner, a transparent window is located on the top wall such that optical access is provided 4 cm upstream and 4 cm downstream from the corner. The detailed schematics of the test section and the actual test section are shown in Fig. 2 and Fig. 3, respectively. The two brass porous segments shown in Fig. 2 were implemented on the inclined wall and lower wall after the sharp corner to collect liquid from the test section. Each brass porous segment is connected to a separate suction pump to collect the attached and detached liquids after the sharp corner without interrupting the separation mechanism. High speed images, which will be discussed in next section, are captured using the high speed side camera that is shown in Fig. 2. After the corner, the duct has an aspect ratio of 1.429 for the remainder of experimental unit. Section four is the gas exit section, which is connected to the LFE. Great care was taken to ensure that the test section is horizontal and the film is uniformly developed across the test section width. To this aim, the facility is mounted on an optic table, which offers a dynamic method for 3D alignment of the whole unit.

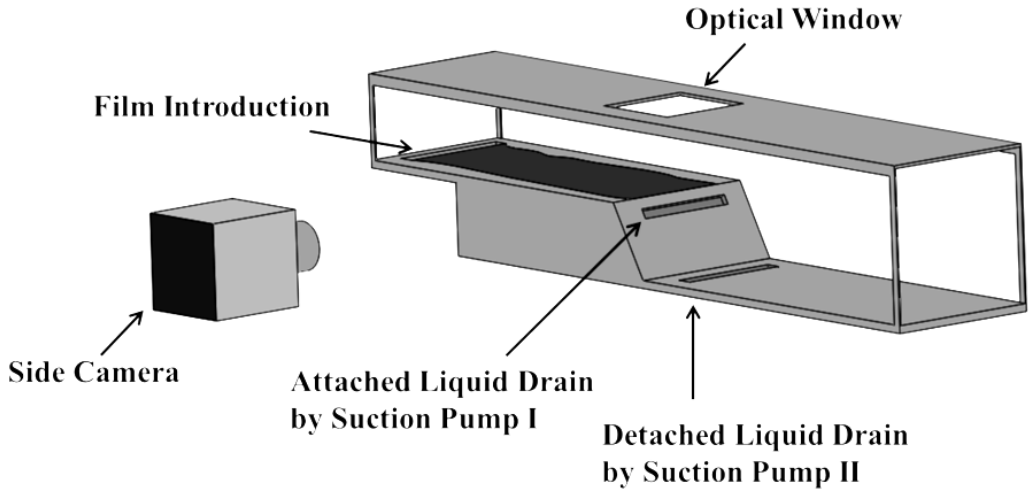

Figure 2. Schematic of test section

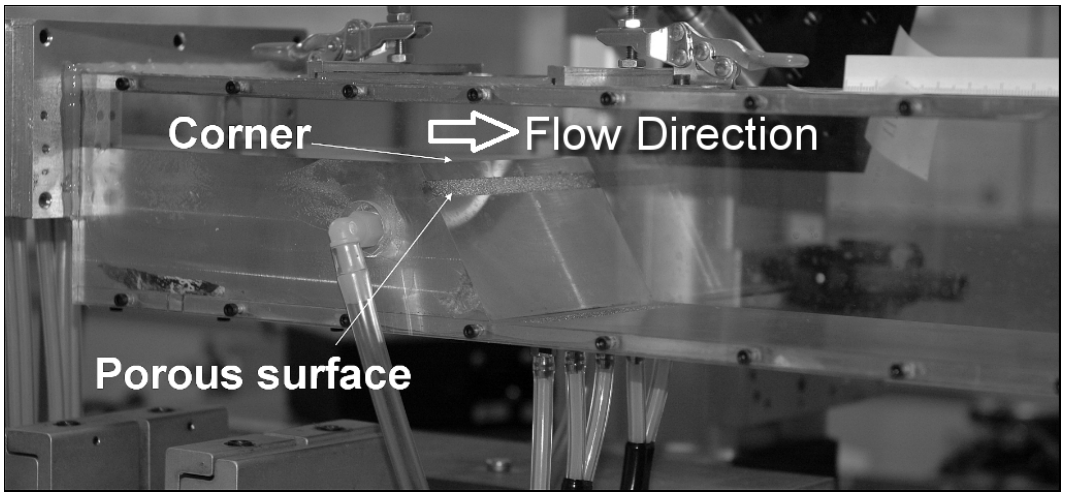

Figure 3. Porous surface and corner of experimental test section

To perform the experiment, vinegar was chosen as the working liquid. To prevent ridges at the edges of shear-driven film due to contact angle effects, it is essential to choose a liquid with a surface tension lower than water. Therefore, instead of using water that has large surface tension $\sigma = 0.072\ N/m$, vinegar (5% acetic acid, CH3COOH, by volume) was chosen as the working fluid for this study, which has $\rho = 1010\ kg/m^3$, $\sigma = 0.058\ N/m$, and $\nu = 1.2\ cP$.

Gas phase velocity varied from 25 m/s to 40 m/s. Liquid Re number ranged between 100 to 300 based on volumetric flow rate and measured liquid width, $Re = \frac{\dot{Q}_f}{W_f \nu}$. To have the Re number in this range, the liquid volumetric flow rate varied from $\dot{Q}_f = 400\ \frac{cm^3}{min}$ to $1000\ \frac{cm^3}{min}$. Gas-liquid flow parameters in this study are presented in a dimensional space to facilitate the interpretation of the results, where liquid volume low rate, gas velocity, and liquid type are directly controlled parameters in this shear-driven film separation problem. Similarly, film thickness and width are reported separately, as opposed to through the liquid Re, to facilitate comparisons to wave dimensions.

The full run duration for each gas-liquid flow condition was 5 minutes. Experimental observation showed that the film characteristics were stable after 2 minutes. The high-speed images were taken after 4 minutes of continual running. Liquid mass separation measurements were done for 120 seconds after stable operation for each gas-liquid flow condition and each test was replicated three times to determine the uncertainty in measurements.

3. HIGH SPEED IMAGE PROCESSING

High speed image processing has been performed to provide liquid film characteristics at specific gas-liquid flow rate conditions. A high speed camera (Photron 1280 PCI) with close-up lenses totaling +7 diopter was implemented in this experiment. The camera captures 2000 frames per seconds at a resolution of 640 X 128. The magnification is 7 and spatial resolution is approximately 55 microns. During high speed image processing, the image is inverted into binary data based on pixel brightness. A threshold value is defined to

Figure 4. Grayscale and corresponding binary high speed images of gas-liquid interface

divide all pixel brightness into two different categories. Pixels with brightness higher than the threshold are converted to saturated white color that corresponds to a brightness of 255, while pixels with lower brightness than the threshold value are assigned with 0 brightness, which is saturated black color. The threshold value in this experiment was adjusted over a wide range, and a value of 170 has been selected to generate binary images. For example, an initial high speed image and its corresponding binary image are shown in Fig. 4.

Since the camera is capturing frames from the side view, the line-of-sight integration effect of wave shapes and amplitudes on the resultant interface profile adds uncertainty to the image processing. Because the camera is capturing images from the side view, all waves along the film span at each axial location are mapped into one plane. Therefore, the shape and height of the interface is determined by the largest wave along the span at each axial location. The line-of-sight effect is represented in Fig. 5. This figure shows how the line-of sight effect defines the observed interface profile. The interface at each time is defined based on the highest disturbance in spanwise direction. The black circles in Fig. 5 represents the interface profile of the liquid film, which is equivalent to the output images from the high speed camera.

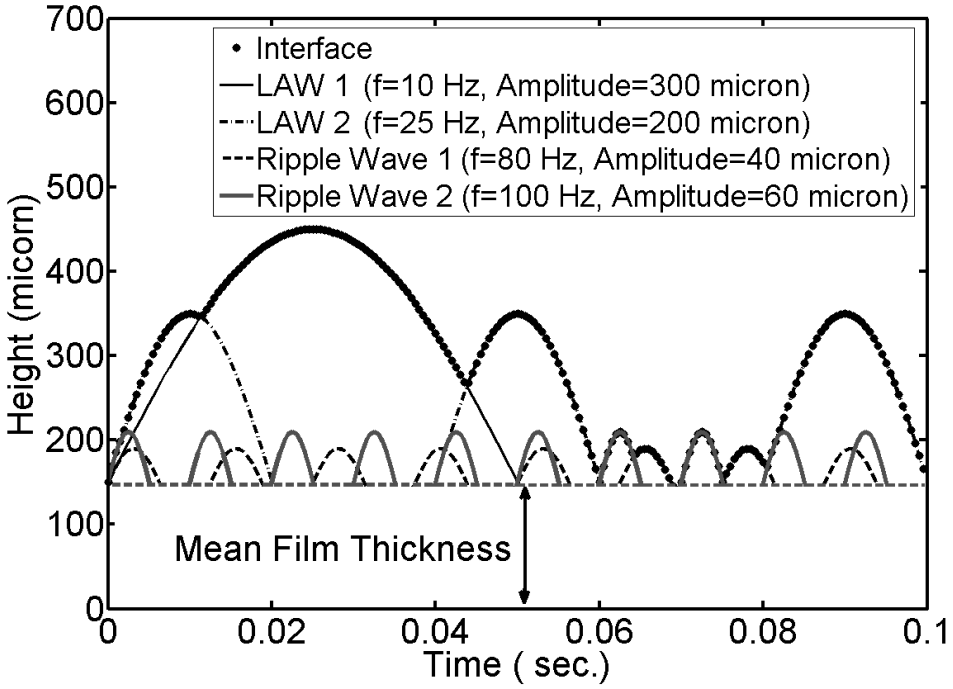

Figure 5. Line-of-sight effect on interface

One aim of this study is to understand the role of LAWs on the liquid separation event. Hence, it is important to be able to capture the chief characteristics of these waves from the imaging. To this end, a numerical simulation has been designed to confirm that LAW characteristics can be extracted from the line-of-sight imaging. This numerical simulation supports the FFT analysis in this paper to demonstrate LAW characteristics can be discovered despite of the existence of the line-of-sight effect. Hence, a randomized combination of LAW and ripple waves with specific known height and frequency range has been considered for an arbitrary time interval to create a simulated interface.

3.1. Interface Numerical Simulation. To simulate LAW and ripple waves at the interface, two distinct ranges for frequencies and amplitudes have been chosen for each wave group. As shown by Bruno and McCready (1988), ripple wave frequencies are approximately one order of magnitude larger than LAW frequencies. In their analysis, ripple waves were the precursor of LAW formation at the interface. This leads to this

Table 1. Wave components of numerical interface signal for hypothetical film thickness of h_f = 150 micron

Wave Type	Ripple Wave	LAW
Wave Amplitude Range(Micron)	30-100	255-500
Wave Frequency(Hz)	50-1000	30-50
Number of Waves	500	5

conclusion that ripple waves are the dominant wave type at the interface. Moreover, Craik (1966) and Hanratty (1983) show that ripple waves have wavelengths and amplitudes much shorter than the film thickness, contrary to LAWs, which have large wavelengths and amplitudes compared to the film thickness. Similarly, Nakamura (1996), Zadrazil *et al.* (2014), and Zhao *et al.* (2013) suggest LAWs have an amplitude of 1.5 to 1.7 times of the liquid film substrate thickness. Hence for this study, LAW heights are considered to be 1.7 of liquid film substrate thickness.

The insight from these studies is used to define the wave components of the interface for this simulation. A hypothetical case where the film substrate thickness is 150 microns was considered for this simulation. Using the assumptions in Bruno and McCready (1988), the LAW frequency range is considered to be from 30 Hz to 50 Hz, while ripple wave frequencies are assumed to be from 50 Hz to 1000 Hz. The upper limit for ripple waves frequency range is determined to be compatible with the high speed camera sample rate of 2000 fps used in this experiment. The ripple wave height range is from 30 micron to 100 micron, which is lower than the substrate thickness. For LAWs, the height range is from 255 micron to 500 micron, which satisfies the $h_{LAW} > 1.7h_{sub}$ condition. It is assumed that the number of LAWs are much smaller than ripple waves on the interface. The detailed information of the wave components is shown in Table 2.

The signal of the liquid film interface from this simulation and the corresponding FFT analysis are plotted in Fig. 6 (a)-(c). The FFT analysis of the individual waves is

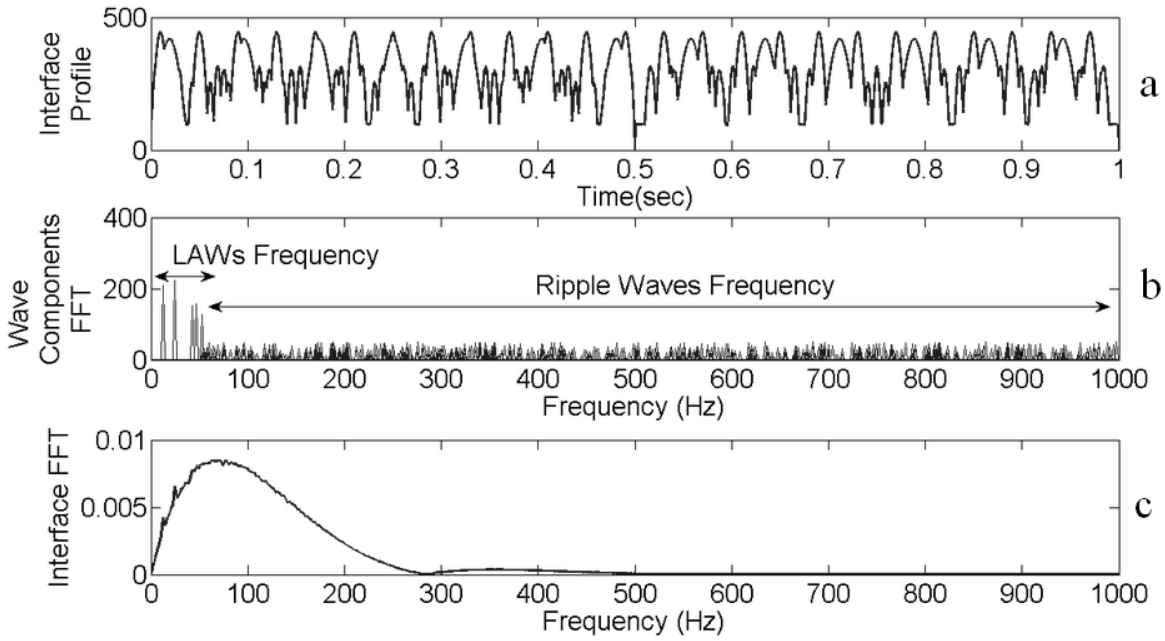

Figure 6. Numerical simulation of interface based on line-of-sight effect

shown in Fig. 6(b). Two distinct regions can be seen on this graph. The LAW region is on the left side from 30 Hz to 50 Hz, while the ripple wave region has a wide range from 50 Hz to 1000 Hz on the right. The FFT of the resultant film interface is shown in Fig. 6(c). The peak of the FFT plot for the interface signal in Fig. 6(c) is near the LAW region. This means in presence of the line-of-sight effect, the frequency characteristics of the interface signal is dominated by the LAWs. This is consistent with the idea that at each axial location, the highest wave forms the interface, and hence it is more probable to lose the frequency information of the small ripple waves. Thus, FFT analysis shows that for a combination of 5 random LAWs and 500 ripple waves, the peak of the FFT plot is nearest the LAW frequency range, and the line-of-sight effect is dominated by the information about LAWs.

The characteristics of the FFT of the simulated line-of-sight interface was explored more in depth. For instance, the LAWs frequency range was varied from 1 Hz to 120 Hz, while a constant ripple wave range was chosen from 200 Hz to 1000 Hz. All other parameters such as number of LAW waves, ripple waves, and their amplitude range remained constant

Table 2. Wave components of numerical interface signal used for FFT peak frequency correlation analysis for hypothetical film thickness of h_f = 150 micron

Wave Type	Ripple Wave	LAW
Wave Amplitude Range(Micron)	30-100	255-500
Wave Frequency Range(Hz)	200-1000	1-120
Number of Waves	500	5

in this case study. The properties of wave component for this numerical case study shown in Table 2. By perturbing the characteristics of the LAW waves, the numerical results in Fig. 7 show a strong linear correlation between the FFT peak frequency and the frequency of largest LAW components that creates the interface profile. These results suggest that the peak frequency of the FFT of the interface correlates well to the frequency of largest LAW component of the interface for waves typical in this experiment.

Furthermore, Fig. 8 depicts the results of another case study that shows a correlation between height of largest LAW component and peak of FFT of the interface. The detailed information of wave components can be found in Table 3. In this numerical analysis, all wave component properties remained constant except the range of LAW amplitudes, which varies from 400 to 1500 micron. As LAW amplitude goes up, the maximum magnitude of the FFT increases. The results of the simulated wave interface suggest the FFT of the interface, while measured across the line-of-sight, provides some insight into the nature of the LAWs on the surface.

The FFT of experimental data is shown in Fig. 9 for vinegar at $U_g = 30\ m/s$ and $\dot{Q}_f = 600\ \frac{cm^3}{min}$, which looks similar to the numerical FFT plot discussed previously in Fig. 6(c). The noted location for each curve on this plot is the location of the measuring point upstream of the corner. Here, the dominant peak of frequency, which provides an indicator of the LAW component frequency at the interface, is around 50 Hz. For the different noted locations, the peak frequency and peak magnitude of FFT of the interface are the

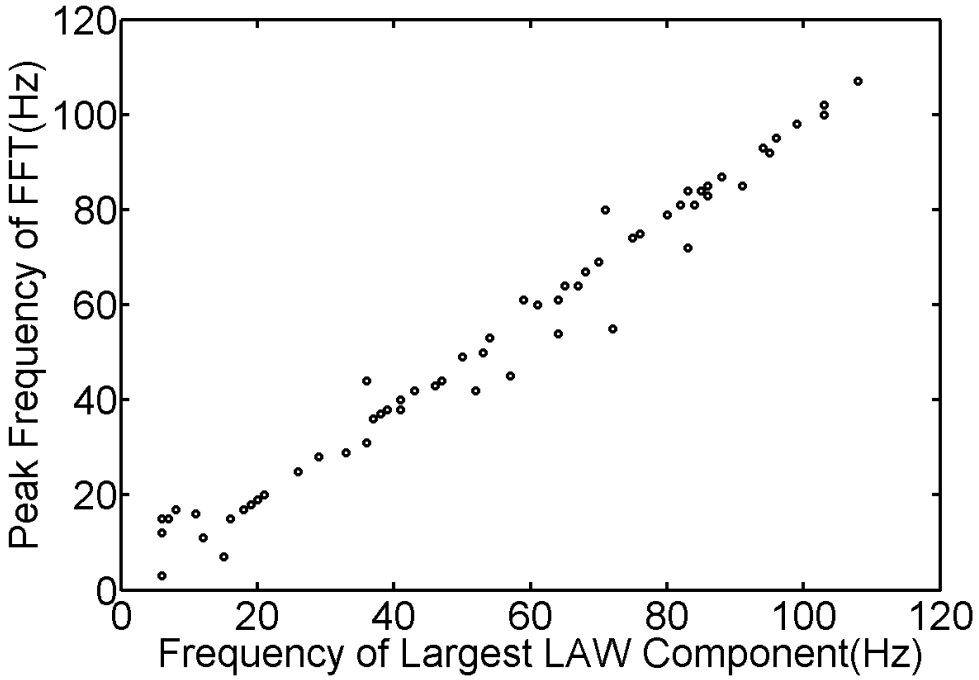

Figure 7. Correlation between frequency of interface LAW components and peak frequency of interface FFT

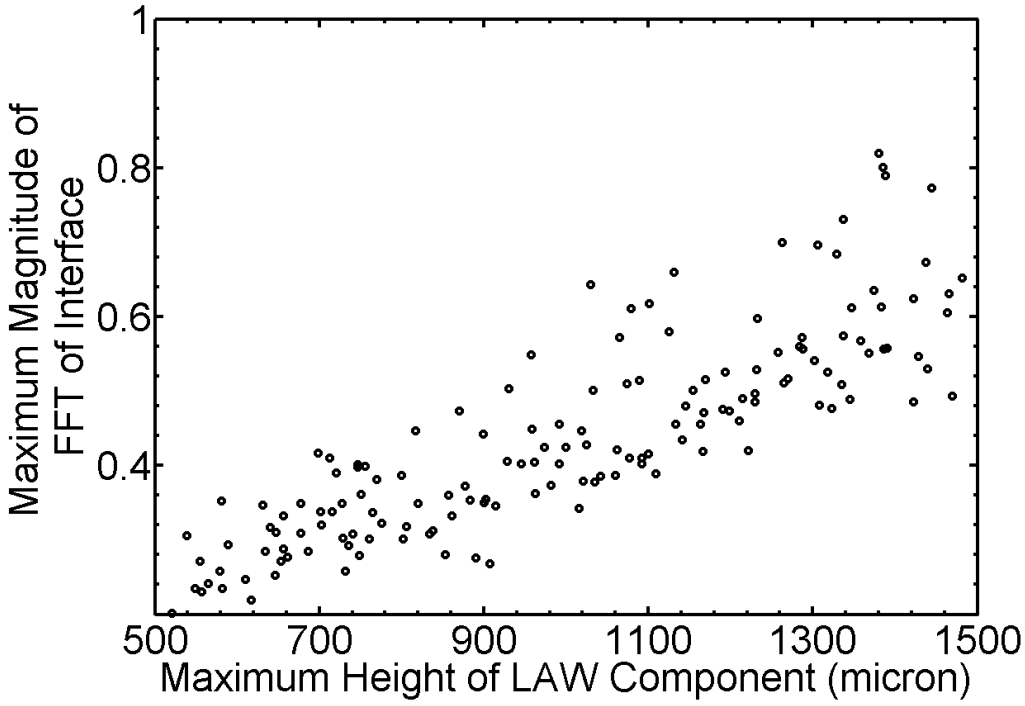

Figure 8. Correlation between amplitude of interface largest LAW components and peak of interface FFT

Table 3. Wave components of numerical interface signal used for FFT peak value correlation analysis for hypothetical film thickness of h_f = 150 micron

Wave Type	Ripple Wave	LAW
Wave Amplitude Range(micron)	30-100	400-1500
Wave Frequency Range(Hz)	200-1000	1-120
Number of Waves	500	5

same, which implies that the dominant LAW frequency and amplitude at the interface are independent of axial location along the wall over the considered range. This observation suggests that the flow regime is well established along the wall.

The FFT results for different liquid flow rates in Fig. 10 at constant gas velocity $U_g = 35\ m/s$ show that as the liquid flow rate increases at the constant gas velocity, the peak magnitude of the FFT goes up. Given the results of the simulated interface study, this implies a higher wave height at the film interface. However, for the lowest liquid flow rate of $\dot{Q}_f = 400\ \frac{cm^3}{min}$ the distribution of frequencies is spread across a large frequency range and no longer dominated by a peak at low frequencies, compared to the higher liquid flow rates. Based on experimental observation, there are no LAWs at this liquid flow rate, so the broader frequency range is related to small ripple waves at the interface, which have higher frequencies but smaller amplitudes compared to the characteristics of LAWs for other liquid flow rates.

4. RESULTS

Shear-driven liquid films are a combination of two layers with different characteristics: the liquid film substrate, which can be defined with mean properties, and the wave layer, which is a combination of ripple waves and LAWs at the interface. Both the substrate

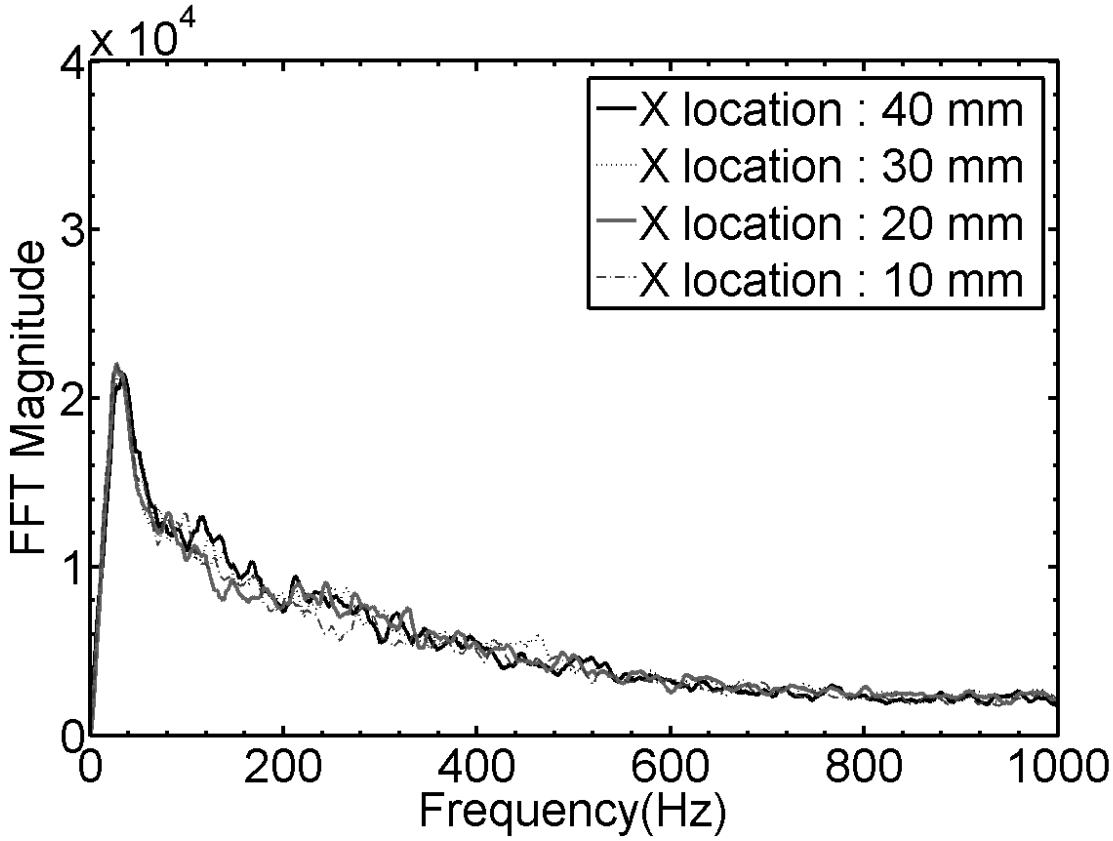

Figure 9. FFT analysis of vinegar at $U_g = 30\ m/s$ and $\dot{Q}_f = 600\ \frac{cm^3}{min}$ at different distances upstream from the corner

and wave layers contribute to liquid mass separation due to inertial and instability effects. Each of these effects will be discussed in this section separately, and then the experimental results will be presented to show how these two effects influence liquid mass separation.

4.1. Inertial Force. Uniform film inertia impacts liquid mass separation by affecting the balance of forces at the corner. Friedrich *et al.* (2008) have considered a 2D control volume that includes the liquid substrate at the corner, and linear momentum conservation is written for this control volume. Using this approach, Friedrich et al. have proposed an analytical force ratio (FR) relation, shown in Equation 1, to predict the liquid mass separation due to the inertial effect at the corner. A schematic of the liquid film at the point of separation is shown in Fig. 5. In this equation, θ is the corner angle and L_b is the charac-

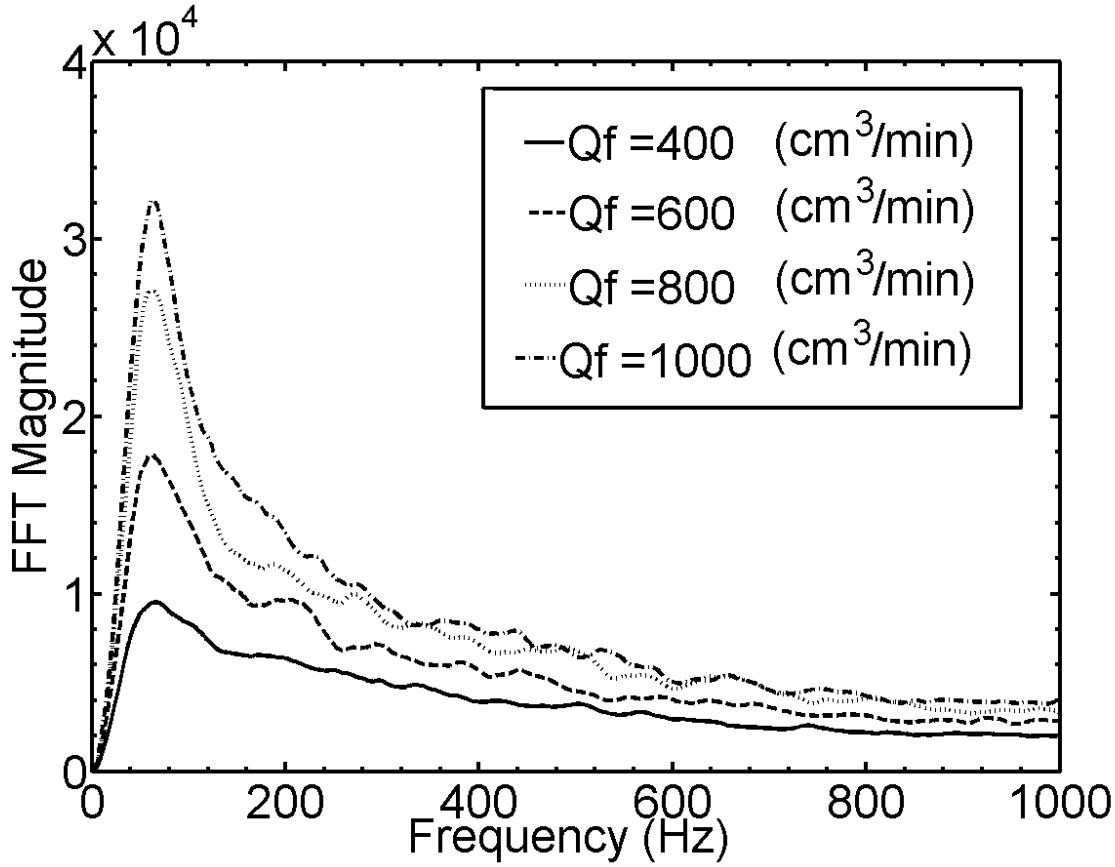

Figure 10. FFT analysis of vinegar for different liquid volume flow rates at $U_g = 35\ m/s$ and 30 *mm* upstream the corner

teristic breakup length. The effect of uniform film inertia is to drive the film to separate from the corner, while surface tension and gravitational forces tend to maintain the liquid film attached to the wall. A force ratio equal to one is defined as the critical value representing equal separating and restoring forces. For FR less than one, the restoring forces are larger than inertia. Therefore, the liquid film should remain attached to the corner. However, for FR larger than one, the destabilizing inertia overcomes the restoring forces at the corner, which leads to liquid mass separation. Specifically, the FR is defined as

$$FR = \frac{\rho_f U_f^2 h_f sin(\theta)}{\sigma sin(\theta) + \sigma + \rho_f g h_f L_b cos(\theta)} \tag{1}$$

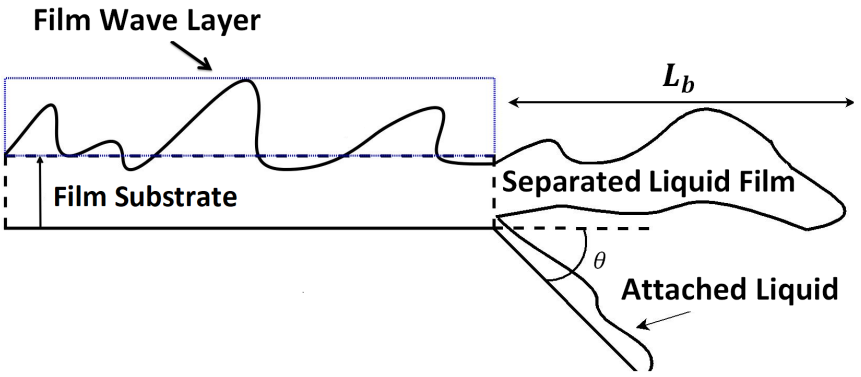

Figure 11. Liquid film at the point of separation

where L_b is the breakup length which is estimated from the experimental correlation presented by Arai and Hashimoto (1985),

$$L_b = 0.0388 h_f^{0.5} Re_f^{0.6} We_{rel}^{-0.5}. \tag{2}$$

This scale estimates the continuous ligament at the point of separation before its breakup into small droplets. The separation process at the corner does not occur in one step. First, liquid film diverges from the corner geometry due to inertial effect while it is still attached to the corner (primary separation), which results in formation of a ligament with a dimension of the breakup length and then it becomes detached from the corner and forms discrete ligaments and droplets (secondary separation). The L_b is an important spatial scale that determines the spatial extent of the primary separation region.

Here, the liquid Reynolds number Re_f is

$$Re_f = \frac{h_f U_f \rho_f}{\mu_f} \tag{3}$$

and the Weber number is defined based on relative velocity between the gas and liquid film:

$$We_f = \frac{h_f \rho (U_g - U_f)^2}{2\sigma}. \tag{4}$$

Comparing the stabilizing surface tension and gravity terms in the denominator, it can be assumed that the gravitational force is negligible with respect to the surface tension term if we have a relatively large turning angle at the corner and a thin film. Therefore, for constant liquid properties, changes in the FR are primarily due to changes in the inertial term.

To calculate the FR term, it is necessary to find the mean film thickness and velocity. Since the line-of-sight effect imposes a bias on the film thickness measurements from side imaging, film thickness is approximated by using the numerical two-phase model presented by Wang *et al.* (2004). This is a model for calculating gas-liquid flow fields in shear-driven flow, which is built from the work of Wittig *et al.* (1991) has been validated in shear-driven film flows.

This 2D numerical model predicts the turbulent air flow field and average shear-driven liquid film characteristics, considering the strong interrelated coupling of both phases. The gas phase flow field characteristics were modeled using finite volume code with k-ϵ turbulence modeling. Due to the waviness of liquid film on the wall, a special wall function was used by Wittig *et al.* (1991) to couple the two phases. It was assumed that the gas-liquid film interface is a very slow-moving rough wall that can be expressed by an equivalent sand grain roughness. Moreover, the liquid film propagation was predicted based on a boundary layer description, which was formulated in a time-averaged manner. Assuming a laminar velocity profile for the liquid phase, the conservation of mass and momentum equations were computed to determine the film velocity and thickness. The details of this rough wall model can be found in Wang *et al.* (2004).

The film thickness results from this rough wall model are plotted with results from a Volume of Fluid simulation and experimental measurements of film thickness by Wegener (2009) using the laser focus displacement (LFD) method in Fig. 12. FLUENT software was also utilized to build the 2D VOF model. The liquid volume fraction determines the location of the interface, which was needed for film thickness calculations. A low-Reynolds

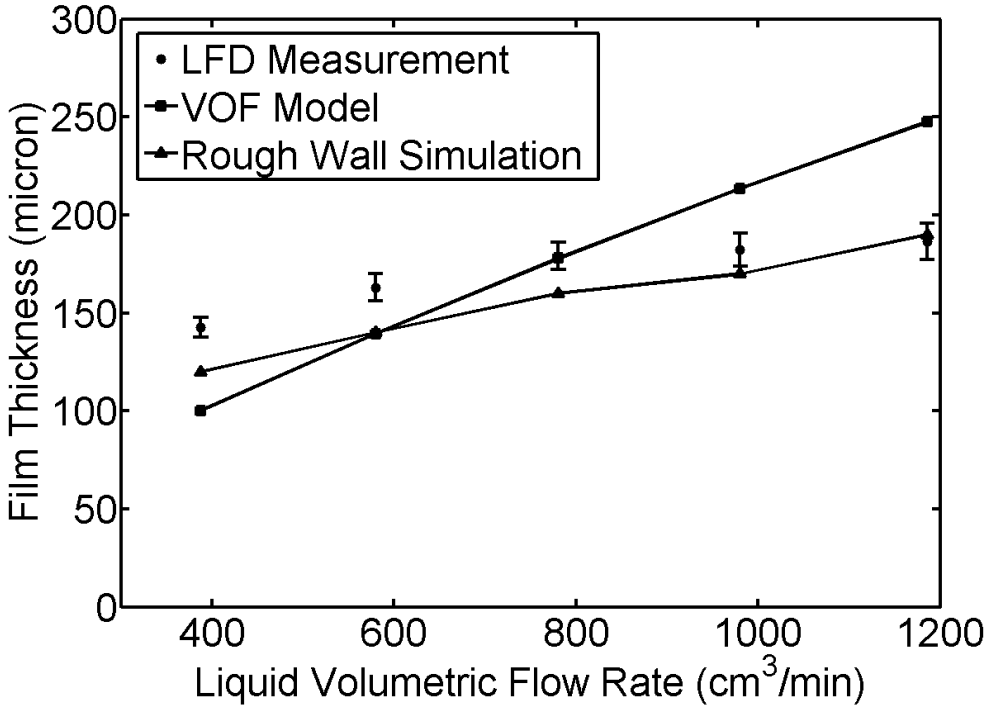

Figure 12. Average film thickness as calculated by Rough Wall Model plotted with the Volume Of Fluid Model and LFD experimental results

k-ϵ turbulent model was used to simulate the gas phase and the SIMPLE algorithm was applied to deal with the coupling between flow field and pressure field. The gas velocity in Fig. 12 is for $U_g = 30m/s$, and the vinegar liquid volume flow rate $\dot{Q}_f$ varying from 400 $\frac{cm^3}{min}$ to 1200 $\frac{cm^3}{min}$. These measurements were made in the flow apparatus described for this work. Comparing the different methods reveals that the film thickness calculations from the rough wall model have approximately 20% difference with LFD measurements, and have better agreement with the experiments than the VOF model. Consequently, the rough wall model was deemed acceptable for the analysis considered here.

Therefore, for a known liquid volume flow rate, the liquid film mean velocity can be calculated by having the film thickness from the rough wall model and film width measurement from the experiment. The film width is measured during the experiment through the optical window on the top wall of the test section.

The FR as a function of the liquid volume flow rate is depicted for vinegar at different gas velocities in Fig. 13. The error bars represent the uncertainty in the measurements, which were calculated by three replications for each operating condition. The FR (representative of the inertial force) increases as liquid volume flow rate increases. Moreover, for constant liquid flow rate, the inertial force is approximately independent of gas velocity except at the highest liquid flow rate observed. For fixed fluid properties, the coupling between the gas and liquid affects the FR term through the change in the mean velocity of the liquid film. Hence, only for the higher liquid flow rate, and thus the thicker film, does the increased gas velocity result in a substantially higher FR. However, this coupling effect at the film interface also leads to the formation of different wave regimes at the interface. This will be discussed in more detail in the next section.

Another important observation is that for all gas velocities and liquid flow rates smaller than $\dot{Q}_f = 800\ \frac{cm^3}{min}$, the FR is less than one. The FR approach is expected to have negligible liquid mass separation for these gas-liquid flow rate combinations. The percent of liquid mass separated at the corner is shown in Fig. 21, where the error bars represent the uncertainty in the mass separation measurements. First, it is important to note that the trends are in good agreement with the FR model presented in Fig. 13. However, the effect of gas velocity on separation appears to be more dramatic than what is presented in Fig. 13 for the FR, particularly at lower film flow rates. Despite the fact that FR is smaller than one for liquid flow rates lower than $\dot{Q}_f = 800\ \frac{cm^3}{min}$, liquid mass separation at the corner is considerable, as shown in Fig. 21. This indicates that the force balance model for the mean film substrate, while capturing some trends appropriately, is not sufficient for capturing the full details of the liquid mass separation. By only considering the liquid film mean characteristics, this model does not capture the more extensive coupling between the gas and liquid phases. Interestingly, the more significant impacts of the gas velocity at a liquid volume flow rate of $\dot{Q}_f = 600\ \frac{cm^3}{min}$ than that predicted by the FR are the flow conditions where LAWs become present, suggesting developed instabilities may be impacting

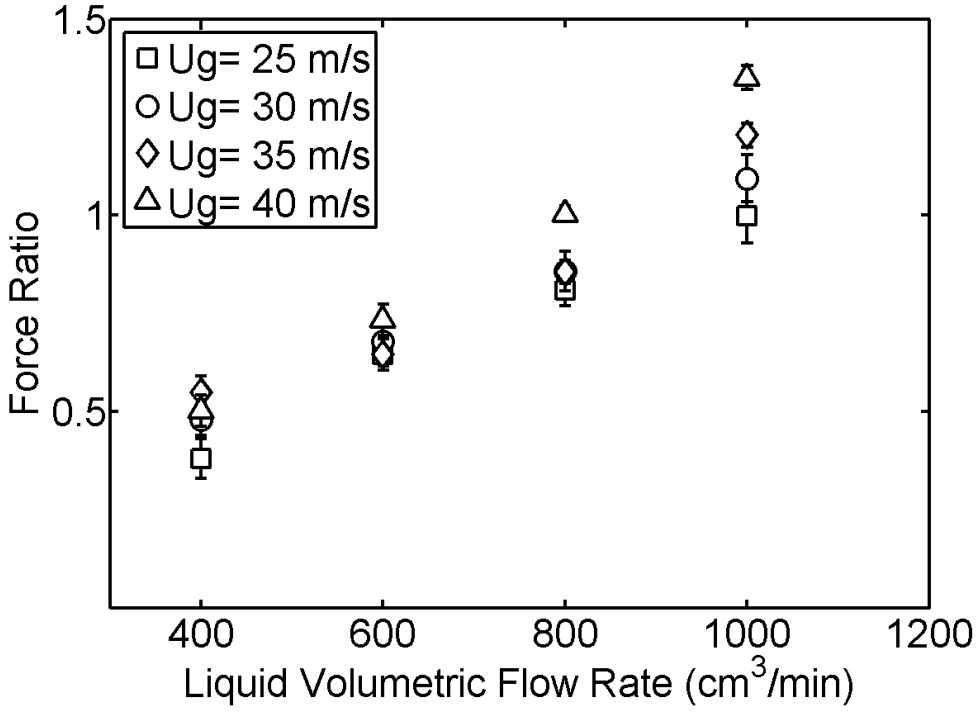

Figure 13. Vinegar dimensionless Force Ratio versus liquid flow rate for different gas velocities

separation. Unfortunately, predicting the exact transition point for the formation of LAWs is difficult. The complicated interaction between the gas and liquid at the interface results in nonlinear instabilities, which lead to LAW formation. Experimental studies show that for specific range of gas velocity, to have LAWs at the interface, the liquid Reynolds number should be sufficiently high. Unfortunately, there is not a general correlation or theoretical study, which can predict the transition between the linear instabilities (ripple waves) and nonlinear instabilities (LAWs) for shear driven liquid films.Bruno and McCready (1988)

These observations are consistent with the high speed imaging shown in Fig. 14, which illustrates a comparison between liquid film interface for vinegar at constant liquid flow rate of $\dot{Q}_f = 800\ \frac{cm^3}{min}$. The gas velocity varies from $U_g = 25\ m/s$ in 14(a) to $U_g = 40\ m/s$ 14(d). The main observed difference between Fig. 14(a)-(d) is the disturbances at the liquid film interface prior to the corner, while the liquid film substrate thickness, which

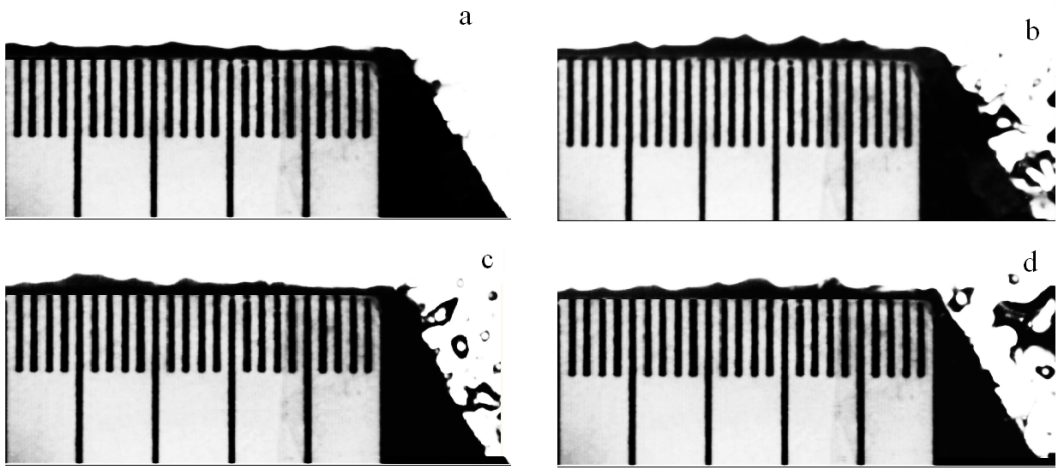

Figure 14. Vinegar at $\dot{Q}_f = 800\ \frac{cm^3}{min}$ (a) $U_g = 25m/s$, (b) $U_g = 30m/s$, (c) $U_g = 35m/s$, and (d) $U_g = 40m/s$

impacts the inertial force, is approximately the same. Hence, coupling between gas-liquid phase through the wave formation is influencing the separation.

In the next section, the LAWs are quantified for each gas-liquid flow rate condition and their frequencies are correlated with the liquid mass separation data.

4.2. LAW Existence on Interface. LAWs at the interface are influential in the liquid mass separation process for a number of reasons. These fast-moving long-lived waves carry significant mass content of the liquid film along the wall and has velocity between 1/5 to 1/10 of the gas phase mean velocity, which is several times larger than mean film substrate. Shedd (2001)Andreussi *et al.* (1985)Alekseenko *et al.* (2014) Experimental studies show that the existence of LAWs is a necessary condition for liquid atomization/entrainment from a horizontal surface into the gas phase in shear driven two-phase flow Andritsos and Hanratty (1987)Woodmansee and Hanratty (1969). Experimental visualizations for vinegar at $\dot{Q}_f = 800\ \frac{cm^3}{min}$ and $U_g = 35\ m/s$ in Fig. 15 show that when LAWs reach the corner, they cannot rotate around the sharp edge and consequently may be detached from the liquid film. Fig. 15(a), (b), and (c) show the liquid film motion near the corner for three sequential frames with 0.0025 seconds time difference.

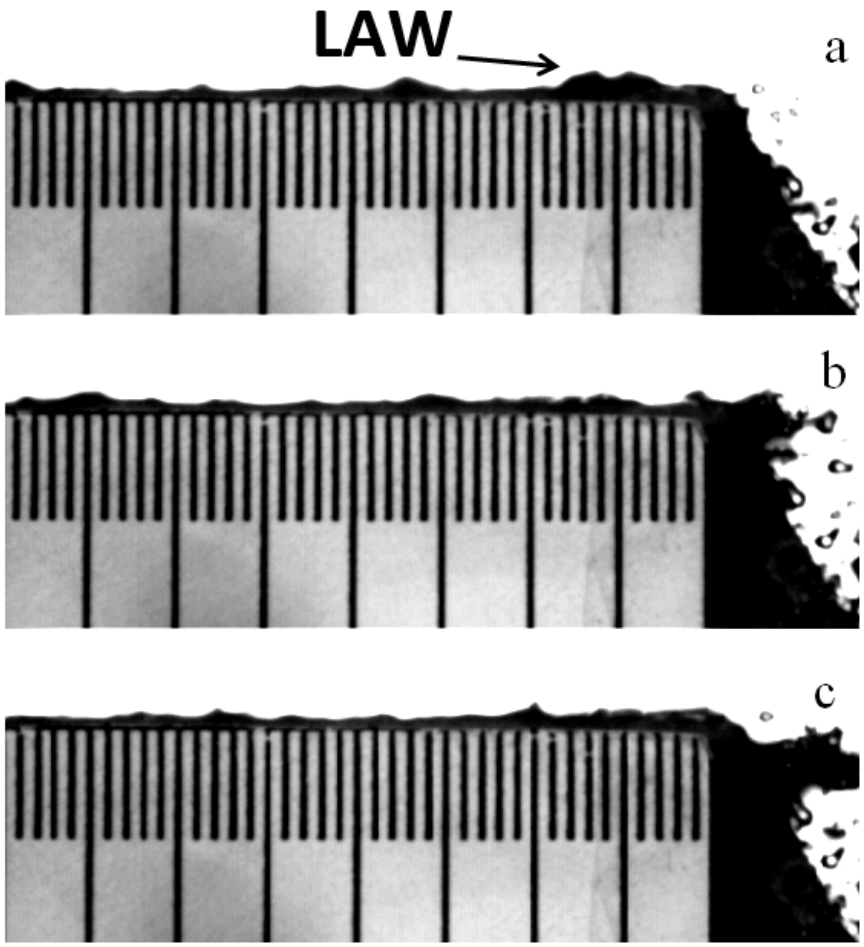

Figure 15. Sequential high speed images of liquid film separation of vinegar at $U_g = 30 m/s$ and $\dot{Q}_f = 800 \frac{cm^3}{min}$

These images suggest that the appearance of LAWs on the interface is a prelude to a higher liquid mass separation regime at the corner. It is important to note that although LAW separation at the corner is a local inertia effect, the liquid mass separation due to LAW is treated differently due to their velocity being much different than the substrate and their occurrence being predictable. These characteristics provide for the potential to develop improved liquid mass separation models.

The liquid film interface along the wall prior to a sharp corner is shown in Fig. 16 for different liquid flow rates of vinegar at $U_g = 30\ m/s$. This high speed imaging shows

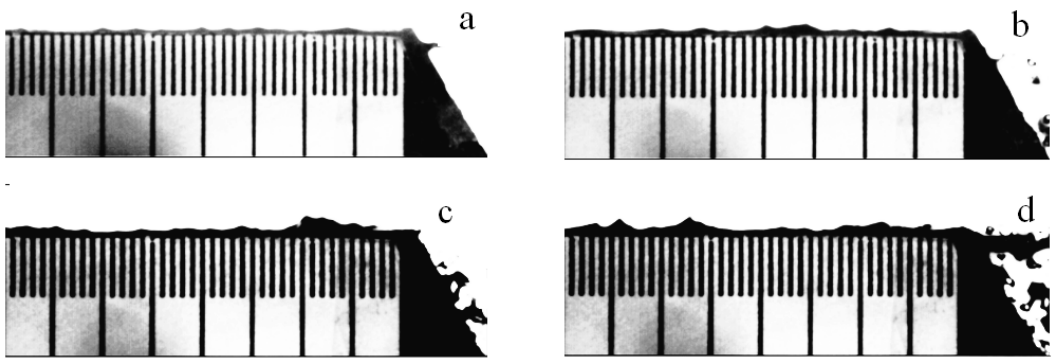

Figure 16. Vinegar at $U_g = 30m/s$ (a) $\dot{Q}_f = 400\ \frac{cm^3}{min}$, (b) $\dot{Q}_f = 600\ \frac{cm^3}{min}$, (c) $\dot{Q}_f = 800\ \frac{cm^3}{min}$, and (d) $\dot{Q}_f = 1000\ \frac{cm^3}{min}$

that by increasing liquid flow rate at constant gas velocity, more LAWs start to appear on the interface, and film separation seems to increase.

The FFT analysis of the surface waves was used to explore the impact of flow conditions on these surface wave properties. The peak frequency and amplitude from the FFT analysis is depicted in Fig. 18 and 17 for different gas-liquid flow rate combinations. First, the FFT peak frequency in Fig. 18 shows a higher frequency for the liquid flow rate of $\dot{Q}_f = 400\ \frac{cm^3}{min}$ at different gas velocities compared to all other liquid flow rates. Moreover, the FFT peak magnitude shown in Fig. 17 suggests that for the $\dot{Q}_f = 400\ \frac{cm^3}{min}$ case, these waves are smaller in amplitude compared to all other liquid flow rates. These results suggest that the waves for $\dot{Q}_f = 400\ \frac{cm^3}{min}$ are related to small ripple waves at the interface and that LAWs begin to appear for $\dot{Q}_f$ greater than $400\ \frac{cm^3}{min}$. For LAWs, as the gas velocity increases from $U_g = 25\ m/s$ to $U_g = 40\ m/s$, as shown in Fig. 18, the FFT peak frequency increases, while the FFT peak magnitude in Fig. 17 remains approximately independent of gas velocity. These frequencies shown in Fig. 18 for $\dot{Q}_f$ greater than = $400\ \frac{cm^3}{min}$ are consistent with LAWs and suggest that the LAWs are of similar height but increase in frequency as gas velocity increases for fixed film flow rate. This suggests that the mass content in LAWs will increase as gas velocity goes up due to a higher frequency of LAWs.

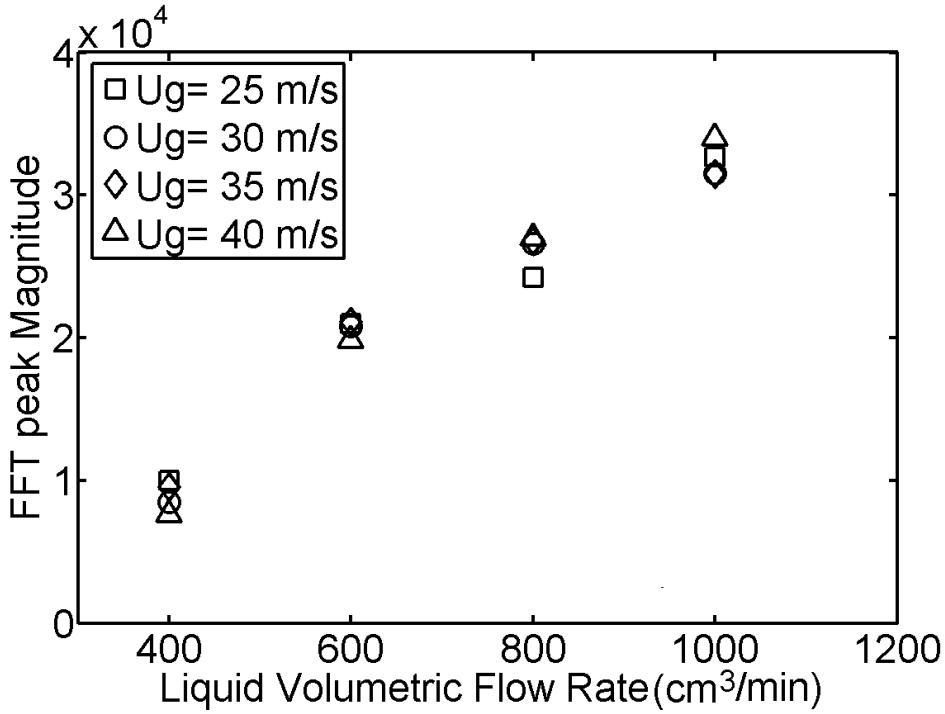

Figure 17. Vinegar FFT peak magnitude for different liquid volume flow rates and gas velocities

This is consistent with the liquid mass separation results which showed sensitivity to gas velocity variation in Fig. 21. The sensitivity of liquid mass separation to gas velocity at lower $\dot{Q}_f$ (e.g., 600 $\frac{cm^3}{min}$) was not supported by the force ratio analysis based on uniform film inertia, which was shown in Fig. 13. Finally, Fig. 17 also indicates an increase in height of the LAWs with flow rate resulting in additional mass residing in these waves.

4.3. Correlation of LAWs to Separated Mass. To confirm these observations, another method using high speed imaging has been used to quantify the probability of LAWs at the interface. In this method, a threshold height value is defined as $1.7h_{sub}$, which distinguished the LAWs from the ripple waves at the interface. At a fixed location 30 mm upstream of the corner, the interface signal is recorded for 10,000 frames and the height threshold was used as a filter to detect the LAWs at the interface. To detect the LAW at this specific axial location, a pixel with height $Y_{pixel} = 1.7h_{sub}$ is selected and called the "tracking pixel." Binary values are defined in such a way that 1 corresponds to white

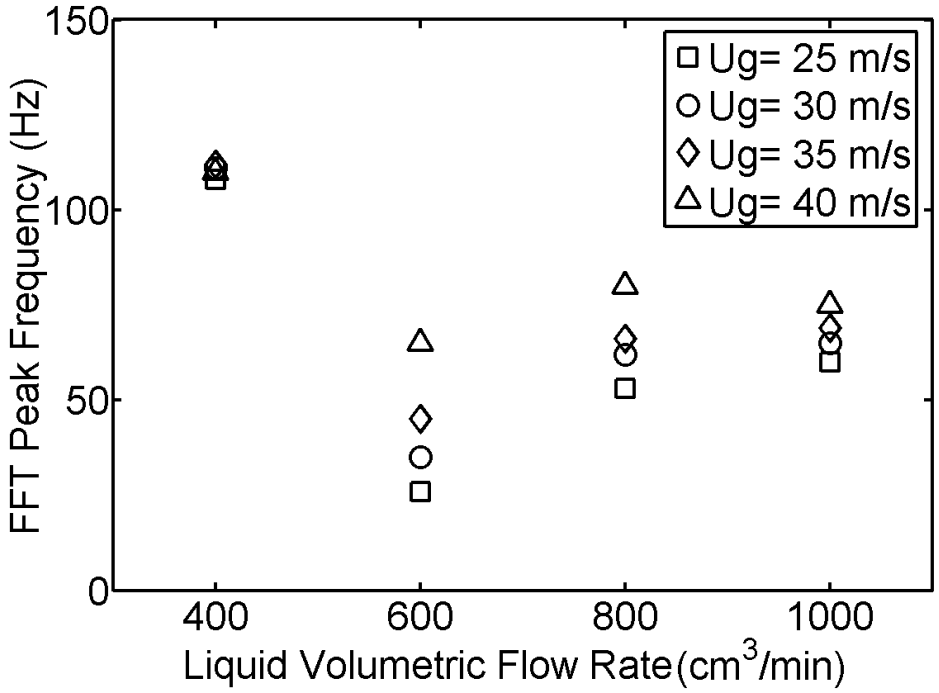

Figure 18. Vinegar FFT peak frequency for different liquid volume flow rates and gas velocities

pixels, which represents the gas phase region, and 0 corresponds to a black pixel, which represents the liquid phase. When LAW is passing through the Y_{pixel}, the binary values remain zero. As soon as the wave leaves the Y_{pixel}, the binary value changes to 1. Based on this definition, the probability of LAWs, which is defined as the number of LAWs in a unit time, was detected by counting the number of transitions from 0 to 1 for all frames. The transition from 0 to 1 is shown in Fig. 19 for a sample binary frame, which shows the variation of film height in stream-wise direction and the transitions between black and white lines are equivalent to the transition between pixel values of 0 and 1.

The LAW count from the high speed imaging analysis is depicted in Fig. 20. These results suggest the liquid flow rate of $\dot{Q}_f = 600\ \frac{cm^3}{min}$ is the threshold for LAW formation at the interface, and despite the small FR values for all gas velocities at this liquid flow rate as shown in Fig. 13, the liquid mass separation (Fig. 21) increases dramatically compared to

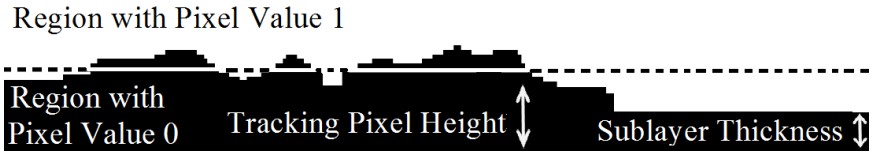

Figure 19. Threshold for calculation of LAW count

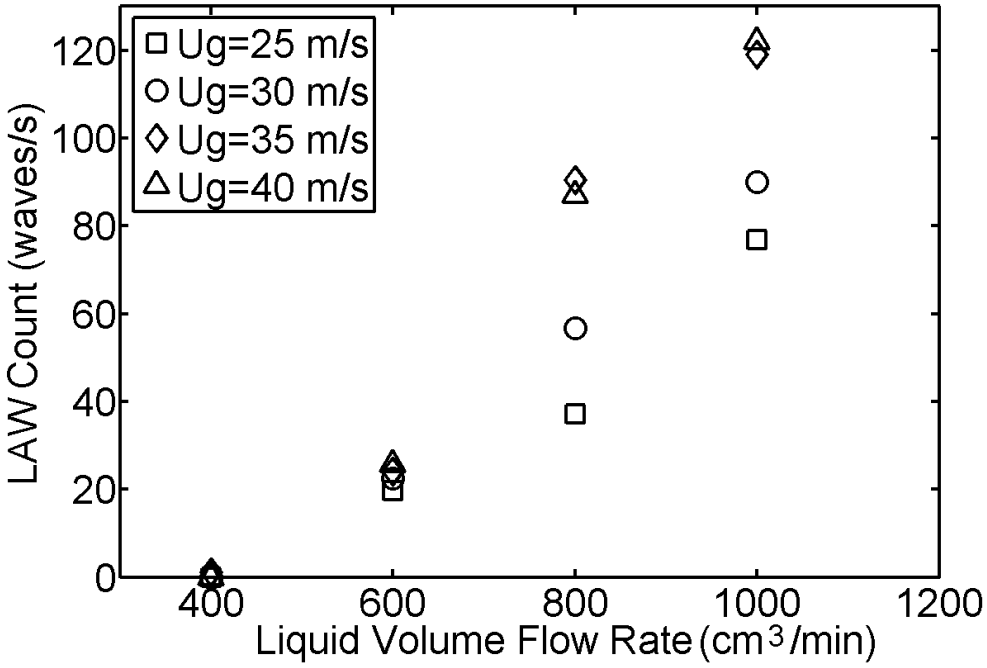

Figure 20. LAW count for vinegar at different gas-liquid flow rate conditions

negligible liquid mass separation at $\dot{Q}_f = 400\ \frac{cm^3}{min}$. Furthermore, at high gas velocities such as $U_g = 35\ m/s$ and $U_g = 40\ m/s$, the LAW counts are approximately constant for specific liquid flow rate; however, the FR results in Fig. 13 show that for these gas velocities, the FR (especially for liquid flow rates greater than $\dot{Q}_f = 600\ \frac{cm^3}{min}$) is sensitive to change in gas velocity. Finally, the LAW formation at the interface correlates well to the start of liquid mass separation for the ranges considered in this study.

Using the LAW threshold and imaging analysis, it is also possible to correlate the amount of separated mass at the corner and mass content of LAWs at the interface.

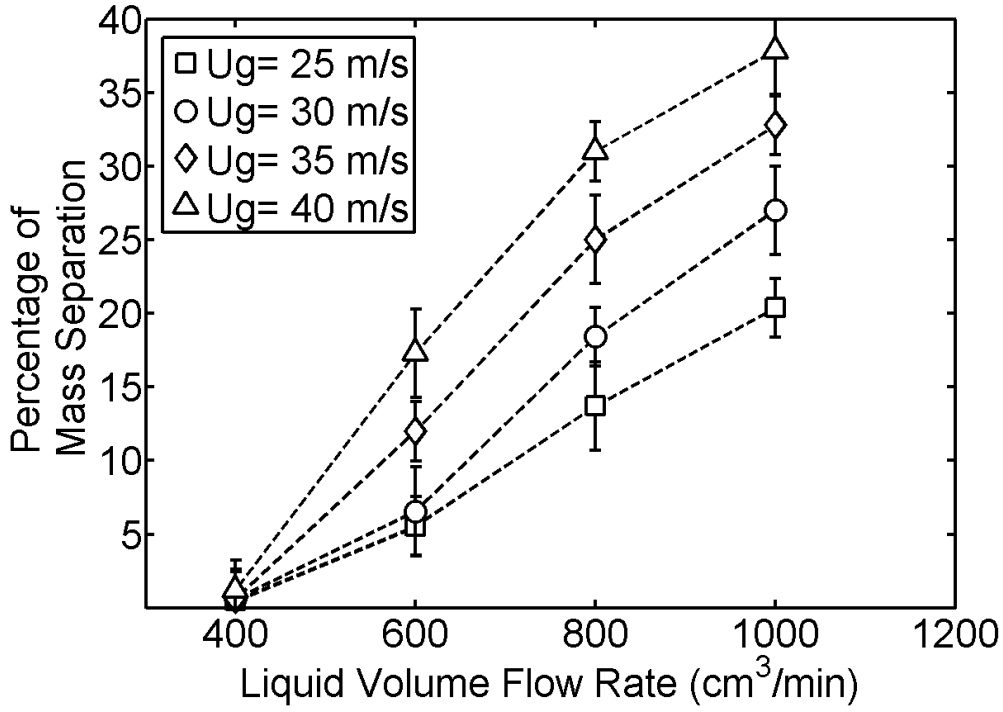

Figure 21. Vinegar mass separation versus liquid flow rate for different gas velocities

Assuming 2D waves in spanwise direction, the mass content in LAWs is proportional to the cross section area of LAWs at the interface. The LAW area was estimated from the image analysis as shown in the schematic of a LAW cross sectional area in Fig. 22. It should be noted that in order to distinguish between the liquid film substrate layer and LAW layer, the LAW area for each frame is defined as the integral of the area confined between the threshold line $h = 1.7h_{sub}$ and the film interface. Then, the LAW area is divided by the film substrate area to give a dimensionless term for analysis, which is called the normalized LAW area. This term, which represents the LAW mass content, is plotted for 10,000 sequential frames in Fig. 23 for vinegar at $U_g = 30\ m/s$ and $\dot{Q}_f = 1000\ \frac{cm^3}{min}$. The time averaged normalized LAW area for this operating condition is equal to 0.2 and is indicated on the figure.

The time averaged values for normalized LAW area versus liquid flow rate for vinegar at different gas-liquid flow conditions are shown in Fig. 24. It is revealed that at

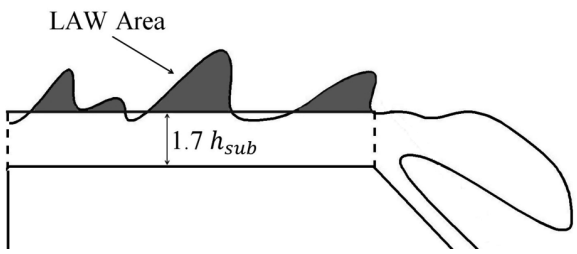

Figure 22. LAW area region upstream of the corner

constant gas velocity as liquid flow rate increases the normalized area increases. Moreover, for constant liquid flow rate, normalized LAW area increases as gas velocity grows. This effect is more significant at higher liquid flow rates where the data shows a more variation compared to lower liquid flow rates. Interestingly, the trends in the normalized LAW area follow well the trends depicted in fig. 21 for liquid mass separation.

It is useful to establish a correlation between gas-liquid non-dimensional parameters and the liquid mass separation at the sharp corner. As is shown in Fig. 25 liquid mass separation is strongly correlated to $Re_g Re_l$ in this study. Over the range of conditions considered in this study, the correlation suggests asymptotic behavior at high values. However, broadening the range of experimental conditions to include more breadth in liquid properties still needs to be considered.

5. CONCLUSION

A shear-driven liquid film is separated from a sharp corner due to two simultaneous effects: uniform film and LAWs at the interface. The main parameter that affects the inertial force is liquid flow rate. By increasing the liquid flow rate at constant gas velocity, the uniform film inertial force increases, which causes a higher percentage of liquid mass separation. The FR analysis based on uniform film inertia is the most practical model available in open literature, because it is easy to implement and also correlates well with liquid mass separation data. However, it does not appear to capture the onset of liquid

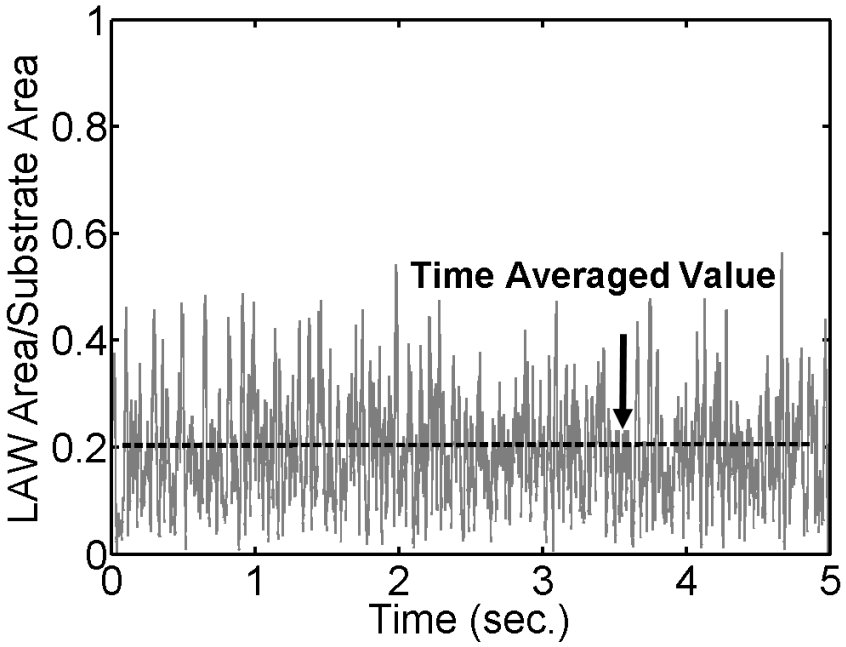

Figure 23. LAW mass signal and the corresponding time averaged value for vinegar at $U_g = 30m/s$ and $\dot{Q}_f = 1000\ \frac{cm^3}{min}$

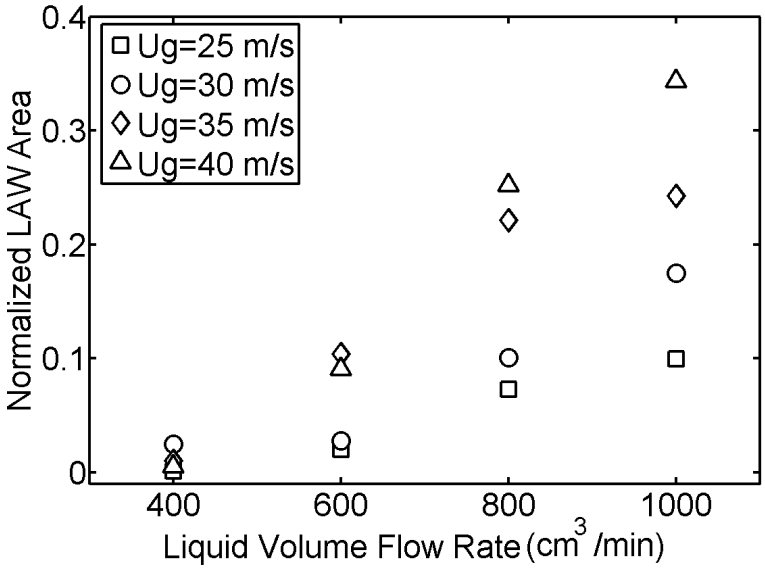

Figure 24. Normalized LAW area for vinegar at different gas-liquid flow rate conditions

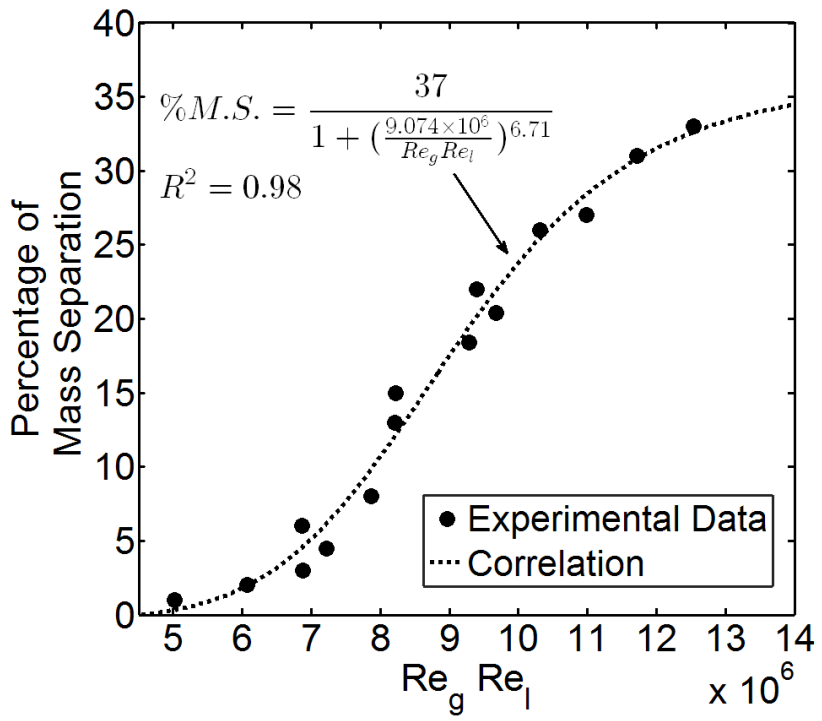

Figure 25. Mass separation correlation

mass separation and the impact of gas phase velocity. This study shows that there is a strong correlation between LAW characteristics such as LAW height, frequency, and mass content of LAWs and onset of mass separation at the sharp corner. For instance, LAWs start to appear at $\dot{Q}_f = 600\ \frac{cm^3}{min}$, which corresponds to the onset of liquid mass separation in this experiment. Also, considering the LAW effect gives better insight to the impact of gas phase velocity on liquid mass separation. For constant liquid flow rates greater than $\dot{Q}_f = 600\ \frac{cm^3}{min}$, the interaction between the gas phase and liquid film increases through the formation of more LAWs at the interface, which result in the more liquid mass separation at the sharp corner.

However, due to the coupled effects of LAWs and the film substrate, the results are insufficient to conclude that uniform film inertia is not contributing to the separation. Additionally, it could not be concluded from the current study that all the mass separated was from LAWs. The challenge to develop a separation model based on LAW is the difficulty to

predict the onset of LAW formation. There is no available theoretical/experimental study to distinguish different shear-driven flow regimes based on the existence of LAWs at the interface. Therefore, the FR model continues to be the most feasible approach to predict the liquid mass separation.

A larger range of fluid properties will be considered as well as corner geometry in future studies to continue the attempt to separate the effect of LAWs and uniform film inertia. This will be necessary to build a robust liquid mass separation criteria, which includes both uniform film inertia and wave instabilities in a predictive model.

ACKNOWLEDGMENT

Particular thanks goes to Mohammad Hossein Behgam, PhD student in electrical engineering, for helping us with the high speed image processing in this research.

REFERENCES

Alekseenko, S. V., Cherdantsev, A. V., Cherdantsev, M. V., Isaenkov, S. V., Kharlamov, S. M., and Markovich, D. M., 'Formation of disturbance waves in annular gas-liquid flow,' in 'Proc. of 17th International Symposium on Applications of Laser Techniques to Fluid Mechanics, Lisbon,' 2014 .

Andreussi, P., Asali, J., and Hanratty, T., 'Initiation of roll waves in gas-liquid flows,' AIChE journal, 1985, **31**(1), pp. 119–126.

Andritsos, N. and Hanratty, T., 'Interfacial Instabilities for Horizontal Gas-Liquid Flows in Pipelines,' International Journal of Multiphase Flow, 1987, **13**(5), pp. 583–603.

Arai, T. and Hashimoto, H., 'Disintegration of a thin liquid sheet in a concurrent gas stream,' Heat Fluid Flow, 1985, **20**, pp. 507–512.

Bacharoudis, E., Bratec, H., Keirsbulck, L., Buchlin, J.-M., and Labraga, L., 'Simplified Model for the Prediction of the Occurrence of Film Atomization in Corner Geometries,' International Journal of Multiphase Flow, 2014, **58**, pp. 325–337.

Bruno, K. and McCready, M., 'Origin of roll waves in horizontal gas-liquid flows,' AIChE journal, 1988, **34**(9), pp. 1431–1440.

Craik, A. D., 'Wind-Generated Waves in Thin Liquid Films,' Journal of Fluid Mechanics, 1966, **26**(2), pp. 369–392.

Friedrich, M. A., Lan, H., Wegener, J., Drallmeier, J., and Armaly, B. F., 'A Separation Criterion with Experimental Validation for Shear-Driven Films in Separated Flows,' Journal of Fluids Engineering, 2008, **130**(5), p. 051301.

Fuster, D., Matas, J.-P., Marty, S., Popinet, S., Hoepffner, J., Cartellier, A., and Zaleski, S., 'Instability regimes in the primary breakup region of planar coflowing sheets,' Journal of Fluid Mechanics, 2013, **736**, pp. 150–176.

Hanratty, T., 'Interfacial Instabilities Caused by Air Flow Over a Thin Liquid Layer,' Waves on Fluid Interfaces, 1983, **11**(1), pp. 221–259.

Matas, J.-P., 'Inviscid versus viscous instability mechanism of an air–water mixing layer,' Journal of Fluid Mechanics, 2015, **768**, pp. 375–387.

Nakamura, H., 'Slug Flow Transitions in Horizontal Gas/Liquid Two-Phase Flows (Dependence on Channel Height and System Pressure for Air/Water and Steam/Water Two-Phase Flows),' Research/Japan atomic energy research institute (Tokyo), 1996, **96**, p. 022.

O'rourke, P. and Amsden, A., 'A particle numerical model for wall film dynamics in port-injected engines,' Technical report, SAE Technical Paper, 1996.

Owen, I. and Ryley, D., 'The Flow of Thin Liquid Films around Corners,' International Journal of Multiphase Flow, 1985, **11**(1), pp. 51–62.

Shedd, T. A., 'Characteristics of the liquid film in horizontal two-phase flow,' Technical report, Air Conditioning and Refrigeration Center. College of Engineering. University of Illinois at Urbana-Champaign., 2001.

Strasser, W. and Battaglia, F., 'The Influence of Retraction on Three-Stream Injector Pulsatile Atomization for Air–Water Systems,' Journal of Fluids Engineering, 2016, **138**(11), p. 111302.

Thunivumani, G. and Gadgil, H., 'Dynamics of Liquid Sheet Breakup in Splash Plate Atomization,' Journal of Fluids Engineering, 2018, **140**(1), p. 011205.

Wang, Y., Wilkinson, G., and Drallmeier, J., 'Parametric Study on the Fuel Film Breakup of a Cold Start PFI Engine,' Experiments in Fluids, 2004, **37**(3), pp. 385–398.

Wegener, J., *Experiments and Modeling of Shear-Driven Film Separation*, MS Thesis, Missouri University of Science and Technology, Rolla, MO, 2009.

Wittig, S., Himmelsbach, J., Noll, B., Feld, H., and Samenfink, W., 'Motion and evaporation of shear-driven liquid films in turbulent gases,' in 'ASME 1991 International Gas Turbine and Aeroengine Congress and Exposition,' American Society of Mechanical Engineers, 1991 pp. V003T06A017–V003T06A017.

Woodmansee, D. E. and Hanratty, T. J., 'Mechanism for the Removal of Droplets from a Liquid Surface by a Parallel Air Flow,' Chemical Engineering Science, 1969, **24**(2), pp. 299–307.

Zadrazil, I., Matar, O. K., and Markides, C. N., 'An Experimental Characterization of Downwards Gas-liquid Annular Flow by Laser-Induced Fluorescence: Flow Regimes and Film Statistics,' International Journal of Multiphase Flow, 2014, **60**, pp. 87–102.

Zhang, Y., Jia, M., Duan, H., Wang, P., Wang, J., Liu, H., and Xie, M., 'Experimental and numerical study of the liquid film separation and atomization at expanding corners,' Technical report, SAE Technical Paper, 2017.

Zhao, F., Qin, L.-Z., Fu, Q.-F., Mo, C.-J., and Yang, L.-J., 'Spray Characteristics of Elliptical Power-Law Fluid-Impinging Jets,' Journal of Fluids Engineering, 2017, **139**(7), p. 071203.

Zhao, Y., Markides, C. N., Matar, O. K., and Hewitt, G. F., 'Disturbance Wave Development in Two-Phase Gas-Liquid Upwards Vertical Annular Flow,' International Journal of Multiphase Flow, 2013, **55**, pp. 111–129.

II. EFFECT OF LIQUID VISCOSITY AND SURFACE TENSION ON MASS SEPARATION OF SHEAR-DRIVEN LIQUID FILM AT A SHARP CORNER

Z. Sadeghizadeh, James A. Drallmeier

Department of Mechanical & Aerospace Engineering

Missouri University of Science and Technology

Rolla, Missouri 65409–0050

Email: zsp7c@mst.edu

ABSTRACT

Formation of a thin liquid film along a wall that is driven by an adjacent high velocity gas has many applications such as liquid atomizers, fuel film transport in internal combustion engines, and refrigerant systems. At a geometric singularity like a sharp corner, the liquid film may remain attached to the wall or become separated depending on gas-liquid flow conditions. Mean film layer inertia and instabilities, which form large amplitude waves at liquid film interface are two mechanisms for the separation of shear-driven films from a sharp corner. Inertial force due to the mean film layer and the interface layer which includes large amplitude waves both influence the liquid mass separation at the corner. In this study, the effect of liquid film properties such as viscosity and surface tension on these processes and ultimately the liquid mass separation of the shear-driven liquid film from a sharp corner was investigated. Experimental results revealed that as liquid film viscosity decreased, more mass became separated from the sharp corner due to an increase in both large amplitude wave amplitudes and mean film layer inertial force. This study also showed that although liquids with smaller surface tension developed a thiner mean film layer and less large amplitude waves at the interface, the resultant high force imbalance between the destabilizing inertial force and surface tension restoring force led to a higher liquid mass separation at the sharp corner.

Keywords: liquid film mass separation, liquid film properties, large amplitude waves, film inertia

1. INTRODUCTION

Gas driven liquid flow occurs often in various engineering applications and has been studied extensively in past decades. However, only a limited amount of work has been done to study the behavior of these films at a sharp expanding corner. This problem is significant in different applications where it may be necessary to have the liquid film attached to the solid wall for instance in demister application or to separate the liquid film from the wall to breakup into ligaments and atomize in gas phase applications like airblast atomizers.
Depending on gas-liquid flow conditions, the liquid film structure is a combination of two distinct layers: a mean film layer and a wavy layer. The mean film layer is defined based on mean properties such as mean film thickness and mean velocity while the wavy layer is a combination of different wave types at the interface. These waves are described as ripple waves (or capillary waves) and large amplitude waves (LAW) based on their amplitudes and frequencies with respect to the mean film thickness. Ripple waves are characterized by small amplitude relative to the mean film thickness and high frequency and they exist at the interface for all gas-liquid flow conditions. However, LAWs appear at the interface for some flow conditions and have large amplitude compared to the mean film thickness and low frequency. These waves carry significant mass content of the liquid film and have a velocity between 1/5 to 1/10 of gas phase velocity, which is several times the mean film velocity.Andreussi *et al.* (1985)Shedd (2001)Alekseenko *et al.* (2014)

Both the uniform mean film layer and LAWs are contributing factors to liquid mass separation at the corner due to their inertia. However, literature has often modeled the liquid film only as a mean film layer or LAW and not the contribution of both. Owen and Ryley (1985) developed a theoretical mass separation model which calculated radial stress distribution on the film at the corner. This model assumed that the liquid has a smooth

interface with linear liquid velocity profile. O'rourke and Amsden (1996) proposed another model to predict liquid separation from the corner by calculating the balance between the mean film layer inertia and the pressure difference between gas and liquid phase at the separation point, which was not verified with experimental studies. Friedrich *et al.* (2008) developed a model based on the momentum conservation of a mean film layer control volume at the point of separation. This practical model has been used by others to predict separation including Zhang *et al.* (2017) who studied the separation of the liquid fuel film at expanding corners under different fuel film forming conditions. The advantage of modeling liquid mass separation based on mean film layer properties is in its simplicity to predict the liquid mass separation based on mean properties of the gas and liquid phase. It should be noted that the uncertainty of this model to predict the onset of separation can be high. For example, experimental results showed liquid mass separation between 10-15% for cases that the proposed model predicted zero liquid mass separation.

In other works, LAWs are assumed to be the only contributing factor to liquid mass separation. In the liquid mass separation model presented by Bacharoudis *et al.* (2014), the mean film layer is neglected and the liquid film is modeled as a series of LAWs with specific frequency and wavelength that negotiate the sharp corner. The force ratio between the destabilizing forces to stabilizing forces for each single disturbance wave turning the corner, determines if the wave either remains attached to the wall or becomes separated from mean film layer at the sharp corner. This approach is more difficult to apply compared to the model by Friedrich *et al.* (2008), which uses only mean values. Also, this model fails to explain the separation of liquid films in cases where liquid is being separated from the sharp corner in the absence of disturbance waves. However, unlike mean film layer models, it appears to predict the onset of film separation more accurately.

Common to both the mean film layer and LAW models is that the inertia is the dominant destabilizing force, which needs to overcome the restoring forces such as surface tension and gravity. However, the mean film layer and LAWs have been considered

separately to enable construction of predictive models for liquid mass separation and the limitations that exist for both approaches suggest that both effects are significant.

There are limited studies available that consider a range of liquid properties on LAW formation and film inertia in shear-driven flows. At a fixed gas-liquid flow rate, the liquid film properties such as viscosity and surface tension influence the film characteristics in terms of mean film thickness, film width, and interface instabilities. Wegener (2009) studied the effect of surface tension and viscosity on liquid film characteristics, using the laser focused displacement(LFD) method to measure mean film thickness and an estimate of film velocity. For all flow conditions in this study an increase in viscosity resulted in formation of thicker mean film thickness and a decreases in mean film velocity. Also, the experimental results showed that surface tension influenced the mean film thickness and mean film velocity indirectly through variation in film width. Increasing in surface tension resulted in smaller film width, which led to thicker mean film thickness and higher mean film velocity. Hoogendoorn (1959) used water and oil as working fluids to study the effect of viscosity and surface tension on film in a stratified flow regime. This flow regime occurs where both phases are separated from one another with a definite interface and usually takes place at low gas velocity in pipes. The observations in this study showed that the transition to stratified flow occurred at higher gas velocity for air-oil mixture compared to the air-water mixture due to surface tension reduction. Moreover, Andreussi *et al.* (1985) studies showed that the liquid viscosity affected the transition between flow regimes in two-phase flow. Weisman *et al.* (1979) prepared a liquid matrix in order to change one liquid properties while the other properties remained approximately constant. This study showed that the transition from smooth stratified flow to wavy stratified regime occurred at higher gas velocity as surface tension decreased. It should be mentioned that the wavy flow regime in all these studies includes both ripple waves and large amplitude waves (LAWs) at the interface. Furthermore, based on observations by Thwaites *et al.* (1976), reducing the liquid surface tension by adding a surfactant led to more damping of ripple waves and

reduction in LAWs frequency at the interface. The limited range of operating conditions studied in the literature along with the assumptions that consider the liquid film either as a smooth surface or a wavy structure are barriers for drawing a general conclusion on the effect of liquid film properties on mean film characteristics, instabilities at the interface and subsequent liquid mass separation. This literature clearly shows liquid film properties impact film characteristics and instabilities at the interface, which are important parameters for prediction of liquid mass separation at expanding corners. Despite the importance of liquid film properties on liquid mass separation, this problem has not studied extensively in literature.

The purpose of this paper is to investigate the effect of liquid film properties on the shear driven liquid films prior to the sharp corner and eventually the liquid mass separation at the sharp corner. The two mechanisms for liquid mass separation at the sharp corner considered in this study are liquid film inertia and LAW. The effects of liquid film viscosity and surface tension were studied on each of theses mechanisms. To isolate the effect of liquid film viscosity from surface tension, a specific liquid matrix has been designed, which included six different liquid types. Experimental results reveal how liquid film viscosity and surface tension influenced liquid mass separation mechanisms through affecting LAW formation and the force imbalance at the sharp corner.

2. EXPERIMENTAL SETUP

The experimental unit, which is shown in Fig 1 was designed to study the characteristics of a shear-driven liquid film and separation phenomena at the sharp corner. The unit consists of three sections: Air entrance section, test section, and air exit section. To clarify the flow direction, X and Y axis were defined in the flow direction and normal to the film, respectively.

The air entrance region, which is 1.43 m long, was designed to provide a fully developed turbulent flow at the test section. The second section which is shown in Fig 3 is

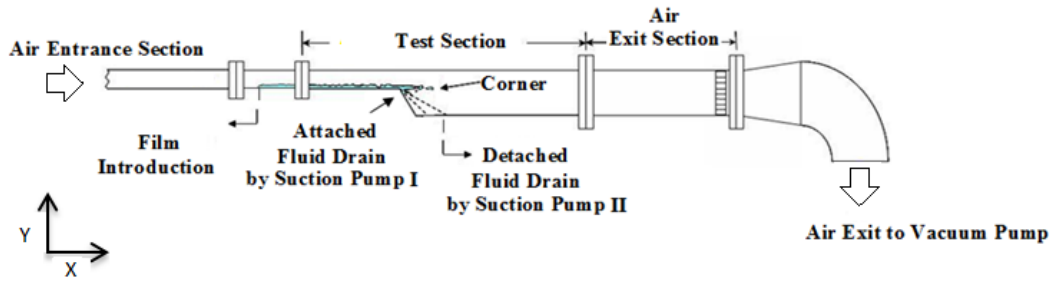

Figure 1. Schematic of experimental unit

the test section. The liquid film was introduced in the test section through a porous brass medium. This location is called film introduction point. The liquid was supplied to the brass at the film introduction point from a pressurized vessel. Then, liquid volume flow rate was adjusted, using a rotameter with an uncertainty of 2.5%. To prevent the brass blockage, a liquid filter has been applied before the brass medium to filter any contamination larger than 8 micron in the liquid. The test section was designed with a sharp corner, which was located 23 cm downstream of the film introduction point and had an angle of 60° to the horizon. The two brass porous segments, shown in Fig 3, were implemented on the inclined surface of the wall right after the corner to collect the attached liquid and the other one on the lower horizontal wall after the sharp corner to collect the separated liquid. Each brass porous segment was connected to a separate suction pump to collect the attached and detached liquids after the sharp corner without interrupting the separation mechanism. The cross section before the sharp corner was a rectangle with a height of 2 cm and width of 10 cm, giving the aspect ratio of 5. In order to measure film width nearest to the corner, an optically transparent window was located on the top wall such that optical access was provided 4 cm upstream and 4 cm downstream from the corner. Also, a side high speed camera was used to take images of the liquid film prior to the corner. An image of the test section used in this experiment is shown in Fig 3.

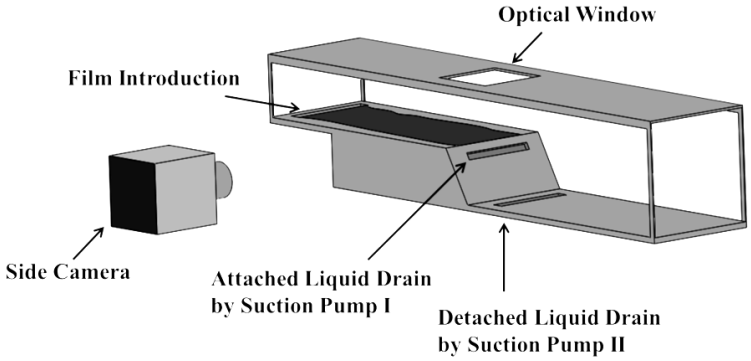

Figure 2. Detailed schematics of the test section

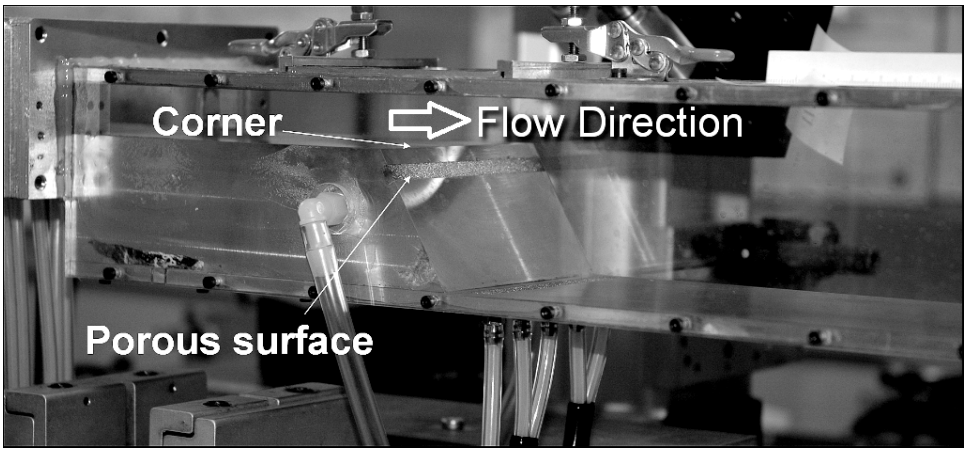

Figure 3. Attached and separated liquid drainage

Section three was the gas exit section, which was connected to a liquid ring vacuum pump to pull the air into the system. A laminar flow element (LFE) measured the air flow rate through the system caused by the vacuum pump, where the volumetric flow rate of air was correlated with the pressure drop through the LFE. Having the cross sectional area of the duct, the average gas velocity was calculated for different flow rates. By adjusting the manual control valve on the suction pump, the average gas velocity in this experiment varied from 25 to 40 m/s. Also, to have horizontal shear flow, the facility was mounted on an optics table, which provided accurate leveling of the test section in all directions.

In this experiment, to have the liquid Re_f number, $Re_f = \frac{\dot{Q}_f}{W_f \nu}$ between 100 to 300, the liquid volumetric flow rate varied from $\dot{Q}_f = 400\ cm^3/min$ to $\dot{Q}_f = 1000\ cm^3/min$. All results in this study are presented in a dimensional space to facilitate the interpretation of the results, where liquid volume low rate, gas velocity, and liquid type are directly controlled parameters in this shear-driven film separation problem. Similarly, film thickness and width are reported separately, as opposed to through the liquid Re_f, to facilitate comparisons to wave dimensions. The full run duration for each gas-liquid flow condition was 5 minutes. Experimental observation showed that the film characteristics were stable after 2 minutes. The high-speed images were taken after 4 minutes of continual running. Liquid mass separation measurements were done for 120 seconds after stable operation for each gas-liquid flow condition and each test was replicated three times to determine the uncertainty in measurements.

Three main liquid film properties, density, surface tension and viscosity affect liquid mass separation. However, in practice the significance of liquid density is reduced due to the fact that most liquids encountered in shear driven flows have negligible variation in density. In this paper, liquid mass separation results are presented for liquids with different surface tensions and viscosities.

For the flow regime considered in this experiment, it was found that liquids needed to have surface tensions lower than $\sigma = 0.072\ N/m$ to prevent ridges at the edges of film due to contact angle effects. Therefore, instead of using water that has large surface tension $\sigma = 0.072\ N/m$, vinegar (5% acetic acid CH3COOH by volume), glycerol-vinegar solutions (GV), and butanol-water (BW) mixtures were chosen as the working fluids. To study the effect of liquid viscosity on liquid mass separation, vinegar and GV mixtures of 10% and 20% glycerol by volume were chosen as the working fluids. To study the surface tension effect on liquid mass separation, butanol which has a small surface tension $\sigma = 0.025\ N/m$ compared to water was mixed with water to vary the surface tension while holding the viscosities nearly identical. To examine the effect of surface tension on liquid mass

separation, butanol-water(BW) mixtures with 1%BW, 2%BW, and 4%BW concentration by volume were chosen for this study. All the measurements of liquid properties were done using a viscometer and tensiometer, with results shown in Table 1. The liquids that were used for viscosity and surface tension tests are called Case 1 and Case 2 in this paper as disigneated in Table 1 .

Table 1. Experimental liquid matrix

Experiment	Liquid Type	$\rho(kg/m^3)$	$\mu(cP)$	$\sigma(mN/m)$
Case 1	Vinegar	1010	1.2	58.6
	10% Glycerol Vinegar Mixture(10%GV)	1028	1.9	60.5
	20% Glycerol Vinegar Mixture(20%GV)	1050	3.08	58.4
Case 2	1% Butanol Water Solution(1%BW)	990	1.15	60
	2% Butanol Water Solution(2%BW)	1016	1.2	49.3
	4% Butanol Water Solution(4%BW)	1016	1.16	40.4

3. HIGH SPEED IMAGING TECHNIQUES

To study the liquid film characteristics prior to the sharp corner, high speed imaging was performed at different locations. In the flow direction a high speed camera (Photron 1280 PCI) used in this study captured high speed images with 2000 frame per second shutter speed. At a resolution of 640 x 128, the high speed images had the magnification and spatial resolution of 7 and 55 micron, respectively. To determine the interface profile, high speed images were converted into binary sets of data based on pixel brightness. The threshold brightness value of 170 was selected to divide pixels into black and white. The pixels with brightness higher than the threshold value were converted to 255, which corresponded to the gas phase, and pixels with brightness value lower than 170 were assigned with black pixels(zero brightness), which corresponded to the liquid phase. The interface was determined by the height of the transitional pixels, where the transition between the

brightness of 0 and 255 occurred. A sample high-speed image with corresponding binary image, are shown in Fig. 4. In this study, waves at the interface are differentiated as

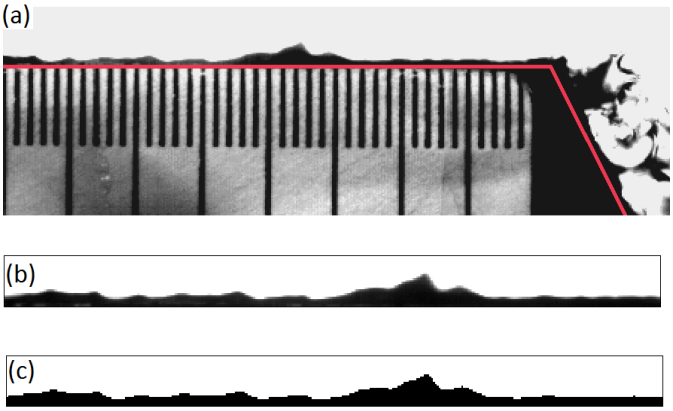

Figure 4. (a):Original high speed image, (b):interface grayscale image, and (c): corresponding binary image from the interface

ripple waves and LAWs, depending on their height ratios (HR), which is the wave height h_w relative to the mean film height h_f. To show the distribution of waves at the interface, the probability distribution function (PDF) versus HR is shown in Fig 5 for a representative test case. The PDF distribution was the result of 10,000 sequential frames. The bimodal distribution of this PDF plot represented two different types of wave at the interface: the first peak at $HR = 0.6$ related to ripple waves and the second peak at $HR = 1.8$ corresponded to LAWs at the interface.

Since one side camera was used for imaging, all waves at the liquid film interface in span-wise(Z) direction were mapped into one plane. This is called the line-of-sight effect. As illustrated in Fig 6, at each X location along the wall, the shape and height of the interface were determined by the waves with the highest amplitude along the Z direction. The black bold line in Fig 6 represents the imaged interface profile of the liquid film, which is equivalent to the observed high speed images in this study. This effect leads to loss of information about the wavelengths of disturbances at the interface.

If the line-of-sight imaging results are to be used to investigate LAW characteristics, it is important to show that the line-of-sight effect did not impact the information regarding

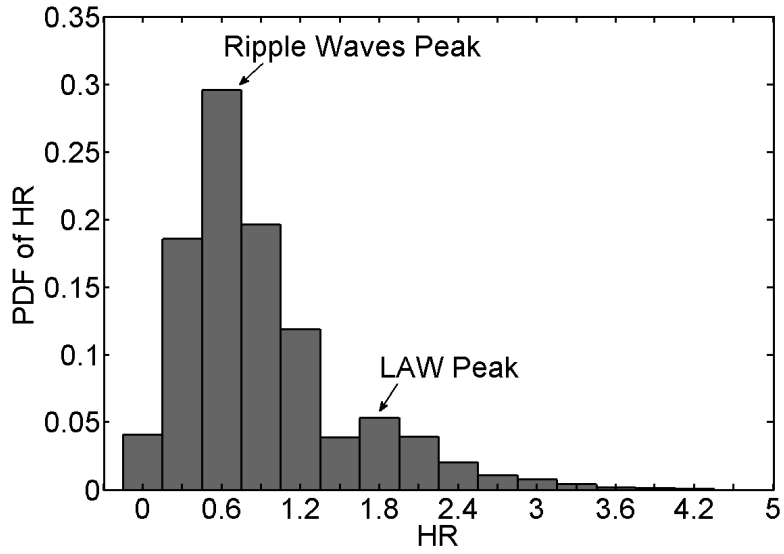

Figure 5. PDF of waves for 10,000 frames at 20 mm upstream from the corner for 2%BW at $U_g = 40\ m/s$ and $\dot{Q}_f = 1000\ cm^3/min$

to the dominant wave characteristics such as the wave frequency and wave amplitude. To this aim, a numerical simulation was designed to create an artificial interface by a randomized combination of LAW and ripple waves, with known height and frequency range for an arbitrary time interval. Then the FFT analysis of the interface was compared with the characteristics of wave components to determine how line-of-sight imaging may affect the perceived frequency and amplitude of the interface.

3.1. FFT of Film Interface. A schematic of a liquid film is shown in Fig 7. The liquid film was assumed to have two layers: mean film layer and wavy layer. The mean film layer is a layer adjacent to the wall that can be estimated by mean properties such as mean film thickness and velocity. However, the wavy layer at the interface is an accelerated disturbed layer, that depending on gas-liquid flow rate conditions, has waves with different frequencies, amplitude, and velocities. Previous studies showed that ripple wave frequencies are one order of magnitude larger than LAW frequencies, have wavelengths and amplitudes much shorter than mean film thickness, and appear prior to LAW formation.Bruno and McCready

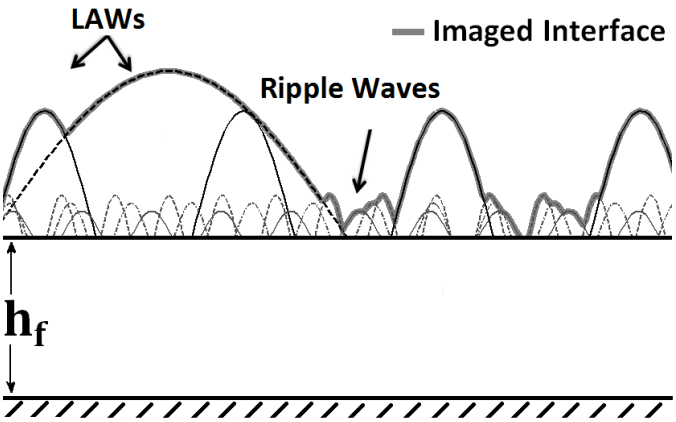

Figure 6. Line-of-sight effect

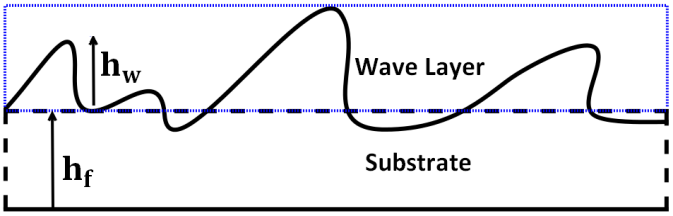

Figure 7. Liquid film layers

(1988) On the other hand, LAWs have large wavelengths and amplitudes compared to mean film thickness.Craik (1966)Hanratty (1983) LAW heights were shown to be 1.5 to 1.7 times greater than mean film layer thickness.Nakamura (1996)Zadrazil *et al.* (2014)Zhao *et al.* (2013). In this study, LAWs were considered to be 1.7 times of the liquid film mean thickness, which is consistent with the characteristic height ratios shown in Fig. 5.

The insight from these studies was used to define the wave components of the simulated film interface with a mean film layer thickness of 150 microns. Using the assumptions from the Bruno and McCready (1988) study, the LAW frequency range was considered to be from 30 Hz to 50 Hz while ripple wave frequencies were assumed to be from 50 Hz to 1000 Hz. The upper limit for the ripple wave frequency range was determined by the high speed camera sample rate, which was 2000 fps in this experiment. The ripple wave height range was from 30 micron to 100 micron, which was lower than the mean film

layer thickness. For LAWs, the height range was from 255 micron to 500 micron, which satisfied the $h_{LAW} > 1.7h_f$ condition. Furthermore, there were fewer LAWs than ripple waves at the interface. The detailed information of the wave components for the simulated interface is shown in Table 2.

Table 2. Wave components of numerical interface signal for simulated film thickness of h_f = 150 microns

Wave Type	Ripple Wave	LAW
Wave Amplitude Range (Micron)	30-100	255 - 500
Wave Frequency Range (Hz)	50 -1000	30-50
Number of Waves	500	5

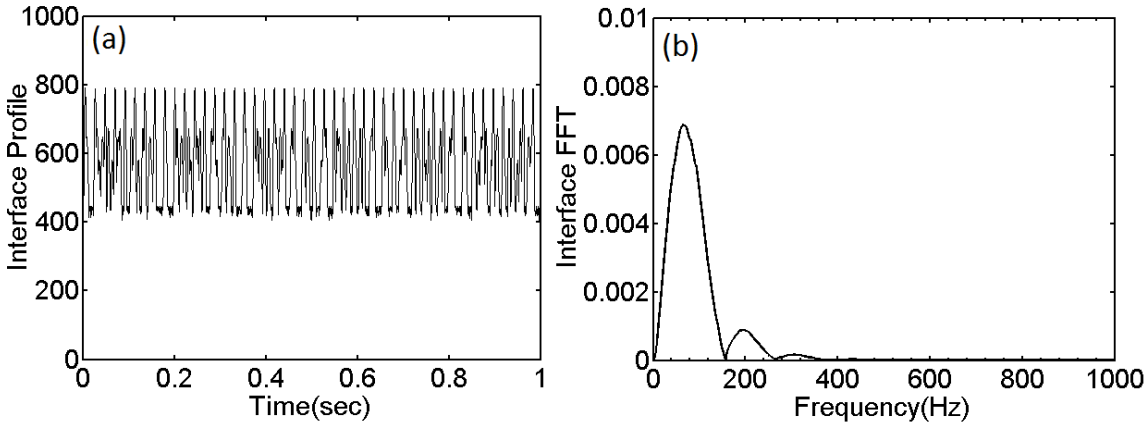

Figure 8. (a):The artificial interface generated by numerical simulation (b): corresponding FFT

The profile of the simulated liquid film interface and the corresponding FFT analysis are plotted in Fig 8(a) and (b). It should be noted that the peak of FFT plot for the interface signal in Figure 8(b) was near the frequency range of the LAWs. This means in the presence of the line-of-sight effect, the frequency characteristics of the interface signal was dominated by the LAWs. Thus, the FFT analysis showed that for a random combination of 5 LAWs and 500 ripple waves, the peak of the FFT plot was nearest to the LAW frequency range

and line-of-sight effect was dominated by the information about LAWs. To further explore the characteristics of the FFT of the simulated line-of-sight interface, the LAWs frequency range was varied from 1 Hz to 150 Hz for a fixed ripple wave frequency chosen from 200 Hz to 1000 Hz. LAW amplitude was varied from 800 to 2000 micron. All other parameters such as number of LAW waves and ripple waves characteristics remained constant in this case study as shown in Table 3.

Table 3. Wave components of numerical interface for FFT correlation of simulated film thickness of h_f = 450 microns

Wave Type	Ripple Wave	LAW
Wave Amplitude Range (Microns)	50-150	800 - 2000
Wave Frequency Range (Hz)	200 -1000	1-150
Number of Waves	500	5

The numerical FFT results of the simulated interface are shown in Fig 9 (a) and (b), which show a strong correlation between the FFT peak frequency and magnitude and LAW's characteristics. The results of the numerically simulated wave interface suggests

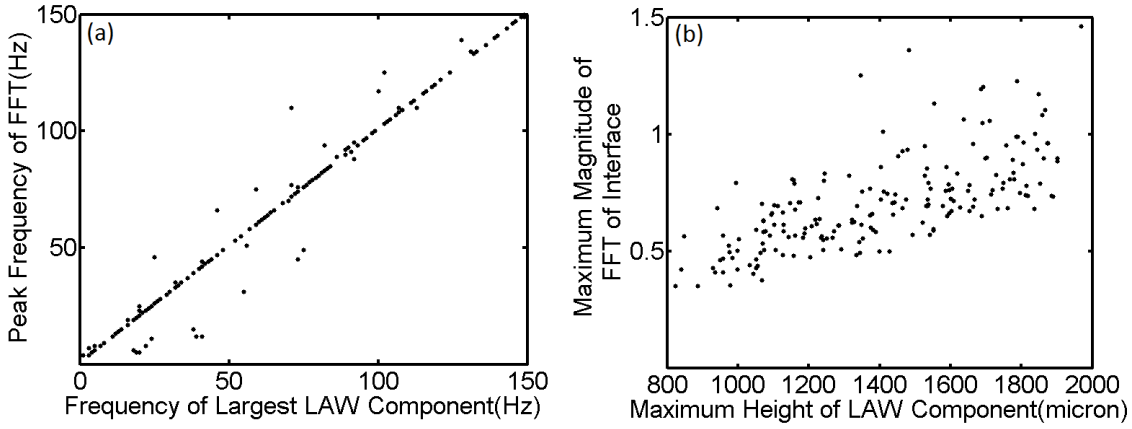

Figure 9. Correlation between LAW characteristics and FFT of the interface (a): frequency correlation (b): amplitude correlation

that all wave information is not lost when viewed from the side, but that the FFT of the line-of-sight measured film interface provides some insight into the frequency and amplitude of the LAWs at the interface.

3.2. Imaging Area. The LAWs can carry the significant mass content of the liquid film. To estimate the LAW contribution to the liquid mass separation at the corner, LAW mass content was considered to be proportional to area of the wavy layer as estimated from the high speed imaging. Therefore, to estimate LAW mass content, the normalized LAW area was defined as the ratio of the wavy layer area divided by the mean film layer area at each gas-liquid flow condition. The high speed imaging technique was used to measure the normalized LAW area. The normalized LAW area was then correlated to the amount of separated mass at the corner for different gas-liquid flow conditions.

4. FORCE BALANCE ANALYSIS METHOD

The force ratio (FR) analysis method, proposed by Friedrich *et al.* (2008) was used to determine the effect of force imbalance on liquid mass separation at the corner. This method is based on the conservation of linear momentum for a bulk ligament at the point of separation. A schematic of the parameters used in this method is shown in Fig 5.

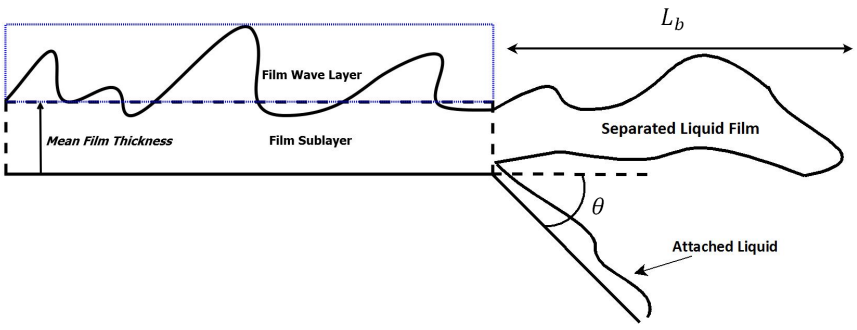

Figure 10. Liquid film at the point of separation

This model determines a force ratio of the destabilizing force over restoring forces as follows

$$FR = \frac{\rho_f U_f^2 h_f sin(\theta)}{\sigma sin(\theta) + \sigma + \rho_f g h_f L_b cos(\theta)} \tag{1}$$

In the FR relation, θ is the corner angle and L_b is the characteristic breakup length, which is estimated from Eq. 2. Arai and Hashimoto (1985)

$$_b = 0.0388 h_f^{0.5} Re_f^{0.6} We_{rel}^{-0.5} \tag{2}$$

Here, liquid Reynold number Re_f is

$$Re_f = \frac{h_f U_f \rho_f}{\mu_f} \tag{3}$$

and relative Weber number is defined as

$$We_{rel} = \frac{h_f \rho (U_g - U_f)^2}{2\sigma} \tag{4}$$

The nondenominational form of FR is as follows

$$FR = \frac{We_f}{1 + \frac{1}{sin\theta} + Fr_{h_f} We_f (\frac{L_b}{h_f})(\frac{1}{tan(\theta)})} \tag{5}$$

where $We_f = \frac{\rho_f U_f^2 h_f}{\sigma}$ and $Fr_{h_f} = \frac{g h_f}{U_f^2}$.

The effect of liquid film inertia is to separate the film from the corner, while surface tension and gravitational forces inhibit liquid film separation. Also, a FR equal to one should correspond to the onset of liquid film separation.

This analysis method correlated well to film separation for a wide range of gas-liquid test conditions. For large corner angles, as θ increases, the gravity term in denominator decreases compared to the surface tension term. Therefore, for one liquid with constant surface tension, the FR represents the mean film layer inertial effect.

To calculate the FR term, it is necessary to find mean film thickness and velocity. Since line-of-sight effects imposed error on film thickness measurements derived from imaging, the film thickness was approximated by using a numerical two-phase model presented by Wang Wang *et al.* (2004). This 2D numerical model predicted the turbulent air flow field and shear driven liquid film properties, considering the strong interrelated coupling of both phases. Gas-phase flow field characteristics were modeled using a Finite Volume code with k-ϵ turbulent modeling. Due to waviness of the liquid film interface, a special wall function, which was suggested by Wittig *et al.* (1991) was considered in this turbulent air model. It was assumed that gas-liquid film interface was a very slow moving rough wall that could be expressed by an equivalent sand grain roughness. Moreover, liquid film propagation was predicted based on a boundary layer description. Details on this numerical model to predict film thickness can be found in Wang *et al.* (2004)Wittig *et al.* (1991).

5. RESULTS

Liquid mass separation results for liquids with different viscosities and surface tensions are presented in this section. Then these results are followed with observed trends seen based on the force balance and imaging analyses.

5.1. Mass Separation. Liquid mass separation results versus liquid flow rate, for liquids with different viscosities and surface tensions are presented in Fig. 11 and Fig. 12, respectively. As shown in Fig. 11, at constant gas velocity, as viscosity increased, the percentage of liquid mass separation decreases at the corner. Additionally, increased gas velocity increased the fraction of liquid mass separation. Experimental results in Fig.12 show that for liquids with different surface tension at constant gas velocity, liquid mass separation increases as surface tension decreases. It is interesting to compare the liquid mass separation results to the observed trends from the force balance and imaging analyses. These tools help determine how the mean film layer and LAWs affect the liquid mass

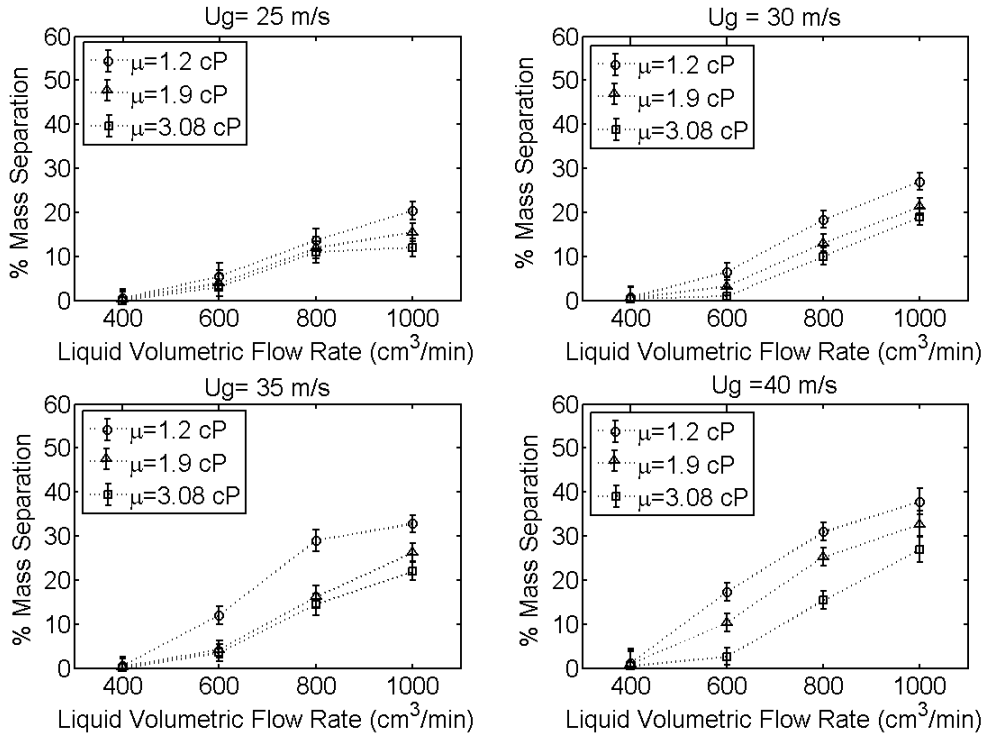

Figure 11. Viscosity effect on liquid mass separation at different gas velocities

separation due to change in inertial force at the point of separation. Since liquid Re_f number includes both film thickness and film width variations, to prevent complexity in presenting the results, liquid volume flow rate has been chosen as the independent variable for presentation of results in this section.

5.2. Force Balance Analysis. In this section the FR analysis was evaluated for liquids with different viscosities and surface tensions. To calculate FR for different liquid properties and gas-liquid flow conditions, the film model discussed in section 4 was used to determine the mean film layer characteristics such as mean film thickness and velocity as the viscosity and surface tension varied.

5.2.1. Viscosity effect on FR. The data in Table 4 represents the effect of viscosity on film width at $U_g = 40\ m/s$ and different liquid flow rates. It should be noted that all film width measurements were performed from the top optical window at a fixed axial location

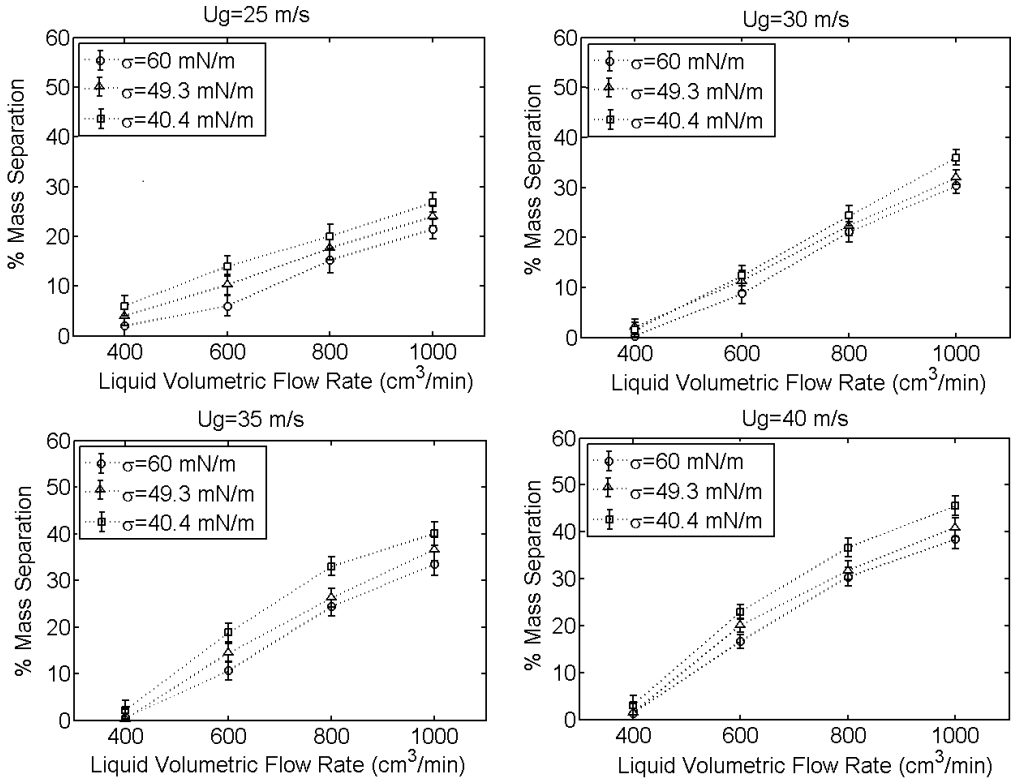

Figure 12. Surface tension effect on liquid mass separation at different gas velocities

10 mm upstream the corner. Also, for the same gas-liquid flow conditions, film thickness was calculated from the film model with results shown in Table 5.

At constant gas-liquid flow rate, as viscosity increased, both liquid film width and thickness increased as well. However, the rate of increase in film thickness was larger than film width. This observation was consistent with previous experimental study presented by Wegener (2009). For a known liquid volume flow rate, the liquid film had lower mean velocity as viscosity increased.

The calculated FR values are shown in Fig. 13, for the lowest and highest gas velocities in this experiment at different liquid flow rates. For the geometry used in this study with relatively high θ angle (e.g. $\theta = 60°$), the restoring force due to gravitational force is only 5% to 10% of the total force on liquid film control volume used in the FR

Table 4. Film width measurements for liquids with different viscosities at $U_g = 40\ m/s$

Film Width (mm) with $\pm 1mm$ Uncertainty			
$\dot{Q}_f\ cm^3/min$	$\mu = 1.20\ cP$	$\mu = 1.90\ cP$	$\mu = 3.09\ cP$
400	75	85	88
600	85	88	91
800	91	92	94
1000	94	95	97

Table 5. Film thickness calculations for liquids with different viscosities at $U_g = 40\ m/s$

Film thickness(micron) from CFD model			
$\dot{Q}_f\ cm^3/min$	$\mu = 1.20\ cP$	$\mu = 1.90\ cP$	$\mu = 3.09\ cP$
400	130	170	200
600	150	190	240
800	170	230	270
1000	190	250	290

determination. Hence, the FR is proportional to the ratio of inertial force to the restoring surface tension force. For the Case 1 experiments, where the surface tension remained constant as viscosity increased, the FR is directly proportional to the inertial force. It should be noted that as viscosity increases, the film inertia decreases because the rate of decrease in mean film velocity is higher than the rate of increase in mean film thickness, which results in a decrease in inertial force. Therefore, FR decreases as the viscosity increases.

The FR results in Fig. 13 showed that, for all different liquid types, at constant gas velocity, as liquid flow rate increased the FR increased; however, the liquid which had lower viscosity demonstrated higher FR compared to the more viscous liquids. So, when viscosity increased the FR values decreased.

These results correlated well with the liquid mass separation trends shown in Fig. 11. Viscosity affected the mean film layer characteristics, which resulted in smaller FR

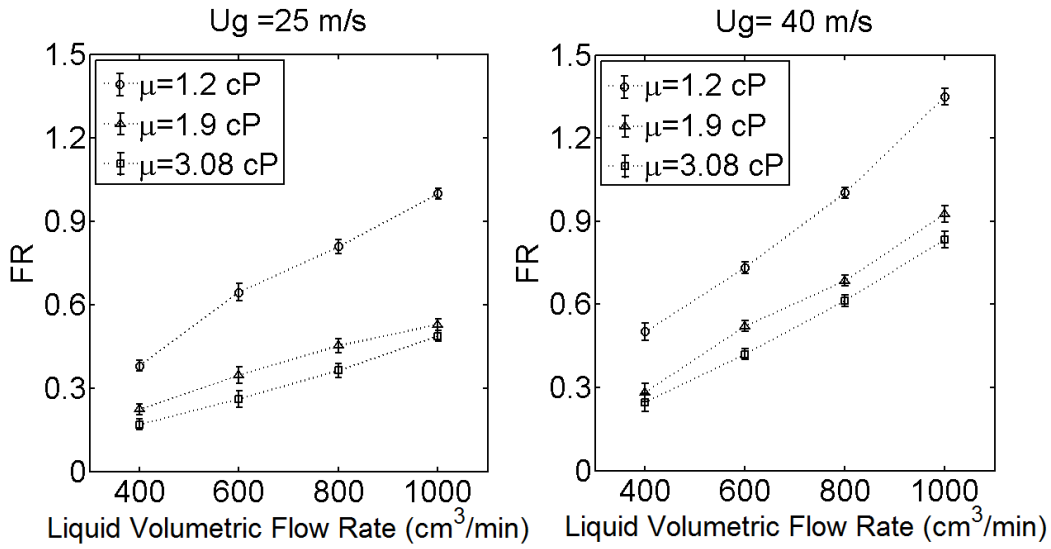

Figure 13. Viscosity effect on FR at different gas velocities

values and eventually lower liquid mass separation at the corner. However, for many tests, particularly at the higher viscosities, the FR was less than one, yet Fig. 11 clearly showed separated mass.

5.2.2. Surface tension effect on FR. Decreasing the surface tension at constant gas-liquid flow rate, resulted in formation of wider films and consequently thiner mean film layers upstream from the corner, which are shown in Tables 6 and 7, respectively.

Table 6. Film width measurements for liquids with different surface tensions at $U_g = 40$ m/s

Film Width (mm) with $\pm 1mm$ Uncertainty			
$\dot{Q}_f$ cm^3/min	$\sigma = 60.0$ mN/m	$\sigma = 49.3$ mN/m	$\sigma = 40.4$ mN/m
400	70	76	83
600	77	88	89
800	91	96	98
1000	95	98	100

Therefore, considering Eq.1, for negligible gravitational restoring force and constant corner angle, the FR was proportional to We_f number at the corner. As it is shown in Table 7 and Table 8, decreasing surface tension resulted in thiner mean film thickness and smaller film velocity, which leads to decreased liquid film inertia.

Table 7. Film thickness calculations for liquids with different surface tensions at $U_g = 40$ m/s

Film thickness(micron) from CFD model			
$\dot{Q}_f$ cm^3/min	$\sigma = 60.0$ mN/m	$\sigma = 49.3$ mN/m	$\sigma = 40.4$ mN/m
400	150	140	130
600	175	170	160
800	180	170	165
1000	190	185	180

Table 8. Film velocity calculations for liquids with different surface tensions at $U_g = 40$ m/s

Film Velocity(m/s) from CFD model			
$\dot{Q}_f$ cm^3/min	$\sigma = 60.0$ mN/m	$\sigma = 49.3$ mN/m	$\sigma = 40.4$ mN/m
400	1.5	1.43	1.38
600	1.7	1.65	1.6
800	1.72	1.67	1.66
1000	1.81	1.76	1.78

The FR versus liquid flow rate for different gas velocities are presented in Fig. 14. The results showed that at constant gas-liquid flow rate, the liquid with lower surface tension had higher FR. Moreover, the FR values in Fig. 14 had dramatically different scales from the FR results in Case 1 for similar gas-liquid flow conditions due to the lower surface tension for Case 2 fluids. Since the onset of liquid mass separation was assumed to be at $FR = 1$, the presented results with FRs much larger than one were suggesting high percentage of liquid mass separation at the corner, which was confirmed with liquid mass

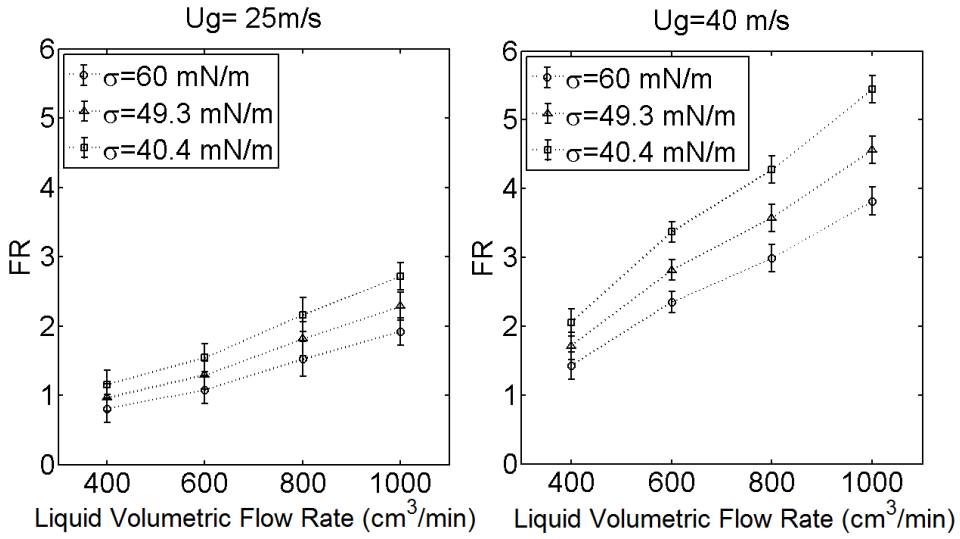

Figure 14. Surface tension effect on force ratio at different gas velocities

separation results in Fig. 12. Also, compared to the same gas-liquid flow conditions in Case 1 experiments, higher percentage of liquid mass separation was observed in Case 2 experiments.

The FR analysis provides a practical prediction tool for liquid film mass separation at the sharp corner due to the variation in liquid film properties. Having the mean film characteristics determine the FR for different gas-liquid flow conditions, these correlated well to liquid film mass separation results. However, for Case 1 experiments, the liquid film mass separation results show that the FR values predicted little to no film separation since most conditions had a $FR < 1$ (Fig. 13). Furthermore, for Case 2 experiments, while the high values of FR reflect the significant effect of liquid film surface tension as a restoring force on separation process, the mass separation results in Fig. 12 seemed to suggest less of an effect.

5.3. LAWs Imaging Analysis. The normalized LAW area is directly proportional to LAW amplitude and frequency. Higher values in both LAW amplitude and frequency imply more mass content in LAWs as these waves propagate towards the sharp corner. Also,

analysis of the simulated film interface in Section 3.1, showed that the peak of interface FFT magnitude and the corresponding peak frequency are proportional to LAW's amplitude and frequency, respectively. Therefore, the FFT peak magnitude and amplitude can be used in this study to discern trends in the LAWs mass content for different flow conditions. In this section, the imaging of the interface for different gas-liquid conditions were analyzed to show how liquid film properties change the LAWs wave characteristics and subsequent mass separation.

5.3.1. Viscosity effect on LAWs. As shown in Section 3 the peak magnitude of the FFT of the line-of-sight imaging is proportional to LAW amplitudes at the interface. Results in Fig. 15 show that for Case 1, increasing the viscosity acted as a damping factor on LAW heights as LAWs propagated along the wall. This effect became larger as viscosity was increased. Furthermore, at a fixed X location, a liquid with higher viscosity had smaller LAW amplitude.

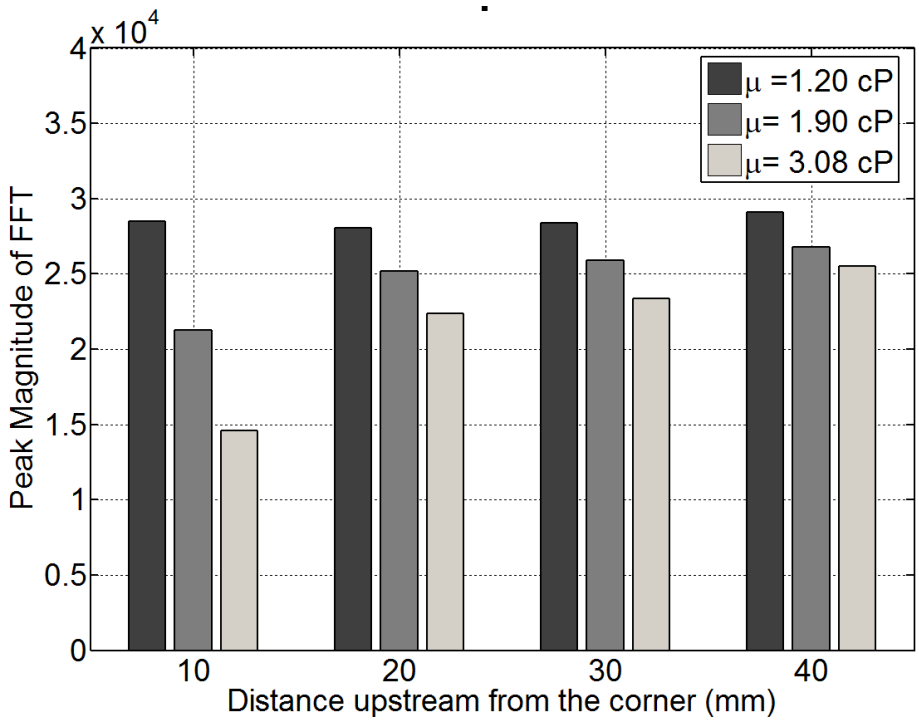

Figure 15. FFT magnitude for liquids at different axial locations upstream form the corner for Case 1: viscosity test

This is consistent with the literature which demonstrates liquids with higher viscosity have higher wave attenuation rates compared to liquids with lower viscosities.Bacharoudis *et al.* (2014)

The peak magnitude and corresponding frequency of interface FFT for liquids with different viscosities are shown in Tables 9 at specific gas-liquid flow condition. It should be noted that the observed trends were the same for all other gas-liquid flow conditions, where the LAWs were present. In this study, the change in FFT peak frequency with viscosity was small. For liquids with different viscosities, the averaged FFT peak frequency was approximately 95 Hz and independent of the measuring location along the X direction. Also, as viscosity increases, the FFT peak magnitude, which is correlated to LAW amplitude, decreases. Therefore, these results suggest the overall LAWs mass content decreases by an increase in viscosity.

Table 9. Viscosity effect on interface FFT at 10 mm upstream from the corner for $U_g = 40$ m/s and $\dot{Q}_f = 800$ cm^3/min

Liquid Type	FFT Peak Frequency	FFT Peak Magnitude x10^4
Vinegar ($\mu = 1.20$ cP)	96.2 Hz	2.15
10%GV ($\mu = 1.90$ cP)	95.4 Hz	2.01
20%GV ($\mu = 3.08$ cP)	94.6 Hz	1.58

The normalized LAW area, obtained as discussed in Section 3.2, versus liquid flow rate for different gas velocities is shown in Fig. 16. At constant gas velocity, by increasing the liquid viscosity, the normalized LAW area decreased. As gas velocity increased, the normalized LAW area was more sensitive to change in viscosity. In addition viscosity affected the onset of LAW formation at the interface with the onset delayed for higher viscosity. For both gas velocities the LAWs start to appear at $\dot{Q}_f = 600$ cm^3/min for vinegar with $\mu = 1.20$ cP. However, for higher viscosity of $\mu = 1.90$ cP the onset of LAW formation occurs at higher liquid volume flow rate of $\dot{Q}_f = 800$ cm^3/min and for the highest viscosity the LAWs did not appear under flow conditions studied in this experiment.

Therefore, increase in viscosity acted as a damping mechanism on LAWs at the interface, which led to the reduction in LAW mass content at the interface and anticipated lower liquid mass separation at the sharp corner. These results are consistent with mass separation results in Fig. 11, which shows a decrease in mass separation due to an increase in viscosity for all flow conditions studied in this experiment. It is important to note that mass separation did exist for the higher viscosity even though Fig. 16 suggests limited, if any, LAW formation.

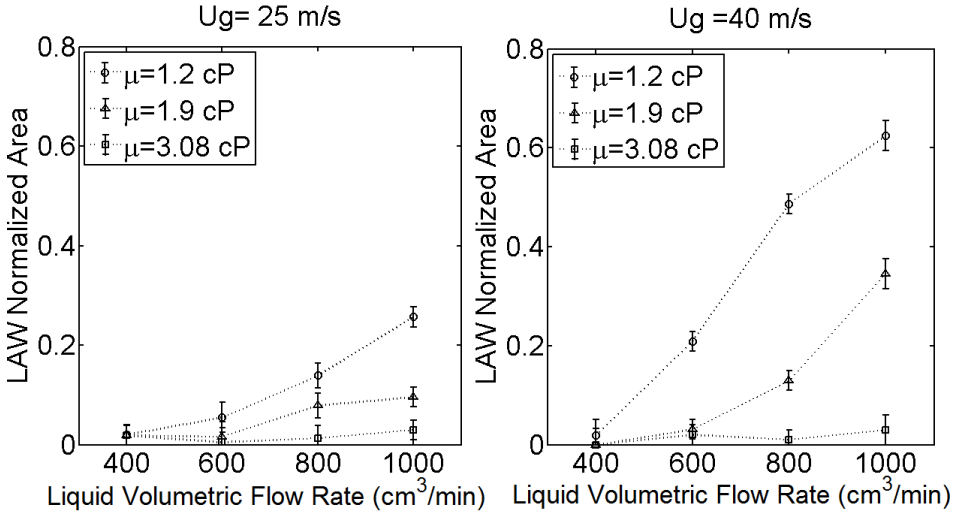

Figure 16. Viscosity effect on LAW normalized area at different gas velocities

5.3.2. Surface tension effect on LAWs. Interface FFT analysis presented in Table 10 shows that the amplitude of LAWs became smaller as surface tension decreased, while the frequency also reduced slightly (≈10%). For Case 2 results shown in Fig. 17, the variation in FFT peak magnitude due to the change in surface tension was present but smaller compared to the viscosity changes at each axial location. For all Case 2 liquids with the averaged viscosity of ($\overline{\mu}$ = 1.17 cP), the LAW's amplitude increased slightly as it propagated along the X. Therefore, by assuming that the LAW mass content was proportional to the LAW peak amplitude and frequency of LAWs, there was smaller mass content in the wavy layer as the surface tension decreased. This is consistent with the

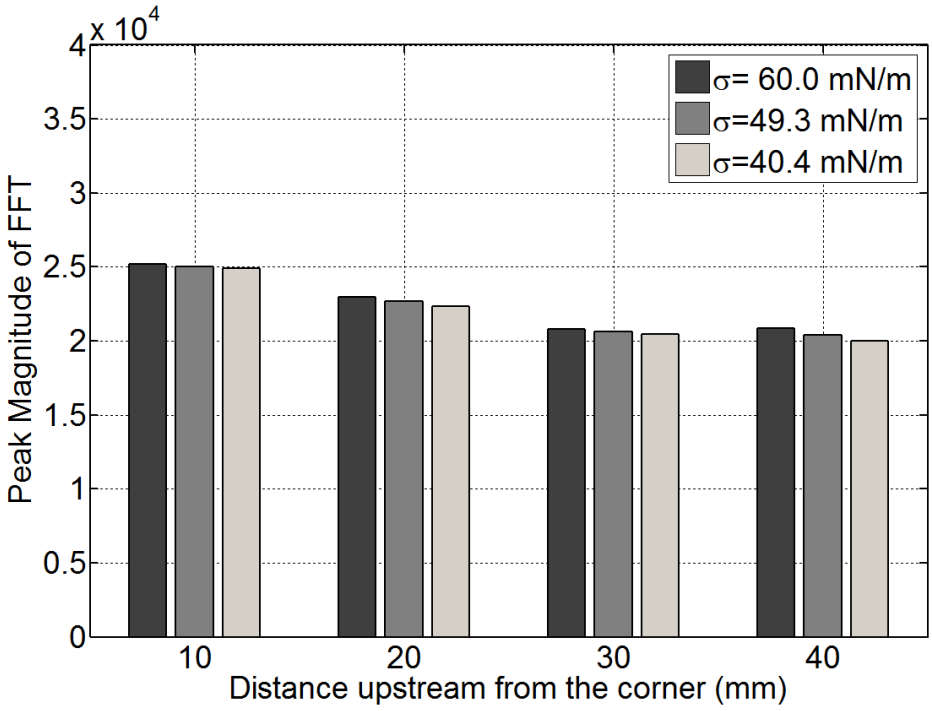

Figure 17. FFT magnitude for liquids at different axial locations upstream form the corner for Case 2: surface tension test

normalized LAW area shown in Fig 18, which shows the normalized LAW area decreased as the surface tension decreased at a constant gas-liquid flow rate. This conclusion was supported by other studies including the work of Hanratty (1983), Whitaker (1964), Pereira and Kalliadasis (2008), and Setyawan *et al.* (2016), where it was shown that the decrease in the surface tension resulted in less formation of LAWs at the liquid interface. Therefore, decreasing the surface tension diminished the LAW mass content at the interface prior to the corner. However, the liquid mass separation results in Fig. 12 showed that despite the fact that reducing the surface tension decreased the LAW formation, liquid mass separation measurably increased. The reduction in surface tension seen in Case 2 clearly showed LAW growth in X direction compared to the fluids used in Case 1. Perhaps one explanation is the effect of the interaction length between the gas and liquid, i.e. the fetch length. The wave interaction at the interface along the wall, results in formation of more LAWs as liquid

Table 10. Surface tension effect on interface FFT at 10 mm upstream from the corner for $U_g = 40\ m/s$ and $\dot{Q}_f = 800\ cm^3/min$

Liquid Type	FFT Peak Frequency	FFT Peak Magnitude x10^4
1%BW ($\sigma = 60.0\ mN/m$)	62.8 Hz	2.5
2%BW ($\sigma = 49.3\ mN/m$)	56.3 Hz	2.1
4%BW ($\sigma = 40.4\ mN/m$)	56 Hz	2

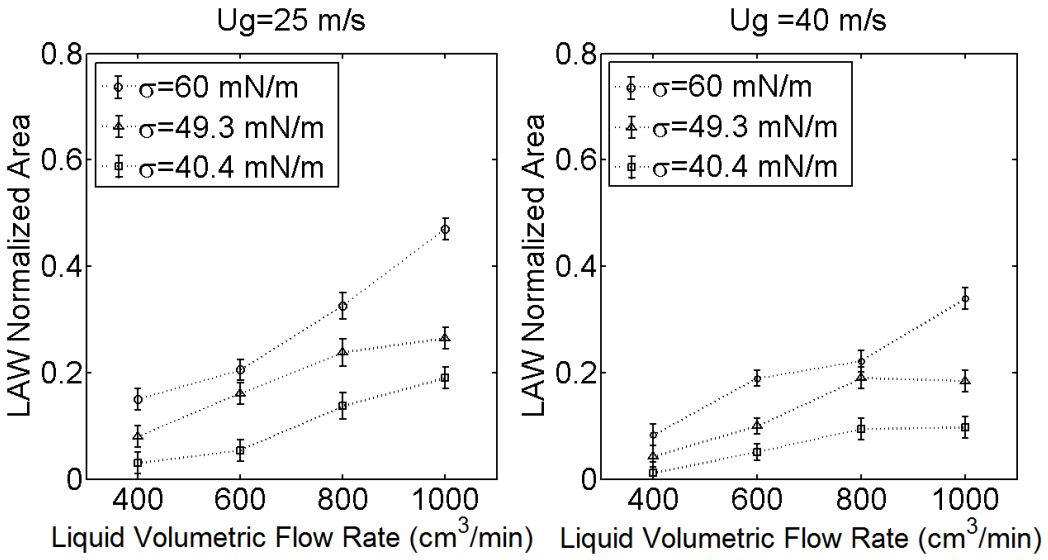

Figure 18. Surface tension effect on normalized LAW area at different gas velocities

film approached the sharp corner. This interaction increases as surface tension decreases. To accurately evaluate the effect of LAWs on liquid mass separation due to surface tension variations, the fetch length between the point of film introduction and the corner is an important factor which needs to be studied in future works.

6. CONCLUSIONS

Liquid film properties such as viscosity and surface tension affect the liquid mass separation of a shear-driven liquid film at the sharp corner through changes in LAW formation and film inertia. Liquid film separation from the corner is then due to two mechanisms:

1) the force imbalance between inertial force and restoring forces such as surface tension and gravity at the point of separation, and 2) formation of LAWs at the interface with considerable mass content with respect to the mean film layer, which results in more liquid mass separation .

For constant gas and liquid flow rates, increasing the viscosity decreased the liquid mass separation at the sharp corner. Higher viscosity decreased the inertial force and consequently the force imbalance at the corner by influencing liquid film mean properties. Also, the LAW mass content at the interface prior to the corner decreased by increasing the viscosity due to wave attenuation.

The surface tension influence on the liquid mass separation was more complex. First, the decrease in surface tension resulted in dramatically higher FR values compared to the viscosity test. This occurred since for the large corner angles, the dominant restoring force was the surface tension. The liquid mass separation results showed that despite the fact that LAW formation was weaken by decreasing the surface tension, the liquid mass separation increased. This may be explained by the increase in the mean film inertia as demonstrated in the FR at the corner. Finally, while a reduction in surface tension reduced LAW formation, those that did form grew faster with axial position.

These results clearly show that neither the inertia of the uniform film layer nor the formation of LAWs can fully describe the film separation at the corner. Liquid mass separation models must consider both the mean film as well as the wavy layer in considering the impact of liquid properties on liquid film separation.

NOMENCLATURE

U Velocity

$\dot{Q}_f$ Liquid Volume Flow Rate

h_f Liquid Film Mean Thickness

W_f Film Width

Re Reynold number

ρ Density

μ Viscosity

σ Surface Tension

We Weber number

f liquid film

g gas

REFERENCES

Alekseenko, S. V., Cherdantsev, A. V., Cherdantsev, M. V., Isaenkov, S. V., Kharlamov, S. M., and Markovich, D. M., 'Formation of disturbance waves in annular gas-liquid flow,' in 'Proc. of 17th International Symposium on Applications of Laser Techniques to Fluid Mechanics, Lisbon,' 2014 .

Andreussi, P., Asali, J., and Hanratty, T., 'Initiation of roll waves in gas-liquid flows,' AIChE journal, 1985, **31**(1), pp. 119–126.

Arai, T. and Hashimoto, H., 'Disintegration of a thin liquid sheet in a concurrent gas stream,' Heat Fluid Flow, 1985, **20**, pp. 507–512.

Bacharoudis, E., Bratec, H., Keirsbulck, L., Buchlin, J.-M., and Labraga, L., 'Simplified Model for the Prediction of the Occurrence of Film Atomization in Corner Geometries,' International Journal of Multiphase Flow, 2014, **58**, pp. 325–337.

Bruno, K. and McCready, M., 'Origin of roll waves in horizontal gas-liquid flows,' AIChE journal, 1988, **34**(9), pp. 1431–1440.

Craik, A. D., 'Wind-Generated Waves in Thin Liquid Films,' Journal of Fluid Mechanics, 1966, **26**(2), pp. 369–392.

Friedrich, M. A., Lan, H., Wegener, J., Drallmeier, J., and Armaly, B. F., 'A Separation Criterion with Experimental Validation for Shear-Driven Films in Separated Flows,' Journal of Fluids Engineering, 2008, **130**(5), p. 051301.

Hanratty, T., 'Interfacial Instabilities Caused by Air Flow Over a Thin Liquid Layer,' Waves on Fluid Interfaces, 1983, **11**(1), pp. 221–259.

Hoogendoorn, C., 'Gas-liquid flow in horizontal pipes,' Chemical Engineering Science, 1959, **9**(4), pp. 205–217.

Nakamura, H., 'Slug Flow Transitions in Horizontal Gas/Liquid Two-Phase Flows (Dependence on Channel Height and System Pressure for Air/Water and Steam/Water Two-Phase Flows),' Research/Japan atomic energy research institute (Tokyo), 1996, **96**, p. 022.

O'rourke, P. and Amsden, A., 'A particle numerical model for wall film dynamics in port-injected engines,' Technical report, SAE Technical Paper, 1996.

Owen, I. and Ryley, D., 'The Flow of Thin Liquid Films around Corners,' International Journal of Multiphase Flow, 1985, **11**(1), pp. 51–62.

Pereira, A. and Kalliadasis, S., 'Dynamics of a falling film with solutal Marangoni effect,' Physical Review E, 2008, **78**(3), p. 036312.

Setyawan, A. *et al.*, 'The effect of the fluid properties on the wave velocity and wave frequency of gas–liquid annular two-phase flow in a horizontal pipe,' Experimental Thermal and Fluid Science, 2016, **71**, pp. 25–41.

Shedd, T. A., 'Characteristics of the liquid film in horizontal two-phase flow,' Technical report, Air Conditioning and Refrigeration Center. College of Engineering. University of Illinois at Urbana-Champaign., 2001.

Thwaites, G., Kulov, N., and Nedderman, R., 'Liquid film properties in two-phase annular flow,' Chemical Engineering Science, 1976, **31**(6), pp. 481–486.

Wang, Y., Wilkinson, G., and Drallmeier, J., 'Parametric Study on the Fuel Film Breakup of a Cold Start PFI Engine,' Experiments in Fluids, 2004, **37**(3), pp. 385–398.

Wegener, J., *Experiments and Modeling of Shear-Driven Film Separation*, MS Thesis, Missouri University of Science and Technology, Rolla, MO, 2009.

Weisman, J., Duncan, D., Gibson, J., and Crawford, T., 'Effects of fluid properties and pipe diameter on two-phase flow patterns in horizontal lines,' International Journal of Multiphase Flow, 1979, **5**(6), pp. 437–462.

Whitaker, S., 'Effect of surface active agents on the stability of falling liquid films,' Industrial & Engineering Chemistry Fundamentals, 1964, **3**(2), pp. 132–142.

Wittig, S., Himmelsbach, J., Noll, B., Feld, H., and Samenfink, W., 'Motion and evaporation of shear-driven liquid films in turbulent gases,' in 'ASME 1991 International Gas Turbine and Aeroengine Congress and Exposition,' American Society of Mechanical Engineers, 1991 pp. V003T06A017–V003T06A017.

Zadrazil, I., Matar, O. K., and Markides, C. N., 'An Experimental Characterization of Downwards Gas-liquid Annular Flow by Laser-Induced Fluorescence: Flow Regimes and Film Statistics,' International Journal of Multiphase Flow, 2014, **60**, pp. 87–102.

Zhang, Y., Jia, M., Duan, H., Wang, P., Wang, J., Liu, H., and Xie, M., 'Experimental and numerical study of the liquid film separation and atomization at expanding corners,' Technical report, SAE Technical Paper, 2017.

Zhao, Y., Markides, C. N., Matar, O. K., and Hewitt, G. F., 'Disturbance Wave Development in Two-Phase Gas-Liquid Upwards Vertical Annular Flow,' International Journal of Multiphase Flow, 2013, **55**, pp. 111–129.

III. EXPERIMENTAL MASS SEPARATION MAP FOR SHEAR-DRIVEN LIQUID FILM AT EXPANDING CORNERS

Zahra Sadeghizadeh, Jeffery L. Wegener PhD, James A. Drallmeier, PhD

Department of Mechanical & Aerospace Engineering

Missouri University of Science and Technology

Rolla, Missouri 65409–0050

Email: zsp7c@mst.edu

ABSTRACT

Partial separation of gas-driven liquid film from an expanding corner is encountered in many applications such as port fuel injected (PFI), premixed charge compression ignition (PCCI) engines, and demisters. However, physical insight about the separation is very limited. Experimental studies show two different flow regimes in shear driven flow: a flow regime where there is no large amplitude waves at the interface and a flow regime with large amplitude waves at the interface. This distinction between these flow regimes is important when considering how liquid mass separates at a corner. Two distinct correlations have been provided in this study according to the flow regime at the film interface. The objective of this paper was to propose a correlation between the gas-liquid flow parameters and corresponding mass separation at the expending corners according to the flow regime at the interface. The controlling parameters, which affected the mass separation at the corner was gas-liquid *Re* number, liquid film properties, and corner angle. In this study mass separation occurred due to both mean film inertia and large amplitude waves at the interface. However, for large corner angle in absence of large amplitude waves at the interface, the mass separation could occur purely due to liquid film inertia.

Keywords: liquid mass separation map, large amplitude waves, film inertia, liquid film properties

1. INTRODUCTION

Separation of shear driven liquid film from a sharp corner has applications in many engineering two-phase flow problems. However, there is limited number of experimental and theoretical studies in the literature, which focus on the separation of shear-driven films at sharp corners. The complexity of this problem demands a deep insight into the important physical aspect of the problem in order to establish a comprehensive model for predicting the liquid mass separation.

Different approaches are available in the literature to study the liquid mass separation from a sharp corner for different applications. Wang *et al.* (2004) studied a liquid film separation for a PFI engine by visualization techniques. Engine conditions were simulated by adjusting air flow rate at each valve lift to characterize different separation regimes at the valve seat.

In a numerical study presented by O'rourke and Amsden (1996) the separation of the film was based on the comparison of the film pressure at the corner edge with the pressure developed inside the air flow above the film interface at the same location. In this approach gas pressure was considered as the main factor that controls film detachment from the corner. However, no experimental analysis was conducted to support this hypothesis. In an attempt to define and quantify controlling parameters for liquid film passing through a bend Owen and Ryley (1985) presented a theoretical analysis to model the radial stress distribution that results in film separation from the bend. In this study, a force balance was applied to a control volume of the film turning around a circular bend. Liquid film atomization was predicted by this model depending on the net force exerted on the film at the point of separation. They assume that the liquid interface is smooth and has linear liquid velocity profile. This model was compared to thin films with a thickness less than 0.1mm and the accuracy of this model depends on the accuracy of mean film characteristics such as mean film thickness and velocity.

Steinhaus *et al.* (2007) presented experimental studies to demonstrate that mass separation is a strong function of the shearing gas flow and only a weak function of the liquid flow rate which is contrary to other published literature. However, in this experimental study the model was able to predict correctly the onset of the film separation but the prediction of mass separated was limited.

Friedrich *et al.* (2008) developed an analytical model based on momentum conservation for a control volume which includes the liquid ligament. A force ratio term was defined for the ligament control volume to predict the the liquid film separation at the sharp edge. This model was developed to predict the mass separation for thin films in range of $0.1\ mm < h_f < 0.5\ mm$ as a function of mean film properties upstream the corner and it showed a high uncertainty for predicting the onset of film separation from the sharp corner. Wegener (2009) experimentally studied liquids with different surface tensions and viscosities to demonstrate that while the general behavior of mass separation for each liquid type correlates well to the Friedrich model, the model does not provide a reliable quantitative correlation for variation with liquid film properties.

All the models discussed have neglected the effect of the wavy layer at the liquid interface on the liquid mass separation mechanism. Experimental observation in shear driven two-phase flow problems show that when large amplitude waves (LAW) form at the interface, they have high inertia. This large inertial force is due to their high velocities relative to the film substrate velocity and the significant mass content that they carry along the wall (Hanratty (1983), Woodmansee and Hanratty (1969), Andritsos and Hanratty (1987), Bruno and McCready (1988), Zhao *et al.* (2013)). When these waves encounter a singularity in geometry, they have a tendency to become detached from the corner, which leads to more liquid mass separation. It should be noted that determining the transition from a flow regime without LAW to a flow regime where LAWs are present is still an unsolved challenge in two-phase flow field. In an attempt to establish a mass separation model which considers the effect of LAW at the interface, a force balance model was presented by Bacharoudis

et al. (2014). However, this model neglected the effect of liquid film properties such as surface tension and viscosity on LAW formation and growth. Furthermore, the inertia due to liquid film substrate was neglected in this study.

The available models in open literature do not capture the complete physics of film separation in a shear-driven flow problem. The purpose of this work is to find a map for liquid mass separation of shear-driven liquid films at expanding corners to help in refining existing models. Large amplitude waves(LAW) and liquid film inertia mechanisms are both considered in the impact on liquid mass separation. Experimental results show two distinct liquid mass separation maps, which depend on the LAW existence at the interface. To determine the effective parameters for the empirical correlation for each flow regime, the variation in mean film properties and LAWs at the interface are described physically. The liquid mass separation map correlations are then based on nondimensional operating conditions, liquid film properties, and the corner geometry.

2. EXPERIMENTAL SETUP

A schematic of experimental setup is shown in Fig. 1. The facility consists of three sections: air entrance section, test section, and air exit section. The liquid film was driven by the gas flow in X direction and Y axis was defined as normal to the film flow direction. The air entrance region with 1.43 m length, was designed to provide a fully developed

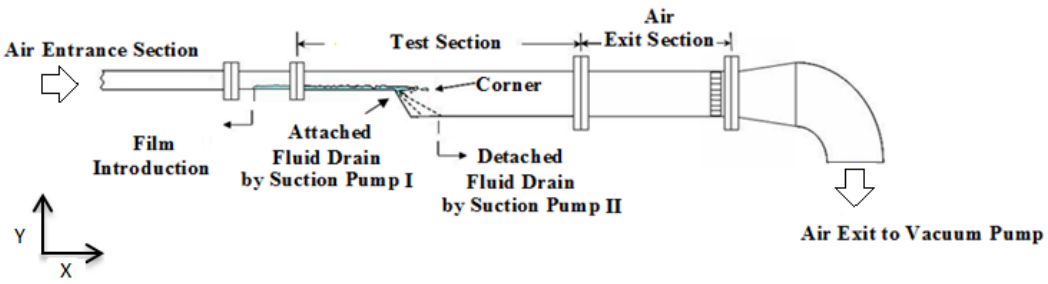

Figure 1. Schematic of experimental unit

turbulent flow prior to the test section. As is shown in Fig. 2 (a) and (b), two different removable test sections were designed for this study. Fig. 2 (a) with corner angle of 60°, was used to test all flow regimes including both flow conditions with LAWs and without LAWs at the interface. The purpose of designing the right angle corner test section (Fig. 2 (b)) was to study the liquid mass separation due to pure film inertia and in absence of LAWs at the interface.

For each test, the liquid film was introduced in the test section through a porous brass medium. This location is called film introduction point. The liquid was sent to the brass at the film introduction point from a pressurized vessel. Liquid volume flow rate was adjusted using a rotameter with an uncertainty of 2.5%. A liquid filter was applied before the brass medium to filter any contamination larger than 8 micron in the liquid. Both test sections were designed with a sharp corner, which was located 23 cm downstream of the film introduction point.

The two brass porous segments, shown in Fig. 3, were implemented on the inclined/vertical surface of the wall right after the corner for each test section to collect the attached liquid, and the other one was located on the lower horizontal wall after the sharp corner to collect the separated liquid. Each brass porous segment was connected to a separate suction pump to collect the attached and detached liquids after the sharp corner without interrupting the separation process.

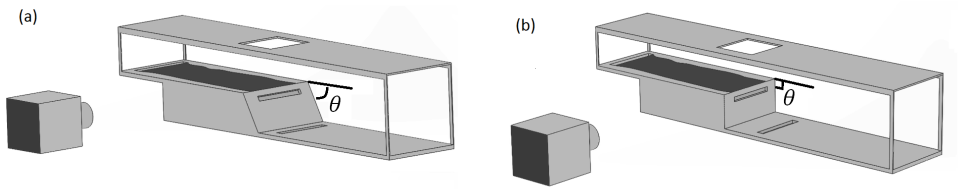

Figure 2. Test sections with different corner angles: (a) $\theta = 60°$(b) $\theta = 90°$

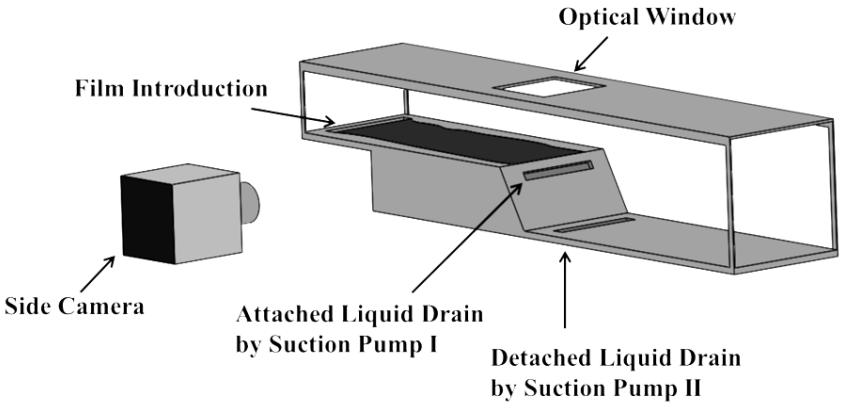

Figure 3. Detailed schematics of the test section

The cross section before the sharp corner was a rectangle with aspect ratio of 5 (height of 2 cm and width of 10 cm). In order to measure film width nearest to the corner, an optical transparent window was located on the top wall such that optical access was provided 4 cm upstream from the corner. To have horizontal shear flow, the facility was mounted on an optics table, which provided accurate leveling of the test section in all directions. Also, a high speed camera was used to take images from the side view of liquid film prior to the corner. An image of the test section used in this experiment is shown in Fig. 4.

Section three was the gas exit section, which was connected to a liquid ring vacuum pump to pull the air into the system. A laminar flow element (LFE) was used to measure the air flow rate through the system caused by the vacuum pump. The volumetric flow rate of air was correlated with the pressure drop through the LFE. Having the cross sectional area of the duct, the mean gas velocity was calculated for different flow rates. By adjusting the manual control valve on the vacuum pump, the average gas velocity in this experiment varied from 25 to 40 m/s. In this study, to have the liquid Re_f number, $Re_f = \frac{\dot{Q}_f}{W_f \nu}$ between 70 to 300, the liquid volumetric flow rate varied from $\dot{Q}_f = 400\ ccm$ to $\dot{Q}_f = 1000\ ccm$.

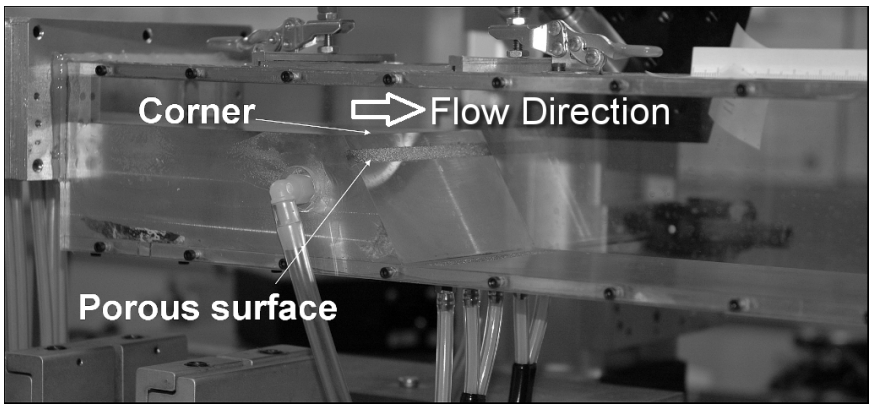

Figure 4. Attached and Separated liquid drainage

2.1. Liquid Matrix. Three main liquid film properties of density, surface tension, and viscosity impact liquid film mass separation. However, in practice the density variation between commonly studied liquids is not as significant compared to variations in liquid surface tension and viscosity. Therefore, in this paper, only liquid film surface tension and viscosity were considered as liquid film variable properties.

In this experiment, it was found that liquids with surface tensions higher than water ($\sigma = 0.072\ N/m$) form ridges at the edges of the liquid film due to contact angle effects. Therefore, all liquids used in this study had surface tensions lower than $\sigma = 0.072\ N/m$.

For the first series of experiments, vinegar (5% acetic acid CH3COOH by volume), glycerol-vinegar mixtures (GV), and butanol-water (BW) mixtures were chosen as the working fluids. In Case 1 experiments, vinegar and GV mixtures were used to study the effect of viscosity, since all these mixtures had nearly the same surface tension. In Case 2 experiments, BW mixtures with approximately the same viscosities were prepared to investigate the effect of surface tension on liquid mass separation. Case 1 and Case 2 experiments were performed for the $\theta = 60^{\circ}$ test section.

From high speed imaging, gas-liquid flow conditions where no LAWs were visible were determined for Case 3 experiments. For vinegar at all gas velocities and a liquid

Table 1. Experimental liquid matrix

Test	Liquid Type	$\rho\ (kg/m^3)$	$\mu\ (cP)$	$\sigma\ (mN/m)$
Case 1	Vinegar	1000	1.2	58.6
	10% Glycerol Vinegar (10%GV)	1028	1.9	60.5
	20% Glycerol Vinegar (20%GV)	1050	3.08	58.4
Case 2	1% Butanol Water (1%BW)	990	1.15	60
	2% Butanol Water (2%BW)	1016	1.20	49.3
	4% Butanol Water (4%BW)	1016	1.16	40.4
Case 3	10% Glycerol Vinegar (10%GV)	1028	1.9	60.5
	20% Glycerol Vinegar (20%GV)	1050	3.08	58.4

volume flow rate of $\dot{Q}_f = 00\ cm^3/min$, no LAW appeared at the interface. Furthermore, the observations showed that (10%GV), and (20%GV) liquid flow rates lower than $\dot{Q}_f = 600\ cm^3/min$ and $\dot{Q}_f = 800\ cm^3/min$, respectively, were the operating conditions, where no LAW formed at the interface. Case 3 experiments were performed for two corner angles of $\theta = 60°$ and $\theta = 90°$ to investigate whether the liquid mass separation occurs where LAWs did not appear at the interface. All liquid properties measurements have been done using a viscometer and tensiometer, which are shown in Table 1.

2.2. High Speed Imaging Technique. A high speed side camera (Photron 1280 PCI) was used in this study to capture high speed images with a shutter speed of 2000 frame per second and a resolution of 640 x 128 pixels. Furthermore, the magnification and spatial resolution of these images were 7 and 55 micron, respectively. To determine the interface profile, high speed images were converted into binary sets of data based on pixel brightness. The threshold brightness value of 170 was selected to divide pixels into back and white. The pixels with brightness higher than threshold value were converted to 255, which corresponded to gas phase, and pixels with brightness value lower than 170 were assigned with black pixels(zero brightness), which corresponded to the liquid phase. The interface was determined by the height of the transitional pixels, where the transition between the brightness of 0 and 255 occurred.

In order ot visualize the presence of LAWs at the interface, high speed imaging has been used in this study to categorize the flow regimes as: shear-driven without LAW and with LAW. A wave hight relative to the mean film thickness ratio of 1.7 was used as a threshold to distinguish ripple waves from LAWs. This assumption is also supported by previous studies. (Nakamura (1996), Zhang *et al.* (2017), Hanratty (1983))

Since a line-of-sight effect imposed error on film thickness measurements if determined from the side view, the film thickness was approximated by using a numerical two-phase model presented by Wang *et al.* (2004). This 2D numerical model predicted the turbulent air flow field and shear driven liquid film properties, considering the strong interrelated coupling of both phases. Gas-phase flow field characteristics were modeled using a Finite Volume code with k-ϵ turbulent modeling. Due to waviness of the liquid film interface, a special wall function, which was suggested by Wittig *et al.* (1991) was considered in this model. It was assumed that gas-liquid film interface was a very slow moving rough wall that could be expressed by equivalent sand grain roughness. Moreover, liquid film propagation was predicted based on a boundary layer description. Typical predicted results are shown in Sadeghizadeh and Drallmeier (2018).

3. ANALYSIS

To determine a liquid mass separation map for different gas-liquid flow regimes, the experimental studies have been divided into two sections. First, the force ratio (FR) analytical model proposed by Friedrich *et al.* (2008) is used to generate a mass separation map. The FR model only considers uniform liquid film properties and ignores the effect of LAWs on mass separation. To include both effects of uniform film inertia and LAW on mass separation, a new mass separation map is presented in section 3.2.

3.1. Mass Separation Map Based on Force Ratio Model. An analytical force ratio (FR) model was established by Friedrich *et al.* (2008) to predict the onset of shear-driven film separation at a sharp corner. This model calculates the force ratio between the

forces leading to separation and the forces that resist the separation by using the conservation of linear momentum perpendicular to the ligament at the point of separation.

As it is shown in Fig. 5, for the liquid film two dimensional control volume at the

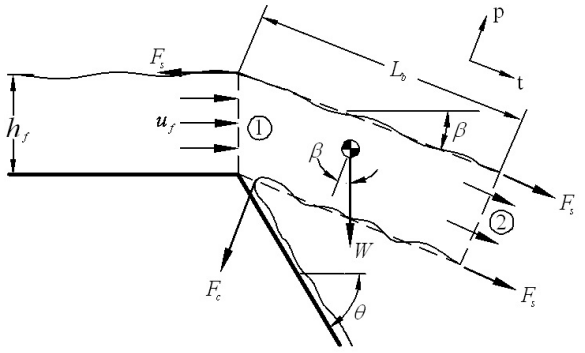

Figure 5. Liquid film at the point of separation

separation point with breakup length of L_b, the nondenominational form of FR is written as

$$FR = \frac{We_f}{1 + \frac{1}{sin\theta} + Fr_{h_f} We_f (\frac{L_b}{h_f})(\frac{1}{tan(\theta)})} \tag{1}$$

Where, $We_f = \frac{\rho_f U_f^2 h_f}{\sigma}$, and $Fr_{h_f} = \frac{g h_f}{U_f^2}$.

In Eq 1, θ is the corner angle and L_b, the estimated length of the film ligament, is estimated from Eq. 2.Arai and Hashimoto (1985)

$$_b = 0.0388 h_f^{0.5} Re_f^{0.6} We_{rel}^{-0.5} \tag{2}$$

Here, liquid Reynold number Re_f is

$$Re_f = \frac{h_f u_f \rho_f}{\mu_f} \tag{3}$$

and relative Weber number is defined as

$$We_{rel} = \frac{h_f \rho (U_g - u_f)^2}{2\sigma} \tag{4}$$

The effect of liquid film inertia is to separate the film from the corner, while surface tension and gravitational forces inhibit liquid film separation. Also, the FR equal to one corresponds to the onset of liquid film separation. Experimental studies by Wegener (2009) show that the restoring gravitational force is negligible compared to the surface tension force for sharp corner geometries with large angles.

The liquid film mass separation results versus the FR is depicted in Fig. 6. Results have been presented for Case 1 and Case 2 experiments and then compared to previous study results presented by Wegener (2009), where the laser focus displacement(LFD) technique was used to measure the mean film thickness and consequently mean film velocity to calculate the FR values.

Using LFD measuring unit, a laser source produces a diverging light beam and the optical train within the unit applies the confocal principle to detect the location of the interface between the gas and liquid phases. While moving the focal point of a converging laser beam, the LFD instrument locates a surface by sensing peaks in reflected light intensity when the laser's focal point is at the interface of two media.

As discussed in Section 2, the liquid mass separation results for Case 1 and Case 2 experiments against the FR show two separated trends. For Case 1 experiments the FR values are smaller compared to the Case 2 experiments. Hence, the FR model does not accurately collapse the impact of liquid film surface tension and viscosity into a single trend.

Results in Fig. 6 demonstrate that the liquid mass separation can not clearly be explained through the FR model. In the FR model the liquid film structure is simplified as a mean layer with smooth interface. However, in fact the liquid film is a complicated

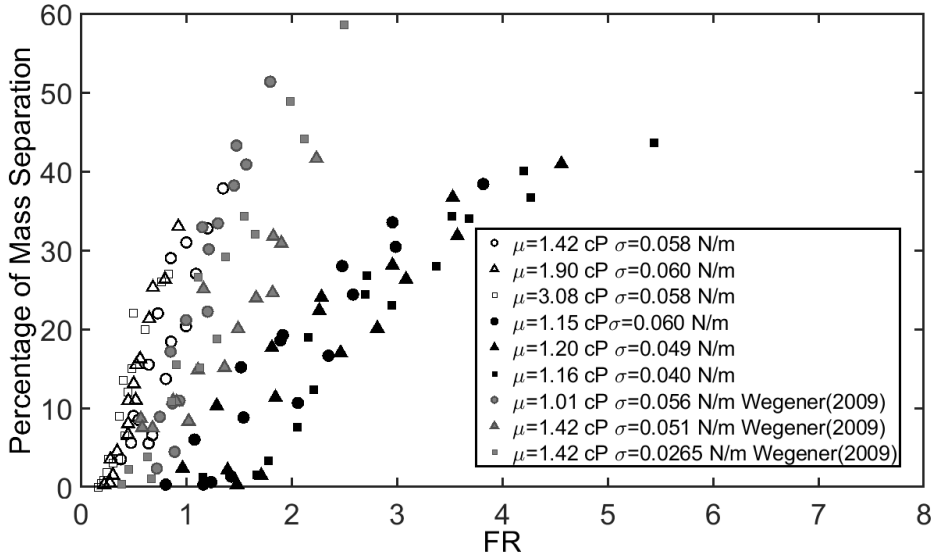

Figure 6. Mass separation versus FR for liquids with different surface tensions and viscosities

structure consisted of film substrate and wavy layer, which includes a combination of different types of disturbance waves such as ripple waves (capillary waves) and LAWs at the interface. Experimental studies in shear-driven flows show that LAWs carry considerable mass fraction of liquid film and contribute significantly to the liquid mass separation. Having the onset of mass separation at a FR of 0.5 implies that, while the FR correlates to the magnitude of the mass separation, the prediction of mass separation inception is not well captured.

3.2. Mass Separation Maps. Physical criteria that impact the force imbalance at the corner and consequently liquid mass separation were considered to determine a correlation between liquid mass separation and non-dimensional operating parameters. The interaction between the gas phase and liquid film is characterized by $Re_g \times Re_f$. For air flow in a fixed test section in this study the Re_g number is equivalent to gas velocity, which is also proportional to mean film velocity in shear-driven flows. (Taylor *et al.* (2014), O'Malley *et al.* (1991), Riley (1987)) Hence, for a constant liquid type, $Re_g \times Re_f$ term represents

the liquid film inertia. To consider the effect of liquid film viscosity and surface tension on liquid mass separation, the non-dimensional terms $\frac{\mu}{\mu_0}$ and We number were considered in this correlation, respectively, where μ_0 is the viscosity of water. The liquid film properties impact the mass separation both through influencing mean film characteristics and LAW formation and growth along the X direction. However, the surface tension also influences the liquid mass separation at the point of separation as a restoring force. The corner angle changes the magnitude of the restoring surface tension force relative to the liquid film inertial force, which consequently impacts the force imbalance at the corner. It should be noted that to determine the Re_f and We number, the mean film characteristics were calculated as discussed in Section 2. (Wittig *et al.* (1991))

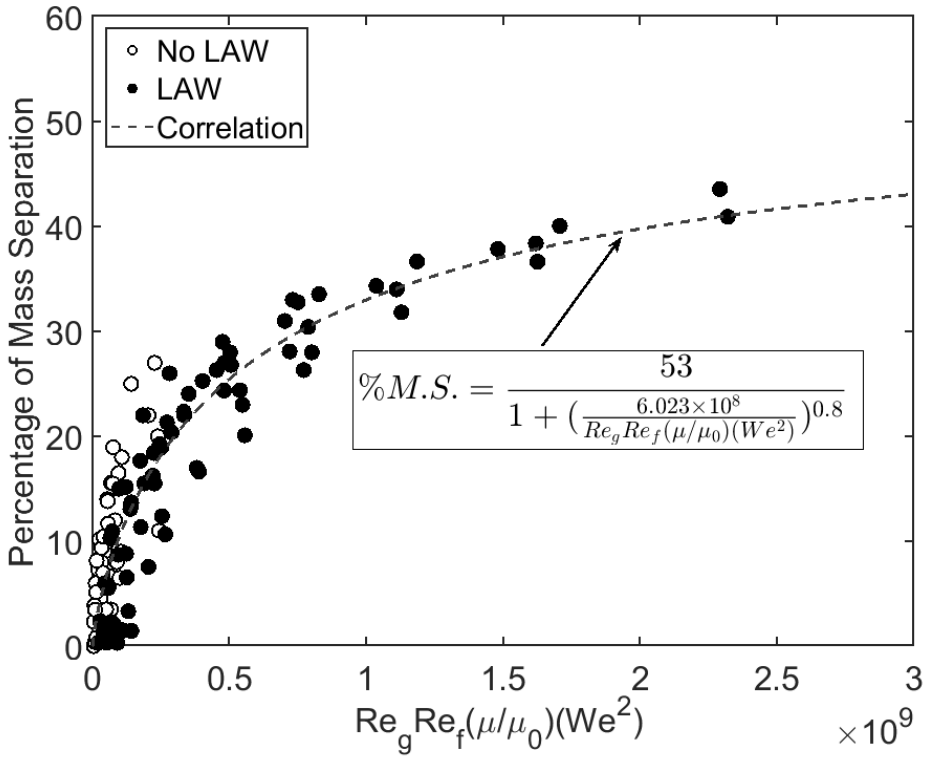

Figure 7. Mass separation map for all flow conditions

The liquid mass separation map including all experiments is depicted in Fig.7. White data points refer to the flow conditions in absence of LAWs (Case 3 experiments),

which were tested for two corner angels of $\theta = 60°, 90°$ and the black data points are for flow conditions in Case 1 and Case 2 experiments, where LAWs appear at the interface. Although both datasets show the same trend in Fig.7, the maximum liquid mass separation in absence of LAWs is smaller than the maximum liquid mass separation for flow regime with LAWs. Also, the correlation suggests asymptotic behavior at high values for the range of conditions considered in this study. However, broadening the range of experimental conditions to include more breadth in liquid properties and operating conditions still needs to be considered. Since both uniform film inertia and LAW effects are influential on liquid mass separation mechanism, the liquid mass separation map was modified by dividing the map into two flow regimes based on LAW existence.

3.2.1. Prediction of mass separation in presence of LAWs. All data for the flow regime with LAW are associated to a fixed sharp corner geometry ($\theta = 60°$). Hence, for specific test section geometry, the non-dimensional parameters that influence liquid mass separation include: $Re_g \times Re_f$, We number, and normalized viscosity $\frac{\mu}{\mu_0}$. These parameters affect the mean film and LAWs characteristics, which impact the force imbalance at the sharp corner.

As is shown in Fig.8, the liquid mass separation correlates well to the defined non-dimensional parameters. In general, the results reveal that liquid mass separation for liquids in Case 1 experiments which have higher surface tension is smaller than liquid mass separation for Case 2 experiments.

3.2.2. Prediction of mass separation for flow regime without LAW (Film Inertia Effect). Empirical correlation for liquid mass separation in the flow regime without LAW is presented in Fig.9. For the flow regime without LAW considered in this study (Case 3 experiments), the surface tension is approximately constant and does not impact the mean film characteristics and LAW formation and growth along the X direction.

In absence of LAWs at the interface, the driving factor for liquid mass separation is the uniform film inertia. To stimulate the liquid mass separation in absence of LAWs,

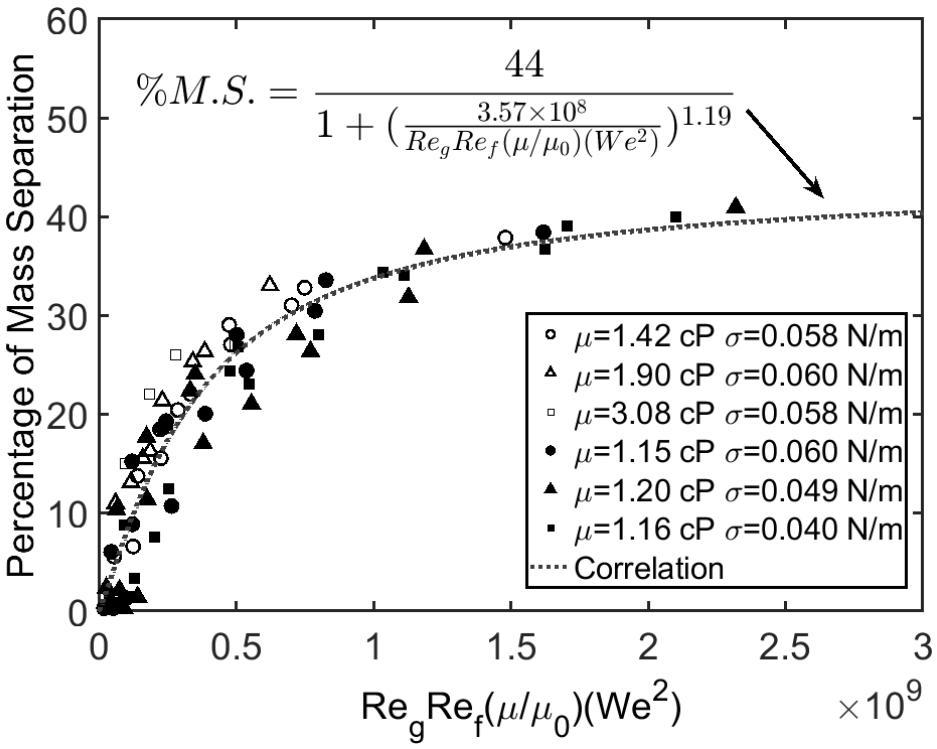

Figure 8. Mass separation correlation for flow regime with LAW

the force imbalance at the point of separation needs to be increased. Different factors impact the force imbalance at the corner. Since the liquid film properties are coupled with the gas-liquid flow conditions and these conditions were fixed in this experiment, the only remaining parameter for increasing the force imbalance was the corner angle. Therefore, in this experiment, the corner angle was increased from $\theta = 60°$ to $90°$ to increase the force imbalance at the corner in absence of LAWs with the ultimate goal to increase the liquid mass separation.

Therefore, the non-dimensional correlation parameters are: $Re_g \times Re_f$ and the normalized viscosity $\frac{\mu}{\mu_0}$. The non-dimensional parameters in Fig.9 are strongly correlated to liquid mass separation results, which is a better correlation compared to Fig.7. Eliminating We number from the effective parameters improves the accuracy of the proposed correlation because the We number includes the effect of viscosity through mean film characteristics

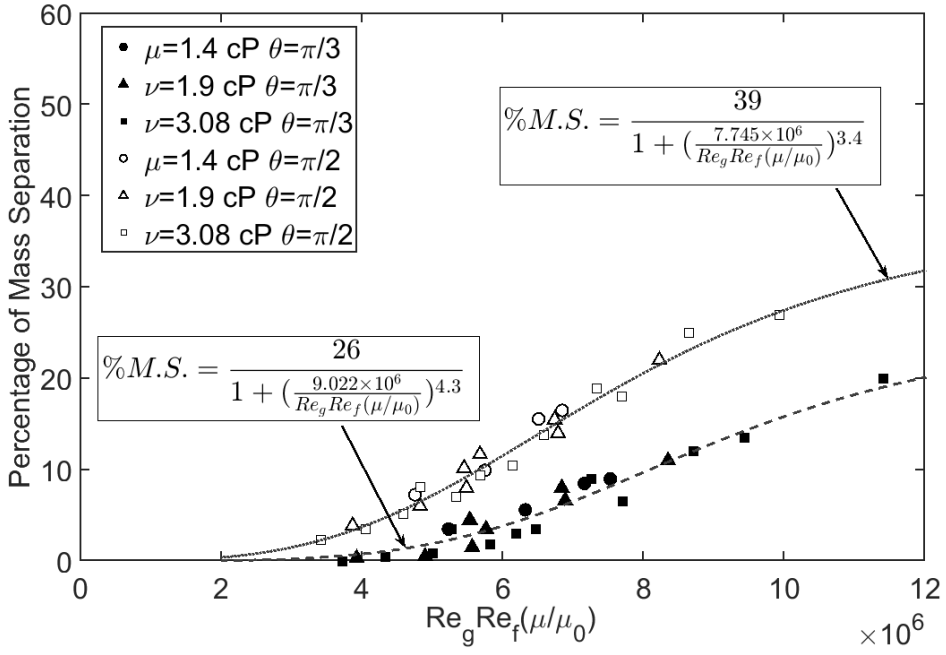

Figure 9. Mass separation correlation for flow regime without LAW

used to define the We number, which results in scattered data in separation map. A sharp corner with larger angle promotes lower restoring force on liquid film control volume at the corner and leads to higher liquid mass separation for the same operating condition. Comparing the mass separation map in Fig.8 and Fig.9 show that presence of LAWs increase the liquid mass separation. When LAWs with significant mass content reach the sharp corner, they become detached from the corner and lead to a higher percentage of mass separation. This is consistent with previous study presented by Sadeghizadeh and Drallmeier (2018)

4. CONCLUSION

Two flow regimes exist in applications where shear-driven liquid film forms at the wall: flow regime without LAW and flow regime with LAW. Liquid mass separation is related to inertial force exerted on liquid film. In the case that there is no LAW at the

interface, the mass separation occurs entirely due to mean film inertia. For cases where LAWs appear at the interface, the liquid mass separation is driven by inertial force of both mean film and LAWs. For each flow regime, an empirical correlation has been proposed in this study. These correlations were determined based on the physical analysis and high speed imaging observations. Compared to the previous models in literature, these correlations presented the liquid mass separation more accurately as liquid film properties such as surface tension and viscosity are varied. The effect of mean film inertia, LAW formation and growth due to the variation in film properties are captured better in these correlations compare to previous models, where the effect of liquid film properties on LAWs were completely ignored in mass separation mechanism.

It should be noted that the challenge to determine the correlation based on the LAW flow regime is that there is no theoretical approach to identify the transition to LAW flow regime and it is essential to use flow visualization techniques to determine the LAW transition for different flow conditions.

REFERENCES

Andritsos, N. and Hanratty, T., 'Interfacial Instabilities for Horizontal Gas-Liquid Flows in Pipelines,' International Journal of Multiphase Flow, 1987, **13**(5), pp. 583–603.

Arai, T. and Hashimoto, H., 'Disintegration of a thin liquid sheet in a concurrent gas stream,' Heat Fluid Flow, 1985, **20**, pp. 507–512.

Bacharoudis, E., Bratec, H., Keirsbulck, L., Buchlin, J.-M., and Labraga, L., 'Simplified Model for the Prediction of the Occurrence of Film Atomization in Corner Geometries,' International Journal of Multiphase Flow, 2014, **58**, pp. 325–337.

Bruno, K. and McCready, M., 'Origin of roll waves in horizontal gas-liquid flows,' AIChE journal, 1988, **34**(9), pp. 1431–1440.

Friedrich, M. A., Lan, H., Wegener, J., Drallmeier, J., and Armaly, B. F., 'A Separation Criterion with Experimental Validation for Shear-Driven Films in Separated Flows,' Journal of Fluids Engineering, 2008, **130**(5), p. 051301.

Hanratty, T., 'Interfacial Instabilities Caused by Air Flow Over a Thin Liquid Layer,' Waves on Fluid Interfaces, 1983, **11**(1), pp. 221–259.

Nakamura, H., 'Slug Flow Transitions in Horizontal Gas/Liquid Two-Phase Flows (Dependence on Channel Height and System Pressure for Air/Water and Steam/Water Two-Phase Flows),' Research/Japan atomic energy research institute (Tokyo), 1996, **96**, p. 022.

O'Malley, K., Fitt, A., Jones, T., Ockendon, J., and Wilmott, P., 'Models for high-reynolds-number flow down a step,' Journal of fluid mechanics, 1991, **222**, pp. 139–155.

O'rourke, P. and Amsden, A., 'A particle numerical model for wall film dynamics in port-injected engines,' Technical report, SAE Technical Paper, 1996.

Owen, I. and Ryley, D., 'The Flow of Thin Liquid Films around Corners,' International Journal of Multiphase Flow, 1985, **11**(1), pp. 51–62.

Riley, N., 'Inviscid separated flows of finite extent,' Journal of engineering mathematics, 1987, **21**(4), pp. 349–361.

Sadeghizadeh, Z. and Drallmeier, J. A., 'Effect of large amplitude waves and film inertia on mass separation at a sharp corner,' Journal of Fluids Engineering, 2018, **140**(8), p. 081301.

Steinhaus, B., Ghandhi, J., and Shedd, T., 'Experimental investigation of liquid film stripping at a sharp corner,' in 'ILASS Americas, Proceedings of the 20th Annual Conference on Liquid Atomization and Spray Systems,' 2007 .

Taylor, N. H., Hewitt, I., Ockendon, J., and Witelski, T., 'A new model for disturbance waves,' International Journal of Multiphase Flow, 2014, **66**, pp. 38–45.

Wang, Y., Wilkinson, G., and Drallmeier, J., 'Parametric Study on the Fuel Film Breakup of a Cold Start PFI Engine,' Experiments in Fluids, 2004, **37**(3), pp. 385–398.

Wegener, J., *Experiments and Modeling of Shear-Driven Film Separation*, MS Thesis, Missouri University of Science and Technology, Rolla, MO, 2009.

Wittig, S., Himmelsbach, J., Noll, B., Feld, H., and Samenfink, W., 'Motion and evaporation of shear-driven liquid films in turbulent gases,' in 'ASME 1991 International Gas Turbine and Aeroengine Congress and Exposition,' American Society of Mechanical Engineers, 1991 pp. V003T06A017–V003T06A017.

Woodmansee, D. E. and Hanratty, T. J., 'Mechanism for the Removal of Droplets from a Liquid Surface by a Parallel Air Flow,' Chemical Engineering Science, 1969, **24**(2), pp. 299–307.

Zhang, Y., Jia, M., Duan, H., Wang, P., Wang, J., Liu, H., and Xie, M., 'Experimental and numerical study of the liquid film separation and atomization at expanding corners,' Technical report, SAE Technical Paper, 2017.

Zhao, Y., Markides, C. N., Matar, O. K., and Hewitt, G. F., 'Disturbance Wave Development in Two-Phase Gas-Liquid Upwards Vertical Annular Flow,' International Journal of Multiphase Flow, 2013, **55**, pp. 111–129.

SECTION

2. SUMMARY AND CONCLUSIONS

The separation of a shear-driven thin liquid film from expanding corners is investigated in this work. Two different mechanisms impact the separation of shear-driven liquid films at expanding corners: liquid film inertia and large amplitude waves. Liquid film inertia affects liquid mass separation through force imbalance at the sharp corner, and large amplitude waves at the interface, contributes to liquid instability at the corner.

Despite the available models in literature, only one of these effects was considered to have impact on liquid mass separation. In this study the coupled effect of these two mechanisms has been studied. Experimental results show that both film inertia and large amplitude wave effects correlate to mass separation results. The results suggest that while both inertia of the film substrate and large amplitude wave effects enhance the mass separation, the correlations between large amplitude wave characteristics and mass separation results provide better insight into the onset of separation and the impact of the gas phase velocity on separation for the conditions studied.

Liquid film properties affect both mean film characteristics and large amplitude waves formation and growth along the wall. To study the effect of liquid film viscosity and surface tension on liquid mass separation, a liquid matrix including six different liquid types has been designed for this study. Increasing the viscosity at constant gas and liquid flow rate decreased the liquid mass separation at the sharp corner. Higher viscosity decreased the inertial force and consequently the force imbalance at the corner by influencing liquid film mean properties. Also, the LAW mass content at the interface prior to the corner decreased by increasing the viscosity due to wave attenuation.

The surface tension impact on the liquid mass separation was more complex. First, the decrease in surface tension resulted in dramatically higher FR values compared to the viscosity test. This occurred since for the large corner angles, the dominant restoring force was the surface tension. The liquid mass separation results showed that even though LAW formation was weaken by decreasing the surface tension, the liquid mass separation increased. This may be explained by the increase in the mean film inertia as demonstrated in the FR at the corner. Finally, while a reduction in surface tension reduced LAW formation, those that did form grew faster with axial position. These results clearly show that neither the inertia of the uniform film layer nor the formation of LAWs can fully describe the film separation at the corner. Liquid mass separation models must consider both the mean film as well as the wavy layer in considering the impact of liquid properties on liquid film separation.

Two distinct mass separation correlations have been proposed in this study. These maps were distinguished based on the existence of large amplitude waves at the interface. In flow regimes without large amplitude waves, the liquid mass is separated from the sharp corner due to pure mean film inertia. The influential parameters are the moment transfer between the gas and liquid phases (proportional to $Re_g Re_l$), the restoring force that resist the liquid film separation, and the corner angle which changes the restoring force magnitude.

The mass separation correlations in presence of large amplitude waves includes the coupled effect of mean film inertia and large amplitude waves simultaneously. Similar to the mass separation map for flow regime without large amplitude waves, the interaction between gas and liquid is a significant correlation factor. Furthermore, the viscosity and Weber number, which impact both mean film properties and large amplitude waves formation and growth are other important correlation parameters.

APPENDIX

Interface Numerical Simulation (line-of-sight effect)

```
clc
clear all;
close all;
%Define the range of interface wave components (ripple waves and LAWs)
    frequency and amplitudes
amp1_S=20; amp2_S=100;amp1_L=255; amp2_L=500;
f1_S=50; f2_S=1000; f1_L=10;f2_L=60;
n_LAW=5;
n_ripp=500;
%---------------------------------------
amp=[];
f=[];
fs=2000;
T=1;
t=0:1/fs:T-1/fs;
nfft=length(t);
amp_S = (amp1_S + (amp2_S-amp1_S).*rand(n_ripp,1))';
amp_L = (amp1_L + (amp2_L-amp1_L).*rand(n_LAW,1))';
f_S = (f1_S + (f2_S-f1_S).*rand(n_ripp,1))';
f_L = (f1_L + (f2_L-f1_L).*rand(n_LAW,1))';
amp=[amp amp_S amp_L];
amp1=amp;
f1=[f f_S f_L];
f=round(f1);
amp=diag(amp);
wave=amp*sin(2*pi*f'*t);

for i=1:length(amp1)
wave_win(i,:)=wave(i,:)'.*hanning(length(t));
end
subplot(3,1,2)
for j=1:length(amp1)
Wave(j,:)=fft(wave_win(j,:),nfft)/length(t);
freq=(fs/nfft)*(0:nfft-1);
hold on
```

```
plot(freq(2:end-1),2*abs(Wave(j,(2:end-1))))
xlim([0 1000])
xlabel('f (Hz)')
ylabel('FFT of All Interface Wave Components')
end
[b,a] = butter(2,0.005,'low');

subplot(3,1,1)
wave_max = max(wave); % Envelope of all waves together
plot(t,wave_max)
xlim([0 1])
xlabel('t(sec)')
ylabel('Interface Profile')
x=(wave_max(:)-mean(wave_max(:))).*hanning(length(t));
WAVE_MAX = fft(x,nfft)/length(t);
[b,a] = butter(2,0.005,'low');
WAVE_MAX(1) = 0;
Y1 = filter(b,a,WAVE_MAX); %FFT Magnitude
subplot(3,1,3)
plot(freq,abs(Y1))
xlim([0 1000])
xlabel('f (Hz)')
ylabel('Interface FFT')
```

Image Processing MATLAB Code for FFT Analysis

```
%Read the High Speed Imaging AVI Files
clc; clear all; close all;
filename = 'AVI_High_Speed_Imaging_Data.avi';
vObj = VideoReader(filename);
mov = aviread(filename);
vidWidth = vObj.Width;
vidHeight = vObj.Height;
for i = 1:vObj.NumberOfFrames
data(:,:,i) = mov(i).cdata;
end
save([filename(1:end-4) '.mat'], 'data','vObj');
%-----------------------------------------------------------------------
clc; clear all; close all;
filename = 'AVI_High_Speed_Imaging_Data.mat';
load(filename)
%-----------------------------------------------------------------------
%Convert grayscale into binary image to determine the interface signal
tr =170;
figure(1);
min_row =90;
max_row = 145;
min_col=30;
max_col=440;
imshow(data(min_row:max_row,min_col:max_col,150))
figure(2)
for i = 1:10
bin_fr = data(min_row:max_row,min_col:max_col,i) > tr;
imshow(bin_fr)
pause(0.001)
end
Col_offset_left = 0;
Col_offset_right=0;
temp1=[];
temp2=[];
sorted=[];
n_frames=8000;
for i = 1:n_frames
i;
```

```
fr_bin = (0.* (data(min_row:max_row,min_col:max_col,i) < tr)) + b@x...
(255 .* (data(min_row:max_row,min_col:max_col,i) > tr));
for j = 1:size(fr_bin,2)
b = find(flipud(fr_bin(:,j)));
if(~isempty(b))
signal(i,j) = b(1);
else
signal(i,j) = 0;
end
end
end
%--------------------------------------------------------------------
%FFT Analysis along the fetch length
fs = 2000;
nfft = 2^17;
freq = ((0:nfft-1)/nfft*fs);
win = hamming(size(signal,1))';
[b,a] = butter(2,0.00035,'low');
x1 = (680/6)*((signal(:,80))- mean(signal(:,80)));
x2 = (680/6)*((signal(:,150))- mean(signal(:,150)));
x3 = (680/6)*((signal(:,270))- mean(signal(:,270)));
x4= (680/6)*(((signal(:,355)))- mean(signal(:,355)));
Loc1=90*680*0.001/6;
Loc2=180*680*0.001/6;
Loc3=270*680*0.001/6;
Loc4=355*680*0.001/6;
figure()
X1 = abs(fft(x1.*win.',nfft));
X2 = abs(fft(x2.*win.',nfft));
X3 = abs(fft(x3.*win.',nfft));
X4 = abs(fft(x4.*win.',nfft));
Y1 = filter(b,a,X1);
Y2 = filter(b,a,X2);
Y3 = filter(b,a,X3);
Y4 = filter(b,a,X4);
Z1 = trapz(freq(1:end/2),Y1(1:nfft/2));
Z2=trapz(freq(1:end/2),Y2(1:nfft/2));
hold on
plot(freq(1:end/2),Y1(1:nfft/2),'r')
```

```
plot(freq(1:end/2),Y2(1:nfft/2),'m')
plot(freq(1:end/2),Y3(1:nfft/2),'b')
plot(freq(1:end/2),Y4(1:nfft/2),'g')
xlabel('Frequency','fontsize',22,'fontweight','b')
ylabel('FFT Magnitude','fontsize',22,'fontweight','b')
legend('X location : 40 mm Upstream From The Corner',...
'X location : 30 mm Upstream From The Corner',...
'X location : 20 mm Upstream From The Corner',...
'X location : 10 mm Upstream From The Corner')
title('X location : 30 mm Upstream From The Corner')
```

REFERENCES

Alekseenko, S. V., Cherdantsev, A. V., Cherdantsev, M. V., Isaenkov, S. V., Kharlamov, S. M., and Markovich, D. M., 'Formation of disturbance waves in annular gas-liquid flow,' in 'Proc. of 17th International Symposium on Applications of Laser Techniques to Fluid Mechanics, Lisbon,' 2014 .

Andreussi, P., Asali, J., and Hanratty, T., 'Initiation of roll waves in gas-liquid flows,' AIChE journal, 1985, **31**(1), pp. 119–126.

Andritsos, N. and Hanratty, T., 'Interfacial Instabilities for Horizontal Gas-Liquid Flows in Pipelines,' International Journal of Multiphase Flow, 1987, **13**(5), pp. 583–603.

Arai, T. and Hashimoto, H., 'Disintegration of a thin liquid sheet in a concurrent gas stream,' Heat Fluid Flow, 1985, **20**, pp. 507–512.

Bacharoudis, E., Bratec, H., Keirsbulck, L., Buchlin, J.-M., and Labraga, L., 'Simplified Model for the Prediction of the Occurrence of Film Atomization in Corner Geometries,' International Journal of Multiphase Flow, 2014, **58**, pp. 325–337.

Bruno, K. and McCready, M., 'Origin of roll waves in horizontal gas-liquid flows,' AIChE journal, 1988, **34**(9), pp. 1431–1440.

Craik, A. D., 'Wind-Generated Waves in Thin Liquid Films,' Journal of Fluid Mechanics, 1966, **26**(2), pp. 369–392.

Friedrich, M. A., Lan, H., Wegener, J., Drallmeier, J., and Armaly, B. F., 'A Separation Criterion with Experimental Validation for Shear-Driven Films in Separated Flows,' Journal of Fluids Engineering, 2008, **130**(5), p. 051301.

Fuster, D., Matas, J.-P., Marty, S., Popinet, S., Hoepffner, J., Cartellier, A., and Zaleski, S., 'Instability regimes in the primary breakup region of planar coflowing sheets,' Journal of Fluid Mechanics, 2013, **736**, pp. 150–176.

Hanratty, T., 'Interfacial Instabilities Caused by Air Flow Over a Thin Liquid Layer,' Waves on Fluid Interfaces, 1983, **11**(1), pp. 221–259.

Hoogendoorn, C., 'Gas-liquid flow in horizontal pipes,' Chemical Engineering Science, 1959, **9**(4), pp. 205–217.

Matas, J.-P., 'Inviscid versus viscous instability mechanism of an air–water mixing layer,' Journal of Fluid Mechanics, 2015, **768**, pp. 375–387.

Nakamura, H., 'Slug Flow Transitions in Horizontal Gas/Liquid Two-Phase Flows (Dependence on Channel Height and System Pressure for Air/Water and Steam/Water Two-Phase Flows),' Research/Japan atomic energy research institute (Tokyo), 1996, **96**, p. 022.

O'Malley, K., Fitt, A., Jones, T., Ockendon, J., and Wilmott, P., 'Models for high-reynolds-number flow down a step,' Journal of fluid mechanics, 1991, **222**, pp. 139–155.

O'rourke, P. and Amsden, A., 'A particle numerical model for wall film dynamics in port-injected engines,' Technical report, SAE Technical Paper, 1996.

Owen, I. and Ryley, D., 'The Flow of Thin Liquid Films around Corners,' International Journal of Multiphase Flow, 1985, **11**(1), pp. 51–62.

Pereira, A. and Kalliadasis, S., 'Dynamics of a falling film with solutal Marangoni effect,' Physical Review E, 2008, **78**(3), p. 036312.

Riley, N., 'Inviscid separated flows of finite extent,' Journal of engineering mathematics, 1987, **21**(4), pp. 349–361.

Sadeghizadeh, Z. and Drallmeier, J. A., 'Effect of large amplitude waves and film inertia on mass separation at a sharp corner,' Journal of Fluids Engineering, 2018, **140**(8), p. 081301.

Setyawan, A. *et al.*, 'The effect of the fluid properties on the wave velocity and wave frequency of gas–liquid annular two-phase flow in a horizontal pipe,' Experimental Thermal and Fluid Science, 2016, **71**, pp. 25–41.

Shedd, T. A., 'Characteristics of the liquid film in horizontal two-phase flow,' Technical report, Air Conditioning and Refrigeration Center. College of Engineering. University of Illinois at Urbana-Champaign., 2001.

Steinhaus, B., Ghandhi, J., and Shedd, T., 'Experimental investigation of liquid film stripping at a sharp corner,' in 'ILASS Americas, Proceedings of the 20th Annual Conference on Liquid Atomization and Spray Systems,' 2007 .

Strasser, W. and Battaglia, F., 'The Influence of Retraction on Three-Stream Injector Pulsatile Atomization for Air–Water Systems,' Journal of Fluids Engineering, 2016, **138**(11), p. 111302.

Taylor, N. H., Hewitt, I., Ockendon, J., and Witelski, T., 'A new model for disturbance waves,' International Journal of Multiphase Flow, 2014, **66**, pp. 38–45.

Thunivumani, G. and Gadgil, H., 'Dynamics of Liquid Sheet Breakup in Splash Plate Atomization,' Journal of Fluids Engineering, 2018, **140**(1), p. 011205.

Thwaites, G., Kulov, N., and Nedderman, R., 'Liquid film properties in two-phase annular flow,' Chemical Engineering Science, 1976, **31**(6), pp. 481–486.

Wang, Y., Wilkinson, G., and Drallmeier, J., 'Parametric Study on the Fuel Film Breakup of a Cold Start PFI Engine,' Experiments in Fluids, 2004, **37**(3), pp. 385–398.

Wegener, J., *Experiments and Modeling of Shear-Driven Film Separation*, MS Thesis, Missouri University of Science and Technology, Rolla, MO, 2009.

Weisman, J., Duncan, D., Gibson, J., and Crawford, T., 'Effects of fluid properties and pipe diameter on two-phase flow patterns in horizontal lines,' International Journal of Multiphase Flow, 1979, **5**(6), pp. 437–462.

Whitaker, S., 'Effect of surface active agents on the stability of falling liquid films,' Industrial & Engineering Chemistry Fundamentals, 1964, **3**(2), pp. 132–142.

Wittig, S., Himmelsbach, J., Noll, B., Feld, H., and Samenfink, W., 'Motion and evaporation of shear-driven liquid films in turbulent gases,' in 'ASME 1991 International Gas Turbine and Aeroengine Congress and Exposition,' American Society of Mechanical Engineers, 1991 pp. V003T06A017–V003T06A017.

Woodmansee, D. E. and Hanratty, T. J., 'Mechanism for the Removal of Droplets from a Liquid Surface by a Parallel Air Flow,' Chemical Engineering Science, 1969, **24**(2), pp. 299–307.

Zadrazil, I., Matar, O. K., and Markides, C. N., 'An Experimental Characterization of Downwards Gas-liquid Annular Flow by Laser-Induced Fluorescence: Flow Regimes and Film Statistics,' International Journal of Multiphase Flow, 2014, **60**, pp. 87–102.

Zhang, Y., Jia, M., Duan, H., Wang, P., Wang, J., Liu, H., and Xie, M., 'Experimental and numerical study of the liquid film separation and atomization at expanding corners,' Technical report, SAE Technical Paper, 2017.

Zhao, F., Qin, L.-Z., Fu, Q.-F., Mo, C.-J., and Yang, L.-J., 'Spray Characteristics of Elliptical Power-Law Fluid-Impinging Jets,' Journal of Fluids Engineering, 2017, **139**(7), p. 071203.

Zhao, Y., Markides, C. N., Matar, O. K., and Hewitt, G. F., 'Disturbance Wave Development in Two-Phase Gas-Liquid Upwards Vertical Annular Flow,' International Journal of Multiphase Flow, 2013, **55**, pp. 111–129.

VITA

Zahra Sadeghizadeh was born in Iran. She attended Sharif University of Science and Technology from 2004 to 2011 and received her B.S. and M.S. degree in Aerospace Engineering. She came to the United States in August 2012 to pursue her Ph.D in Aerospace Engineering.

Since she was passionate about teaching, she was the graduate teaching assistant and instructor in the Mechanical and Aerospace Engineering Department while she was pursing her Ph.D. In July 2018 Zahra received her Ph.D. in Aerospace Engineering from Missouri University of Science and Technology.